

MICROCHANNEL RADIATOR: AN INVESTIGATION OF MICROCHANNEL
TECHNOLOGY WITH APPLICATIONS IN AUTOMOTIVE
RADIATOR HEAT EXCHANGERS

Gus Thomas Checketts

Thesis Prepared for the Degree of
MASTER OF SCIENCE

UNIVERSITY OF NORTH TEXAS

August 2014

APPROVED:

Yong X. Tao, Major Professor and Chair of the
Department of Mechanical and Energy
Engineering

Tingzhen Ming, Committee Member

Jiangtao Cheng, Committee Member

Costas Tsatsoulis, Dean of the College of
Engineering

Mark Wardell, Dean of the Toulouse Graduate
School

Checketts, Gus Thomas. *Microchannel Radiator: An Investigation of Microchannel Technology with Applications in Automotive Radiator Heat Exchangers*. Master of Science (Mechanical and Energy Engineering), August 2014, 126 pp., 18 tables, 53 figures, 58 numbered references.

Microchannels have been used in electronics cooling and in air conditioning applications as condensers. Little study has been made in the application of microchannels in automotive heat exchangers, particularly the radiator. The presented research captures the need for the design improvement of radiator heat exchangers in heavy-duty vehicles in order to reduce aerodynamic drag and improve fuel economy. A method for analyzing an existing radiator is set forth including the needed parameters for effective comparisons of alternative designs. An investigation of microchannels was presented and it was determined that microchannels can improve the overall heat transfer of a radiator but this alone will not decrease the dimensions of the radiator. Investigations into improving the air-side heat transfer were considered and an improved fin design was found which allows a reduction in frontal area while maintaining heat transfer. The overall heat transfer of the design was improved from the original design by 7% well as 52% decrease in frontal area but at the cost of 300% increase in auxiliary power. The energy saved by a reduction in frontal area is not substantial enough to justify the increase of auxiliary power.

The findings were verified through a computational fluid dynamic model to demonstrate the heat transfer and pressure drop of microchannel tubes. The results confirmed that heat transfer of microchannels does improve the thermal performance of the radiator but the pressure drop is such that the net benefit does not outweigh the operating cost. An additional CFD study of the new fin geometry and air-side heat transfer predictions was conducted. The results of the study confirmed the theoretical calculations for the fin geometry.

Copyright 2014

by

Gus Thomas Checketts

ACKNOWLEDGEMENTS

First, I would like to express deep gratitude to the Almighty God for continually guiding and directing his research, educational path, and personal life and for bringing him to this point. There has been evidence of divine guidance during the course of this research and I would be eternally ungrateful and untrue if I did not attribute this success to my Supreme Maker.

I would also like to thank my advisor Dr. Yong Tao for his continual input, direction, advice, and supervision of this work and for his constant desire to push his students to become their best. Without his expertise, achievements, and professional attitude, the realization of this study would not have been possible.

A big thanks goes to Dr. Tingzhen Ming for his support in the technical details of the research and for his constant input on how to improve and develop the studies conducted. A special thanks goes to Dr. Rambod Rayegan and Dr. Junghyon Mun for their willingness to answer questions and provide insight and for their continual support through this process.

I would like to thank the members of my Thesis Defense Committee, Dr. Yong Tao, Dr. Jiangtao Cheng, and Dr. Tingzhen Ming, for their support in seeing this work come to fruition.

I would like to recognize Bill Kahn, Rick Mihelic as the other personnel at Peterbilt who played various roles in the success of this work.

Finally, I would like to thank my family and friends for all of their encouragement and support. Huge thanks goes to Sarah, Elliana, and Kaden for their patience and support for the past few years and for their constant encouragement. I would also like to recognize the support and direction of my father and the continual concern and prayers of my mother and family members in this endeavor.

TABLE OF CONTENTS

	Page
ACKNOWLEDGEMENTS	iii
LIST OF TABLES	vi
LIST OF FIGURES	vii
NOMENCLATURE	ix
CHAPTER 1. INTRODUCTION	1
1.1 Incentive for Research	1
1.1.1 Improving Vehicle Performance.....	2
1.1.2 Requirements for Heavy Duty Vehicle Manufacturers	4
1.1.3 Fuel Economy and Aerodynamics	6
1.1.4 Drag Reduction and Frontal Area	7
1.2 Introduction to Microchannels	10
1.3 Overview of Conducted Research	10
CHAPTER 2. LITERATURE REVIEW	12
2.1 Radiator Studies	12
2.2 Microchannel Studies.....	15
2.3 Mathematical Modeling Studies	18
CHAPTER 3. THEORY	20
3.1 Introduction to Parametric Approach.....	20
3.2 Working Conditions.....	21
3.3 Geometry.....	22
3.4 Heat Transfer Analysis	24
3.5 Heat Transfer Analysis Comparison.....	28
3.6 Fluid Flow Characteristics	29
CHAPTER 4. TOPICS OF RESEARCH AND EXPERIMENTAL PROCEDURES	33
4.1 Design Study.....	33
4.2 Study of Microchannel Tubes.....	33
4.3 Study of Fins	38

4.4	Operating Conditions	39
CHAPTER 5. CALCULATIONS, TEST METHODS AND RESULTS.....		44
5.1	Simulation and Calculations	44
5.2	Optimization of Model.....	63
5.3	CFD Verification	65
CHAPTER 6. CONCLUSION.....		76
6.1	Design Improvements	76
6.2	Material Benefits.....	77
6.3	Conclusion	78
6.4	Future Research	79
APPENDIX A. MATHEMATICAL MODELING CODE		81
APPENDIX B. CFD RESULTS		109
REFERENCES		122

LIST OF TABLES

	Page
Table 1.1: Classification of heavy duty vehicles for GHG emission requirements beginning model year 2014 [4, p. 3].	5
Table 1.2: Aerodynamic improvement options for line-haul trucks [5, p. 4]	6
Table 1.3: Comparison of aerodynamic truck design	8
Table 1.4: Parameters used to compare heat exchangers	11
Table 2.1: Material comparison values taken from MatWeb and literature.	14
Table 3.1: Parameters used to compare heat exchangers	20
Table 3.2: Measured and calculated dimensions of radiator under investigation	24
Table 4.1: Nusselt Number and friction factor for laminar flow through smooth tubes of various cross-sectional geometry [10, p. 437].	37
Table 4.2: Material properties of different fluids at T=20°C [53] [54]	43
Table 4.3: Freezing and boiling points of commonly used coolants [55].	43
Table 5.1: Comparison of radiator designs	64
Table 5.2: Results of design improvements made	65
Table 5.3: Results of CFD Simulation for Mass Flow Average Temperature at Outlet	68
Table 5.4: Results of CFD Simulation for Pressure Drop Across Tubes	68
Table 5.5: Results of simulation for convection heat transfer coefficient	69
Table 5.6: Dimensions of fin geometry	72
Table 5.7: Pressure drop across louver fin geometries	74

LIST OF FIGURES

	Page
Figure 1.1: Energy losses associated with HDVs [2]	2
Figure 1.2: Classification of heavy duty vehicles effective MY 2014 [2].....	5
Figure 3.1: Corrugated serpentine louver fin and flat tube configuration and dimensions [16]...	23
Figure 3.2: Image of radiator fin and tube configuration under investigation.....	23
Figure 3.3: Thermal resistance model of a radiator to determine the total thermal resistance of the radiator	25
Figure 3.4: F Correction factor for LMTD method as a function of P and R [48].	29
Figure 4.1a&b: Original tube and fin configuration and proposed tube and fin configuration	34
Figure 5.1: Total thermal resistance calculated, showing air-side convective resistance, coolant-side convective resistance, and total thermal resistance.	46
Figure 5.2: Hydraulic diameter vs. Reynolds number	47
Figure 5.3: Hydraulic diameter vs. internal convection coefficient.....	48
Figure 5.4: Hydraulic diameter vs. internal thermal convection resistance.....	48
Figure 5.5: Hydraulic diameter vs. pressure drop.....	49
Figure 5.6: Mass flow rate vs. maximum heat transfer for an array of 1100 tubes of varying hydraulic diameters	50
Figure 5.7: Mass flow rate vs. pressure drop for an array of 1100 tubes of varying hydraulic diameters	51
Figure 5.8: Mass flow rate vs. maximum heat transfer for an array of 1500 tubes of varying hydraulic diameters	51
Figure 5.9: Mass flow rate vs. pressure drop for an array of 1500 tubes of varying hydraulic diameters	52
Figure 5.10: Effects of hydraulic diameter on R_{pipe} . The highest resistance value corresponds to the original radiator (flat tube) design.	52
Figure 5.11: Effects of louver length (fin length) on the external convection coefficient comparing against louver pitch.....	54

Figure 5.12: Effects of tube depth on the external convection coefficient comparing against louver pitch	55
Figure 5.13: Effects of fin pitch on the external convection coefficient comparing against louver pitch.....	55
Figure 5.14: Effects of air frontal velocity (from fan) on the external convection coefficient comparing against louver pitch.....	56
Figure 5.15: Effects of fin surface area on external convection resistance	57
Figure 5.16: Comparison of <i>hair</i> and <i>A</i> to <i>R_{fin}</i>	58
Figure 5.17: Effects of fin length on air-side pressure drop	59
Figure 5.18: Effects of fin pitch on pressure drop	59
Figure 5.19: Effects on tube depth on pressure drop	60
Figure 5.20: Effects of fin pitch, fin length, and tube depth on pressure drop using normalized relationship.....	60
Figure 5.21: Comparison of total heat transfer and auxiliary power. Also, a comparison to the frontal area and auxiliary power is given to determine the optimal solution.....	62
Figure 5.22: CFD model and boundary conditions for original flat tube, round microchannel slab and a square microchannel slab	67
Figure 5.23: CFD model with boundary conditions for microchannel square tube slab	67
Figure 5.24: CFD model with boundary conditions for microchannel round tube slab	68
Figure 5.25: Temperature profile at the tube outlet	69
Figure 5.26: CFD model of original fin geometry.....	70
Figure 5.27: CFD model of proposed new fin geometry	71
Figure 5.28: Volume rendering of fluid temperature of the original fin as a result of heat transfer from the wall through the fin and into the free stream air.	72
Figure 5.29: Volume rendering of new fin	73
Figure 5.30: Pressure profile of original fin.....	74
Figure 5.31: Pressure profile of new fin	75
Figure 6.1: Frontal area reduction.....	77

NOMENCLATURE

A	Total convective heat transfer surface area including fins and tube surfaces
A_c	Cross sectional area of single tube
$A_{contact}$	Area of contact between fins and tubes for contact resistance
A_f	Total convective surface area of fins
A_{fin}	Surface area of a single fin
A_{fr}	Frontal area of radiator
A_{rad}	Surface area of applicable radiating surfaces
c_p	Specific heat capacity at constant pressure
Dh_{air}	Hydraulic Diameter of air flow through radiator from single space between fins
Dm	Major tube diameter or, for flat tubes, tube width
D_h	Hydraulic Diameter $D_h = 4A_c/P$
D_{eq}	Equivalent Diameter $D_{eq} = \sqrt{(4A_c)/\pi}$
Fl	Fin length, length of fin from base
Fp	Fin pitch, spacing between each fin
G	Mass velocity $G = \dot{m}_{pipe}/A_c$
h	Convection heat transfer coefficient
k_{fin}	Thermal conductivity of fin material
k_{pipe}	Thermal conductivity of tube material
L	Length of tube
Ll	Louver length, length of louver fin
Lp	Louver pitch, spacing between each louver fin

L_{fin}	Length of fin from base
\dot{m}	Mass flow rate
Nu	Nusselt Number
N_{pipe}	Number of tubes in radiator
P	Perimeter of inside of tube
P_f	Perimeter of single fin normal to the flow
Pr	Prandtl Number $Pr = c_p \mu / k$
Re	Reynolds Number
Td	Tube depth, length of flat tube along air-flow direction
Tp	Tube pitch, spacing between tubes
r_i	Tube internal equivalent radius $r_i = D_{eq}/2$
r_o	Tube external equivalent radius $r_o = r_i + t_{wall}$
R_{pipe}	Thermal resistance of conduction through the pipe wall
R_c	Thermal resistance of the internal convection of the flowing coolant
R_{fin}	Overall thermal resistance of convection by air including the pipe exterior
R_{rad}	Thermal resistance of radiation for any radiating surfaces to the surroundings
R_{tc}	Contact resistance of fins and tubes, for brazed materials this is usually negligible
R_{total}	Total thermal resistance of the radiator
T_{enter}	Temperature of air entering radiator
T_{exit}	Temperature of air after passing through radiator
T_{in}	Temperature of coolant entering radiator
$T_{m,air}$	Mean air temperature $T_{m,air} = (T_{enter} + T_{exit})/2$

T_m	Mean coolant temperature $T_m = (T_{in} + T_{out})/2$
T_{out}	Temperature of coolant exiting radiator
T_s	Temperature of tube surface in K
T_{surr}	Surrounding air and surface temperature for radiation in K
V_{air}	Air velocity of forced air entering radiator area
\dot{V}_{air}	Volumetric flow rate of forced air
η_f	Efficiency of a single fin
$\eta_{overall,fin}$	Overall fin efficiency including the contact resistance of the fins to the base
δ_f	Fin thickness
θ	Louver angle in degrees
μ	Dynamic Viscosity of coolant fluid at T_m
ρ	Density of coolant fluid at T_m
σ	Boltzman's Constant $\sigma = 5.67 \times 10^{-8} \frac{W}{m^2 K^4}$
ϵ	Emissivity of material surface

CHAPTER 1

INTRODUCTION

With the increase in globalization of goods, services, markets, economies, and organizations, the need for transportation has increased. Unfortunately this increase in transportation also comes with the associated costs of energy, mainly in the form of fossil fuels, as well as an increased concern of greenhouse gas (GHG) emissions, particularly CO₂ as byproducts of fuel combustion. According to the EPA, 28% of all GHG emissions are from the transportation industry [1]. The EPA has increased its regulations on the transportation industry and this has demanded new innovations and investigations in fuel efficiency and new technology. This document discusses the feasibility of a particular application of a new technology called microchannels in automotive radiators with the intent to improve the overall fuel efficiency of Heavy Duty Vehicles.

1.1 Incentive for Research

In October 2011 the North American Council for Freight Efficiency (NACFE) presented the U.S. Heavy Duty Vehicle Green House Gas and Fuel Efficiency Final Rule, a set of standards that the transportation industry would be required to meet beginning with the model year 2014 and continuing through 2018 [2]. These new standards were projected to reduce oil imports by 530 million barrels less of oil, decrease fuel consumption resulting in \$50 billion in fuel savings, decrease CO₂ and other greenhouse gas (GHG) emissions by 270 MMT (million metric tons), and operating costs for thousands of businesses including \$49 billion in net benefits.

The new fuel efficiency final rule targets the energy losses associated with heavy duty vehicles (HDV) including engine losses, aerodynamic losses associated with air pressure drag,

inertial losses such as braking, rolling resistance losses due to mechanical friction, drivetrain losses, and auxiliary loads (see Figure 1.1). HDV manufacturers are looking at many different approaches to resolving these issues such as reducing the weight of the vehicles using lighter weight materials, improving rolling resistance by looking at developing tire technology, using waste heat recovery technologies, improving engine performance or reducing engine size, and using various methods to reduce aerodynamic drag [3].

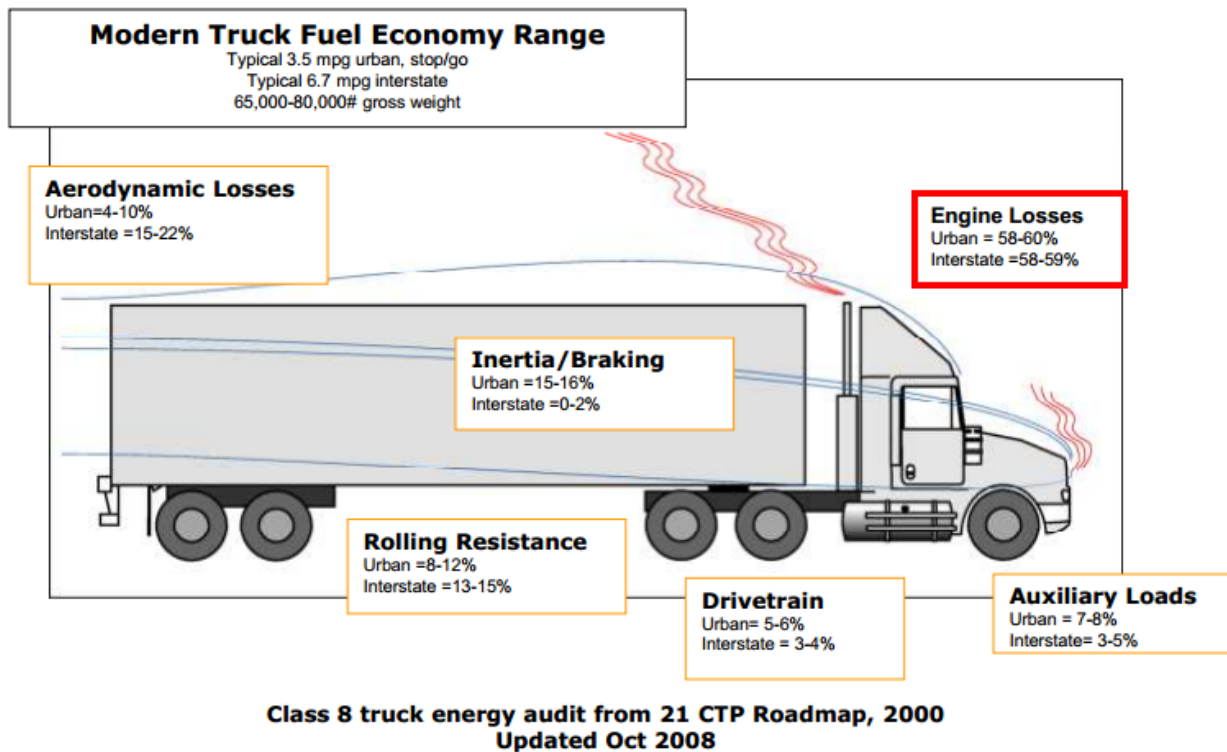


Figure 1.1: Energy losses associated with HDVs [2]

1.1.1 Improving Vehicle Performance

As government regulations on emissions and fuel efficiency increase, the automotive industry is continually required to meet or exceed these standards by implementing new technologies. Some of the new technologies and practices suggested by the EPA include the following.

1.1.1.1 Fuel Switching

By utilizing alternative fuels that produce less CO₂, the overall GHG emissions will be decreased. Alternative fuels include sources such as biofuels, hydrogen, electricity from renewable sources such as wind or solar, or fossil fuels that are less CO₂ intensive. Examples of fuel switching can be the utilization of public busses that are fueled by compressed natural gas (CNG) rather than diesel or gasoline, utilizing electric or hybrid automobiles that can be recharged by electricity generated from low carbon fuels, or using renewable fuels such as low-carbon biofuels [1].

1.1.1.2 Improve Fuel Efficiency

Improving the fuel efficiency of vehicles has increased in priority for both environmental regulating organizations throughout the world, such as US EPA, as well as for consumers of the vehicles. Since the price of fossil fuel is extremely unstable and is generally one of the largest expenses for the lifetime of a vehicle, it is desirable to improve fuel efficiency. Improving fuel efficiency also means that there are fewer GHGs produced for the same amount of energy needed for the vehicles. Through developing technologies such as hybrid or electric vehicles, energy storage systems from braking, weight reduction through advanced material substitutes and designs, and aerodynamic drag reduction, the fuel efficiency of vehicles should be improved greatly [1].

1.1.1.3 Improve Operating Practices

Additional benefits of fuel efficiency can be obtained through adopting driving and maintenance practices that minimize fuel use. These include practices such as driving sensibly such as avoiding rapid acceleration and braking and following the speed limit, as well as

reducing engine idling, improved planning and routing, and following recommended maintenance schedules [1].

All of these practices and implementations of technology will help reduce the contribution of GHGs from transportation vehicles, but in order to give clear direction, give quantifiable criteria, and to enforce implementation of new technology, new regulations have been developed and put in place.

1.1.2 Requirements for Heavy Duty Vehicle Manufacturers

Beginning in the model year 2014, the truck sector of HDVs will be divided into 3 distinct categories as seen in Table 1.2 and Figure 1.2. These vehicles will be required to meet separate standards for both engines and vehicles for each category. This requirement will ensure that both the engine performance and the overall vehicle will have improvements related to GHG reduction. The categories will have separate standards for the reduction of CO₂, N₂O, CH₄, and HFCs, and incentives are provided to encourage early introduction of GHG reducing technologies. The program is credit-based which means that for the manufacturer, the fleet as a whole must meet the standards, i.e., some of the fleet that have higher emissions and that may not meet the standards will be offset by the lower emitting vehicles that exceed the standards, resulting in the average vehicle compliance [4, p. 2]. Each vehicle family must be certified with a Certificate of Conformity prior to being introduced into U.S. Commerce, i.e., the vehicles must be compliant before they can be removed from the manufacturer's lot.

Table 1.1: Classification of heavy duty vehicles for GHG emission requirements beginning model year 2014 [4, p. 3].

Heavy Duty Vehicles		
Categories	Covers	Description
Heavy-duty pickups and vans	Classes 2b-3	<ul style="list-style-type: none"> –Products that are typically chassis-certified for criteria pollutants (8,500-14,000 lb GVWR) –Common trade names are Ram 2500-3500, E250-350, & Silverado 2500-3500 –Engines and chassis are certified as one unit
Combination tractors	Classes 7,8	<ul style="list-style-type: none"> –Typical semi-truck tractors with a 5th wheel attachment –Includes both day & sleeper cab configurations and GVWRs above 26,000 lb –Typically manufactured by companies such as Daimler Trucks NA (Freightliner), Volvo-Mack, International, and Paccar (Kenworth-Peterbilt)
Vocational vehicles	Classes 2b-8	<ul style="list-style-type: none"> –Covers all vehicles not falling into one of the categories above – Box/delivery trucks, buses, fire trucks, cement mixers, refuse haulers, etc – Covers class 2b through class 8 weight ratings (GVWR: 8,500-80,000 lb) – Typically have separate chassis manufacturers and body builders

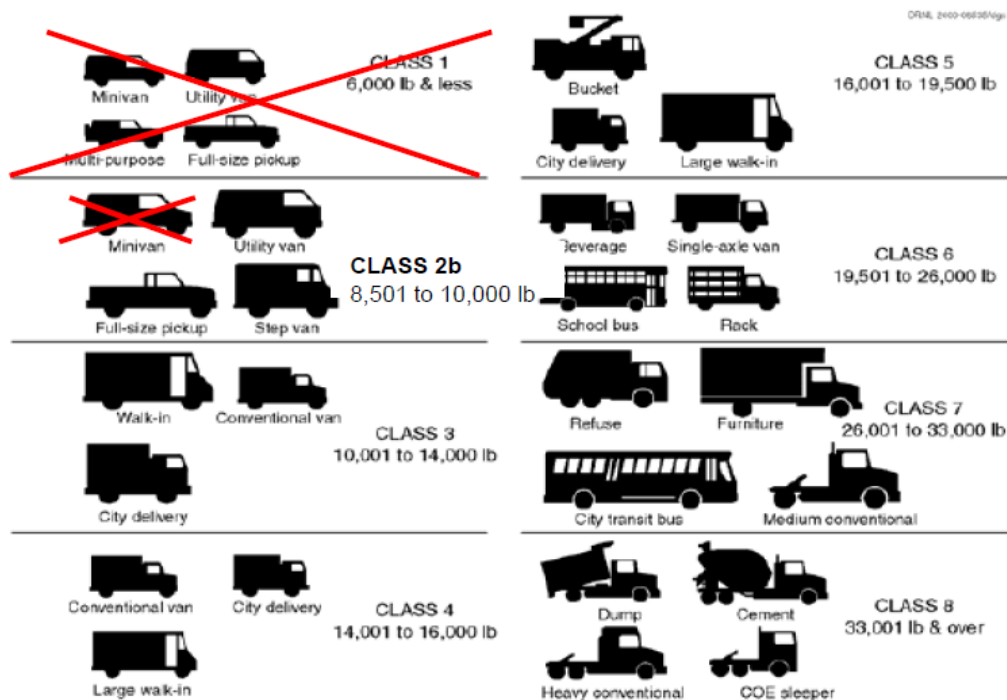


Figure 1.2: Classification of heavy duty vehicles effective MY 2014 [2]

1.1.3 Fuel Economy and Aerodynamics

The aerodynamics of HDVs can be complex and hard to manage, particularly with regards to the trailer geometry or the load that is being pulled by the truck. But for any given load, there should be a goal of reducing aerodynamic drag as much as possible. A rule-of-thumb for the automotive industry is for every 2% reduction in drag there is a 1% increase in fuel economy [3]. For line-haul tractors there have been many improvements in the aerodynamic drag in both the tractors and the trailers within the past few years. These improvements include the interface between tractors and trailers such as the trailer gaps and cab roof deflectors as well as improvements to the tractors such as side skirts, cab extenders, and air dams. Table 1.1 shows suggested best practices after-market add-ons that can be used to improve aerodynamic drag.

Table 1.2: Aerodynamic improvement options for line-haul trucks [5, p. 4]

AERODYNAMICS		
If you use/have:	vs.	MPG Improves
Trailer Gaps		
25 Inches	35 Inches	0.5-1%
25 Inches	45 inches	1-2%
25 Inches	65 Inches	2-5%
Cab Roof Devices		
Standard Deflector	Nothing	Up to 6%
Full Roof Fairing	Nothing	Up to 15%
Full Roof Fairing	Raised Roof Sleeper that is 10-14 inches shorter than trailer	4-10%
Other Devices		
15-inch Cab Extenders	Nothing	1-4%
Air Dam Front Bumper	Standard	Up to 3%
Tractor Side Skirts	Tanks or Nothing	Up to 3%
Nothing	Bug Deflector	Up to 1.5%

All of these features can help to reduce aerodynamic drag but there is a limit to the improvement of an existing truck. Often, further improvements require a paradigm shift or “thinking outside the box.” When looking at the entire envelop of the truck, major improvements in the overall design require looking at the system as a whole and then looking at the individual components of that system. One small system in the truck that sometimes is overlooked is the radiator.





1.1.4 Drag Reduction and Frontal Area

Almost all radiators are liquid-to-air heat exchangers placed at the front-most position of the vehicle so as to maximize the airflow across the radiator as the vehicle is moving, thus removing the most heat possible from the radiator and ultimately from the vehicle’s engine. The current design of automotive radiators has nearly been maximized in its potential efficiency with the current restraints and practices of automotive radiator manufacturing. Over the past decades, automotive radiator heat exchangers have continually evolved with advancing technology to enhance heat transfer while reducing the auxiliary load requirements on the engine for the cooling system.

The need for radiators still exists due to the impossibility of achieving 100% thermal efficiency of the energy produced from the combustion of fuel in the engine. High temperatures are produced in the engine because of the waste heat of the combustion process. To prevent damage to the engine and to maintain a steady combustion cycle and power output, radiators are necessary to cool internal combustion engines. The technology of radiators has developed tremendously from the first automobiles, but the need for more efficient vehicles has pushed the technology to new levels.

There is now motivation to reduce the size of automotive radiators primarily to reduce the pressure drag caused by a large flat frontal area of the vehicle since the placement of the radiator is necessary to maximize airflow across the radiator, thus maximizing the heat transfer from the engine. The primary motivation to reduce pressure drag by reducing radiator size is the fuel savings associated. For the standard American line hauler semi-truck, there is the potential for a significant increase in the aerodynamic pressure drag associated with the front leading edge of the truck. There are currently competing designs for aerodynamic improvement of the frontal area of trucks. Two of the more prominent approaches are making the frontal area more convex or narrower at the leading edge, and the other is the cab-over approach with the whole frontal area being a flat face. See Table 1.3 for a comparison.

Table 1.3: Comparison of aerodynamic truck design

Truck	Image
Peterbilt 579	
Peterbilt Walmart Concept Super Truck	
Modified Peterbilt 372	
Peterbilt 367 with Oversize Load	

As can be seen in Table 1.3, the modern Peterbilt 579 truck [6] has a large frontal area that is governed by the size of the radiator, thus a reduction in frontal area would be beneficial to the aerodynamic drag reduction.

The Peterbilt Walmart Concept Super Truck is a new and innovative approach to the implementation of current technology. The concept truck features an electric hybrid that runs on Lithium Polymer batteries that are recharged by a gas turbine that can run on diesel, gasoline, or biofuels [7]. The aerodynamic features of this truck are due to the fact that there is no radiator and thus a narrow nose can be created for the frontal area. This being a concept car, its adoption into mainstream trucking may be in the far future and, meanwhile, internal combustion engines will still require radiators.

The Peterbilt 372 has been recorded to have achieved 11 MPG fuel economy and the aerodynamics of the truck play a significant role in that. The tear-drop shape produces less drag since there are fewer cavities and more direct diversion of the air to the sides and above the truck [8]. This cab-over design does not necessitate the reduction of frontal area as much as the long-bed design but it may potentially have higher aerodynamic drag due to the large and abrupt frontal area. A reduction of radiator size can always benefit any vehicle in saving space, thus the incentive to reduce the radiator size remains.

Regardless of the tractor aerodynamics, the load that is being pulled behind the tractor also plays a significant role. As can be seen in the image in Table 1.3, the Peterbilt 367 [9] with an oversized load will have significant drag, possibly enough to counter any gains from improvements on the tractor. Although this may be the case, a reduction of aerodynamic drag on the tractor can still improve fuel economy, therefore, to reduce the frontal area may be worthwhile.

This report will study an automotive heat exchanger radiator used in a heavy duty vehicle to determine the possibility of reducing the frontal area of a heavy duty truck by reducing the size of the radiator utilizing the developing technology of microchannels.

1.2 Introduction to Microchannels

Microchannels have developed over the past decade as an effective means of reducing the volume of a heat exchanger and increasing the heat-transfer performance. The basic concept of utilizing microchannels in the design is as follows:

$$h_c = Nu_D \frac{k}{D_h} \quad (1)$$

where h_c is the convective heat transfer coefficient of the cooling fluid, Nu_D is the Nusselt Number, k is the thermal conductivity of the fluid, and D_h is the hydraulic diameter of the fluid channel. As is seen in Eq. 1 by decreasing the hydraulic diameter, the internal force convection coefficient, h_c , is increased even if the flow is laminar (it is a generally accepted theory that at fully developed laminar flow in circular pipes $Nu_D = 3.66$) [10, p. 761]. This increase in the internal convection coefficient leads to less thermal resistance and enhanced heat transfer rates within the cooling fluid as compared to conventional fin-and-tube heat exchangers.

Microchannels also offer the benefits of decreased size and weight and potential cost savings in materials and, due to their high effectiveness even at laminar flows, microchannels can improve auxiliary systems such as fan power or pumping power in addition to their heat transfer benefits.

1.3 Overview of Conducted Research

The current study of this work is to investigate the overall improvement of a heat exchanger radiator system by looking at the following key factors:

Table 1.4: Parameters used to compare heat exchangers

Symbol	Parameter	Units
R_{total}	Total thermal resistance of the radiator	K/W
U_{total}	Total heat transfer of the radiator	W/m ² ·K
Q_{max}	Maximum Heat Transfer	
A_{fr}	Frontal area of the radiator	m ²
P_{pump}	Pumping power determined by the coolant flow through the radiator	W
P_{fan}	Fan power required to move air through the air-side of the radiator	W
ϵ	Heat Exchanger Effectiveness	-
NTU	Number of Transfer Units	-

The goal of this study was to see by how much (in percent of original design) of each parameter can be improved without hurting the other parameters. For the total thermal resistance, it is desirable to have the lowest resistance possible in order to have a high heat transfer rate. The total heat transfer rate is the inverse of the total resistance multiplied by the total external convective surface area and it is desirable to have this be as high as possible. The overall goal is to decrease the frontal area of the truck both in height and width to facilitate a more convex front to reduce drag and, by reducing the height and width of the radiator, this may be realized. Both the pumping power and fan power are auxiliaries to the cooling system but are essential to maintaining steady state heat transfer. It is desirable to decrease these auxiliary power consuming parameters to decrease the parasitic load on the engine if possible.

Within this study a heat transfer analysis method of the thermal performance of the current radiator will be presented. Also a literature review of the current state of Microchannel Heat Exchangers (MCHX) and microchannel technology will be given. A method for the re-design and analysis of a microchannel heat exchanger will be conducted to determine the feasibility and potential gains or losses of a MCHX radiator. Energy and materials costs and savings will be discussed to present a holistic approach to the overall improvement of the radiator cooling system.

CHAPTER 2

LITERATURE REVIEW

2.1 Radiator Studies

In this study, an automotive radiator was analyzed to determine the heat transfer and pressure drop performances of the coolant, thermal conductivity, and air-side heat transfers. The geometry of the radiator was composed of a flat tube and serpentine louver fin geometry.

2.1.1 Radiator Design Studies

Radiator design optimization has been studied by numerous approaches and researchers [11-14]. Several studies have been made particularly with regards to a flat tube and louver fin geometry configuration [11] [13] [15-24]. Oliet et al. conducted a parametric approach to the design of radiators presenting their findings on air mass flow and coolant mass flow versus heat removed, and air and coolant flow versus pressure drop. As the flow rate increases, so does the pressure drop and the increase of air flow allows for more heat transfer than the increase of flow of the coolant. Additional findings indicated that the overall heat transfer coefficient is largely dependent on the Reynolds number or flow regime when the working fluid or fluid flow arrangements are varied. Another insight was that I-flow lay-ups of tubes or straight tubes is preferred over U-bypass or continuous tubes because of the significant decrease in pumping power, although with the straight tubes there is a slight decrease in cooling capacity. Further it was realized that a cooling capacity vs. pressure drop reveals a powerful correlation in finding the optimal design of a heat exchanger. Another significant contribution is that the air inlet temperature of the radiator has little effect on the total heat transfer when compared with the flow rate of air [15]. A study conducted by Chong et al. showed that an automotive radiator can

be used in cooling a dense-array photovoltaic system to improve electricity generation efficiency [25].

2.1.2 Radiator Coolant Studies

Several studies have been conducted on the coolant to be used in the radiator [15] [26]. These have suggested that pure deionized water has a greater ability to remove heat than either 50% or 60% ethylene glycol mixtures; however, the improvement is not as significant as coolant flow rate or tube diameter. It has also been suggested that adding nanoparticles such as Al_2O_3 and CuO to the working fluid can enhance the heat transfer [26]. In one study it was found that for a 2% volume fraction of copper nanoparticles, the overall heat transfer coefficient would increase up to 13%, or provide a 3.8% enhancement in overall heat transfer, but this addition of particles also increases the pumping power [27].

2.1.3 Radiator Material Selection Studies

The study of material selection for radiators has varied greatly from configurations using all copper to combinations of copper-brass, copper-aluminum, pure aluminum, carbon foam, and plastics.

According to Charyulu et al., copper has the greatest thermal advantages of all the materials. A number of studies were conducted of different material types and it was found that having copper fins (regardless of whether the tube material is copper, brass, or carbon steel) will have a greater effect on the heat transfer than using any other material. Aluminum has the second best performance of all the other materials [28].

There is a new material in development called graphite foam that is claimed to have thermal conductivities as high as $180 \text{ W/m}\cdot\text{K}$ along with extremely low density [12] [29]. Further investigation on this material may be beneficial for future research.

Table 2.1 shows the materials that are commonly used in automotive heat exchangers and compares the thermal conductivity to weight. As can be seen in the table, the material selection varies greatly. Some of the earliest microchannels manufactured used plastics or other polymer materials [30]. As manufacturing technology has increased, the use of more conventional materials, such as copper and aluminum, to produce microchannels has become more feasible. The table identifies the benefits of various materials but aluminum is one of the most commonly used in automotive heat exchangers because of the benefits of weight, cost, and the resistance to galvanic corrosion compared to copper.

Table 2.1: Material comparison values taken from MatWeb and literature.

Material	Thermal Conductivity, k (W/m·K)	Density (kg/m ³)	Thermal Conductivity/Weight Ratio	Additional Advantages
PMMA Plastic [30]	0.190	1180	.00016	
Carbon Foam	175-180 [26]	620-700 [29]	.4375-.4500	70% porosity a
Copper	385-401	7940-8930	.0431-.0505	
Aluminum	205-250	2700	.0759-.0925	Manufacturability, cost
Brass	109-233	7600-8860	.0123-.0306	
Carbon Steel	24-93	7750-8080	.0029-.0120	
SS AISI 304&316	16.2-21.5	8000	.0020-.0027	
Cupro Nickel	30	8800	.0034	

2.1.4 Fouling in Tubes and Fins

According to Charyulu et al., a 55% excess in fouling in tubes corresponds to a 10% decrease in the rate of heat transfer for an automotive heat exchanger [28]. Bell and Groll performed a study on the particulate fouling of louver fins and discovered that louver fins with fin pitches less than 2.0 mm were more sensitive to fouling [24].

2.1.5 Mathematical Modeling and Simulation

Many approaches have been made to simulate the heat transfer and pressure drop characteristics associated with automotive radiators. The work of Oliet et al. has developed a

software called CHESS (Compact Heat Exchanger Simulation Software) that is capable of solving the heat transfer and pressure drop of various arrangements of HVAC and automotive heat exchangers [13] [18-20]. Many of the authors utilize the ϵ -NTU method or the LMTD method to mathematically simulate the heat transfer performance of the radiator [14]. Chang et al. performed a study to reveal the accuracy to which louver fin geometry heat transfer could be predicted by comparing the theoretical values to the measured values and found that “83% of the corrugated louver fin data are correlated within $\pm 15\%$ with mean deviation of 7.55%.” [16]

2.2 Microchannel Studies

The purpose of the current study is to investigate the feasibility, practicality, and performance of an automotive heat exchanger utilizing newly developed microchannel technology. A literature review is presented below on the relevant works and studies of microchannel heat exchangers. In 2003, one of the first articles concerning microchannel heat exchangers came from ASHRAE as an introductory overview to the technology. Although much of the information in the documented has changed with advancements, the original statement of marketable benefits or “market factors” still applies:

Because MCHXs impact system cost in several ways besides the heat exchanger, it is crucial to perform a system analysis when considering the application of MCHXs to a specific unit. The reduced size and weight of MCHXs can result in a smaller and lighter system, for example, reducing the chassis size of a packaged unit. In addition, lower airside pressure drop may decrease the required fan or blower size and, hence, component costs. Lastly, the significantly lower internal volume of an MCHX reduces the required refrigerant charge. [31]

2.2.1 Microchannel Overview

Microchannels are defined as channels or tubes that have a hydraulic diameter of less than or equal to 1 mm [24] or, according to Fan and Luo from $1\mu\text{m}$ -1mm, or

Micro-scale: 1–100 μm (micro-structured exchanger);
Meso-scale: 100 μm –1 mm (meso-structured or millistructured exchanger);
Macro-scale: 1–6 mm (compact exchanger); and

Conventional scale: >6 mm (conventional exchanger). [33]

According to Khan et al., “while traditional heat exchangers employ conventional tubes ($\geq 6\text{mm}$) with various cross-sections, orientations, and even the enhanced surface textures, the technology is nearing its limits. Microchannels (broadly $\leq 1\text{ mm}$) represent the next step in heat exchanger development.” [34]

Khan goes further to say:

Traditional heat exchangers generally use the flow passage sizes of 6 mm and larger with various geometry, orientations, and enhanced surfaces. However, the research into efficiency gains based on heat transfer augmentation, size shrinking, and thermal resistance diminution techniques has almost reached its limits with respect to the sizes and shapes of flow passages that are commercially available today... Microchannels are broadly characterized by small flow passages of 1 mm in diameter or less, which allows for heat transfer surface densities to be $10,000\text{ m}^2/\text{m}^3$ or more; this value contrasts with compact heat exchangers having a density of $700\text{ m}^2/\text{m}^3$. Owing to their higher heat transfer, lower weight, and their space, energy, and materials savings potentials over their traditional tube and enhanced surface heat exchanger counterparts, microchannels can meet all the above-mentioned challenges. [34]

According to Khan et al., potential applications for microchannel heat exchangers (MCHX) include energy, automotive, off-highway vehicles, aerospace, HVAC, cryogenic, power, electronics, and others [34]. Khan further goes on to describe how microchannel technology works:

For a given heat duty, the high heat transfer property of microchannels results in shorter channel lengths. Undesired axial heat conduction is minimized because the channel length and fluid residence time are shortened and because the entire bulk fluid is in close contact with the microchannel walls. The fluid flow in MCHX is parallel and usually well distributed over a large number of small passages. This distribution reduces the flow velocity in each individual channel. Therefore, the shorter parallel channel lengths and minimal axial heat conduction, combined with the well-distributed flow, result in a low channel side pressure drop, and hence reduce the liquid side pump capacity. [34]

2.2.2 Application of Microchannel Technology in Automotive

Much of the reviewed literature has suggested that microchannels could be used in automotive applications but there have not been any studies found that have directly verified this

fact. Khan et al., referring to microchannel technology stated, “Applications for automotive heat exchangers exist as proprietary or in-house packages only.” [34] Several studies include a microchannel slab with louver fin geometry [35], but none of the literature has openly stated that the applications were for automotive radiator purposes.

2.2.3 Heat Transfer Modeling of Microchannels

For the heat transfer numerical modeling of microchannel technology, there have been some discrepancies in the past between the predicted and measured values for heat transfer. This is a source of investigation for many studies involving microchannel technology to determine if conventional heat transfer is applicable at this small scale [34].

2.2.4 Working Fluid in Microchannels

Several fluid types have been used in microchannels as the working fluid in cooling including distilled deionized water [35] [36], glycol mixtures [30], various oils [34], and carbon dioxide CO₂ [37].

2.2.5 Geometry of Microchannels

Several geometries of microchannels were reviewed among the literature including wavy fins in a microchannel heat sink which increased the heat transfer due to a constantly developing boundary layer [38], pin fin array geometry for a microchannel heat sink [39], geometric designs of cross-mixing flow in a microchannel [40], diffusion bonded microchannel cross-flow [41], LIGA manufactured rectangular cross flow microchannels [30], transient liquid phase bonded copper microchannels [42], a ring shaped microchannel using guide vanes [43], a laser machining fabricated rectangular microchannel design [44], a MEMS fabrication copper rectangular fin and channel layout cross-flow microchannel heat exchanger for electronics [45], and flat microchannel slabs with annular holes [24].

Schneider et al. investigated a phenomena called hydrodynamic cavitation in microchannels that can be induced by the geometry and conditions of the heat exchanger. The cavitation demonstrated an improvement in heat transfer by 67% compared to the same system with the same flow rate without hydrodynamic cavitation [46]. Further study of flow boiling in microchannels was studied by Kandlikar [47]. Kaneko et al.'s study suggested that their diffusion bonded microchannel cross-flow design could be utilized as a condenser heat exchanger sustaining up to 15 MPa of pressure [41].

2.2.6 Materials Used in Microchannel Designs

The materials used in microchannel designs vary from aluminum to additive manufactured materials. One study compared the design of a microchannel heat exchanger for a domestic refrigerator using aluminum and copper. It was found that, due to the high thermal conductivity of copper, the two heat exchangers were comparable in weight, with the copper design being smaller, although both heat exchangers transferred similar loads of heat [48].

2.3 Mathematical Modeling Studies

2.3.1 Flat Tube Mathematical Models

Yang et al conducting a study involving a comparison of the heat transfer and pressure drop of circular tube heat exchangers versus flat tube heat exchangers and found that under the same conditions, the flat tube heat exchangers increase 24% in heat transfer coefficient, decrease pressure drop by 12-20%, and the coefficient of integral performance increases up to 22-34% [49]. Kim et al studied the effect of aspect ratio of flat tubes on heat transfer coefficient and pressure drop and found that as the aspect ratio increases, so too does the heat transfer coefficient but so does the pressure drop across the tubes. Kim et al further discovered that the equivalent diameter rather than hydraulic diameter of flat tubes can be used in round-tube correlations to

more accurately predict heat transfer but that pressure drop correlations depend on the method of prediction [50]. Vajjha et al developed a Nusselt Number relationship for nanoparticle fluid flow through a flat tube [51]. Quiben et al. offered an effective correlation for the pressure drop through a flat tube with a corrected friction factor for two phase flow [44].

2.3.2 Louver Fin Mathematical Models

The majority of literature points to the correlations made by Chang and Wang [16] and was the mathematical model utilized in this work. Perrotin et al. verified that the Chang and Wang correlation is fairly accurate through their CFD study of louver fins [52].

2.3.3 Microchannel Mathematical Models

For microchannels, the majority of the literature used conventional heat transfer mathematical equations to predict the thermo-hydraulic effects of the flow through microchannels. In their review of mathematical modeling of microchannels, Khan and Fartaj found that investigations showed a conformity of traditional heat transfer characteristics for microchannels but a divergence in the conventional pressure drop and friction factor theories [53]. According to some research the friction factor decreases as Re increases and the value of f is 20 to 30% of the conventional value [53]. It is also hypothesized that the critical Reynolds number for microchannels is $Re_c = 1100$ [53]. According to Khan and Fartaj the pressure drop for microchannels is a function of the Poisselle number ($Po = f Re$) and is defined as

$$\Delta p = \frac{32 \dot{m} \nu L}{17\pi D_h^4} \quad (2)$$

where L is the microchannel tube length, ν is the kinematic viscosity and D_h is the hydraulic diameter. An investigation of this equation may be useful in the analysis of the microchannel geometry.

CHAPTER 3

THEORY

3.1 Introduction to Parametric Approach

As part of the search for ways to improved radiator efficiency, there have been numerous studies involving tube geometry and configuration to improve the heat transfer of the coolant as well as studies on improving the air-side with various fin geometries, configurations, and materials. In determining the performance of one radiator against another it is essential to know the comparable parameters. The current study will demonstrate the process of performing a mathematical analysis of an existing radiator in order to determine the effect of modifications of the design. The parameters which will be used to determine radiator performance are given in Table 1.4 and are given again below for the convenience of the reader in Table 3.1. Once these factors have been calculated, they may be used in comparing other existing or theoretical designs of radiators.

Table 3.1: Parameters used to compare heat exchangers

Symbol	Parameter	Units
R_{total}	Total thermal resistance of the radiator	K/W
U_{total}	Total heat transfer of the radiator	W/m ² ·K
A_{fr}	Frontal area of the radiator	m ²
P_{pump}	Pumping power determined by the coolant flow through the radiator	W
P_{fan}	Fan power required to move air through the air-side of the radiator	W
ϵ	Heat Exchanger Effectiveness	-
NTU	Number of Transfer Units	-

These parameters have been used in numerous studies to compare different geometries and configurations but the author has chosen these particular parameters because they are the most practical parameters to use and they identify the key interests in reducing energy consumption and enhancing heat transfer.

This paper will set forth the theoretical and mathematical approach to analyzing a serpentine louver fin and flat-tube automotive radiator heat exchanger beginning with the heat transfer characteristics through the coolant, continuing to the heat transfer through the tube walls, and finally the heat transfer to the air by the louver fins. This will be followed by an analysis of the pressure drop of the coolant followed by a pressure drop of the air across the radiator. Finally the previously specified parameters will be used to compare the radiator in question with modified versions of the design for finding an optimal performance design.

The current radiator heat exchanger is composed of thin, long, flat tubes with serpentine louver fin arrays between the tubes. The tubes and fins are both of aluminum with the fins being brazed to the tubes for a near zero contact resistance. The working coolant fluid is 50% ethylene-glycol and water mixture. Air is used to remove the heat from the radiator with a single large fan. Operating conditions are similar to the actual performance conditions of the radiator. The geometry of the flat tube is advantageous since it has a high surface area to volume ratio. This particular geometry of flat tube is very narrow with a resultantly small hydraulic diameter.

Louver fins are one of the most effective extended surfaces available, having a high surface area to volume ratio and a relatively low pressure drop. The following method described is to analyze the current radiator to identify its performance as a benchmark for further investigative study to improve and optimize the heat transfer of the radiator and reduce the overall frontal area.

3.2 Working Conditions

The mathematical approach to the design and analysis of a heat exchanger has been developed over years of study, testing, and evaluations. There are thousands of publications, theories, and equations used to determine every characteristic of a heat exchanger from the heat

transfer through a moving fluid through certain geometry to the theoretical airflow characteristics and pressure drop through a fin array of specified geometry and configuration. The key in determining the characteristics of a heat exchanger are to know the principles, theories, and equations associated with each type of geometry and design. The radiator that will be analyzed in this study is one of a louvered serpentine fin and flat tube design. For this particular configuration, numerous publications were reviewed to determine the appropriate theoretical equations that could be utilized in the analysis. In order to verify the theoretical predictions, it is always necessary to perform physical tests to compare against the calculated predictions.

For testing and analysis of a radiator the following is a list of working conditions that are required for accurate analysis of the radiator:

- Temperature of coolant into radiator
- Temperature of coolant exiting radiator
- Pressure drop of coolant through the radiator
- Flow rate of the coolant
- Physical properties of the coolant (density, viscosity, thermal conductivity, heat capacity)
- Velocity/flow rate of air entering air-side of radiator
- Temperature of air entering air-side of radiator
- Temperature of air exiting air-side of radiator
- Pressure drop of air through the radiator
- Physical properties of the air (density, viscosity, thermal conductivity, heat capacity)
- Geometry, dimensions, configurations and
- Material properties of the radiator (tubes, fins, etc.)

These are the parameters necessary to repeat the analysis method set forth in this paper and consist of the general parameters necessary to analyze any heat exchanger.

3.3 Geometry

This study involves a flat tube and serpentine louver fin configuration of an automotive heat exchanger. In order to effectively analyze the heat exchanger, all the geometric dimensions need to be known. Figure 3.1 shows these dimensions in detail and Figure 3.2 shows images of

the flat tube and fin configuration. Table 3.2 contains a list of the necessary dimensions for the analysis.

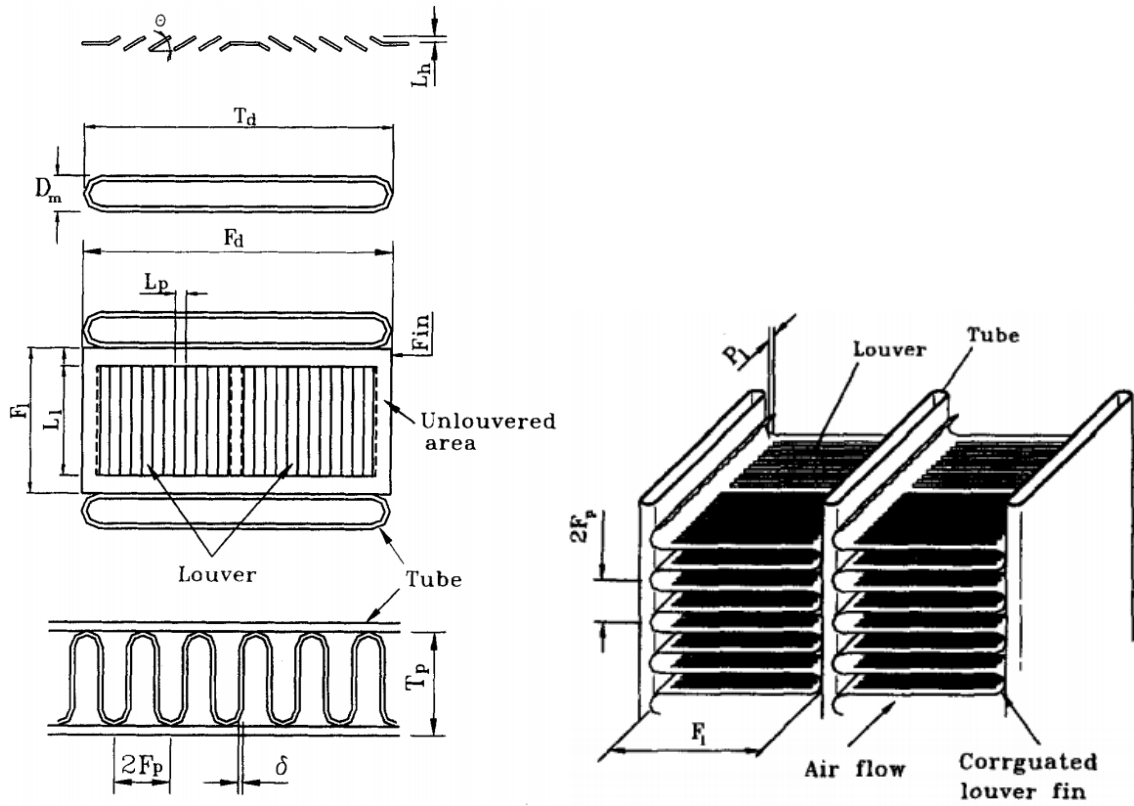


Figure 3.1: Corrugated serpentine louver fin and flat tube configuration and dimensions [16]



Figure 3.2: Image of radiator fin and tube configuration under investigation

Table 3.2: Measured and calculated dimensions of radiator under investigation

Symbol	Dimension Description	Value	Units
L	Axial length of tube. In this study the length is the height of the radiator	933.45	mm
W	Total width of the radiator	917.62	mm
T_d	Tube depth. For this study the tube depth is the same as the fin depth and the depth of the radiator	52.24	mm
D_m	Mean diameter or Tube width	2.38	mm
A_c	Cross sectional area of tube	73.116	mm ²
F_L	Fin length	7.77	mm
t	Tube thickness	0.45	mm
P	Internal tube perimeter	102.31	mm
N_{pipe}	Number of tubes	91	tubes
F_p	Fin pitch	1.54	mm
L_l	Louver length	5.77	mm
L_p	Louver pitch	0.861	mm
δ_f	Fin thickness	0.1	mm
θ	Louver angle	30	°
T_p	Tube pitch	10	mm
A	Total air side convective heat transfer surface area (fins and tubes)	58.406	m ²
A_i	Internal surface area of tubes	8.690	m ²
A_o	Total free flow area for air	0.656	m ²
A_{fr}	Frontal area of radiator ($L \times W$)	0.857	m ²
D_h	Hydraulic diameter of tubes $D_h = (4A_c)/P$	2.86	mm

3.4 Heat Transfer Analysis

3.4.1 Thermal Resistance Model

To determine the heat transfer characteristics of the radiator a thermal circuit was used to model the thermal resistances of each part of the radiator as can be seen in Figure 4.1. The model shows that the total thermal resistance of the system is between the temperature of the free stream fluid in the pipes, $T_{\infty,i}$, and the temperature of the free stream air outside the radiator. The heat is first transferred through the fluid in the pipe having resistance, R_c , then through the pipe wall with resistance, R_{pipe} , then to the air by convection, R_{fin} which includes fin and base convection, or by radiation, R_{rad} , which includes any radiation heat transfer to the surrounding

surfaces which can be assumed to be approximately equal to the air temperature for most cases. The following equation is then used to determine the total thermal resistance of heat transfer for the radiator:

$$R_{total} = R_c + R_{pipe} + \frac{1}{\frac{1}{R_{fin}} + \frac{1}{R_{rad}}} \quad (3)$$

Generally it is found that the thermal resistance of the air-side heat transfer has the largest effect on the total thermal resistance of the radiator and that the radiation does little to contribute to the heat transfer but cannot be dismissed if the temperature difference between the radiating surface and the surroundings is substantial.

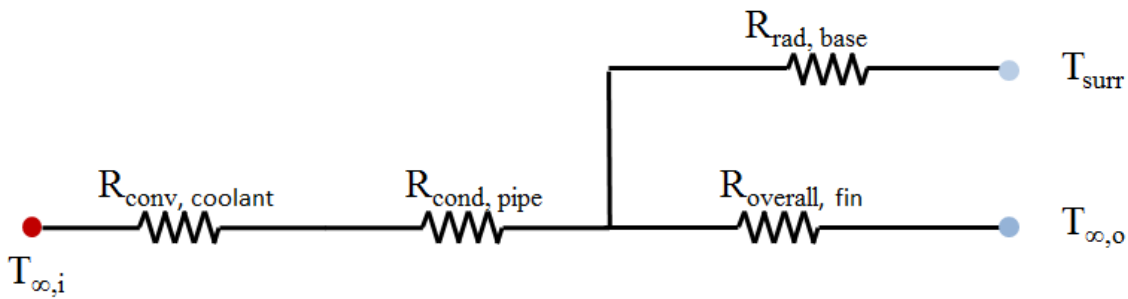


Figure 3.3: Thermal resistance model of a radiator to determine the total thermal resistance of the radiator

3.4.2 Thermal Resistance of Internal Convection of Coolant

The thermal resistance through the coolant in the radiator can be described by the equation

$$R_c = \frac{1}{h_c A_i} \quad (4)$$

where h_c is the convection coefficient for the coolant and A_i is the total internal surface area of all tubes. To determine h_c we use the following equation

$$h_c = Nu_D \frac{k}{D_h} \quad (5)$$

where k is the thermal conductivity of the fluid, D_h is the hydraulic diameter of the tube, $D_h = \frac{4A_c}{P}$, and Nu_D is the Nusselt Number which can be found by using traditional heat transfer methods for round tubes. For the particular flat tube heat exchanger of interest, the following equation from Junqi et al [17, p. 2070] is applied for fully developed turbulent flow:

$$Nu_D = 0.012(Re_D^{0.87} - 280)Pr^{0.4} \left(1 + \left(\frac{D_h}{L} \right)^{2/3} \right) \quad (6)$$

where

$$Re_D = \frac{\dot{m}_{pipe} D_h}{A_c \mu} \quad (7)$$

based on the mass flow rate of the coolant through a single pipe (\dot{m}_{pipe}), the hydraulic diameter (D_h), the tube cross sectional area (A_c), and the dynamic viscosity (μ), Prandtl Number $Pr = c_p \frac{\mu}{k}$, and the total length of the pipe (L).

For the microchannel study the Nusselt correlation for turbulent flow was

$$Nu_D = 0.023Re_D^{4/5}Pr^{0.3} \quad (8)$$

and for laminar flow with uniform heat flux for circular tubes, the correlation

$$Nu_D = \frac{48}{11} \quad (9)$$

was used and for square tubes with uniform heat flux

$$Nu = 3.61 \quad (10)$$

3.4.3 Thermal Resistance of Conduction through Tube Wall

The heat transfer through the pipe wall can be found by approximating the flat tube of uniform wall thickness as a cylinder and using the equation

$$R_{pipe} = \frac{\ln \left[\frac{r_o}{r_i} \right]}{N_{pipe} 2\pi L k_{pipe}} \quad (11)$$

where $r_i = \frac{D_{eq}}{2}$ and D_{eq} is the equivalent diameter found by using the internal cross sectional area

A_c as $D_{eq} = \sqrt{\frac{4A_c}{\pi}}$ and $r_o = r_i + t_{wall}$.

3.4.4 Thermal Resistance of Convection to Air

The most critical part of the heat exchanger is the air side since the air is the end heat sink for the engine. The contributor to the total thermal resistance of the radiator is generally on the air-side and is defined as

$$R_{fin} = \frac{1}{\eta_{overall} h_{air} A} \quad (12)$$

where A is the total convective surface area, $\eta_{overall}$ is the overall efficiency of the fins defined by the following equations:

$$\eta_{overall} = 1 - \frac{A_f}{A} \left(1 - \frac{\eta_f}{C1} \right) \quad (13)$$

$$\eta_f = \frac{Tanh[m L_{fin}]}{m L_{fin}} \quad (14)$$

$$C1 = 1 + \eta_f h_{air} A_f \left(\frac{R_{tc}}{A_{contact}} \right) \quad (15)$$

$$m = \left(\frac{P_f h_{air}}{k_{fin} A_{fin}} \right)^{1/2} \quad (16)$$

where η_f is the fin efficiency, R_{tc} is the contact resistance between the fins and tubes, and h_{air} is the convective heat transfer coefficient. In calculating this value it is imperative to know the geometry and configurations of the fins. For the louver fin and flat tube geometry being analyzed the method proposed by Chang and Wang [16] is employed:

$$h_{air} = j \frac{\dot{m}_{air} c_{p,air}}{A_o Pr_{air}^{2/3}} \quad (17)$$

$$j = Re_{Lp}^{-0.49} \left(\frac{\theta}{90}\right)^{0.27} \left(\frac{Fp}{Lp}\right)^{-0.14} \left(\frac{Fl}{Lp}\right)^{-0.29} \left(\frac{Td}{Lp}\right)^{-0.23} \left(\frac{Ll}{Lp}\right)^{0.68} \left(\frac{Tp}{Lp}\right)^{-0.28} \left(\frac{\delta f}{Lp}\right)^{-0.005} \quad (18)$$

$$Re_{Lp} = \frac{V_{air} Lp \rho_{air}}{\mu_{air}} \quad (19)$$

where j is the Colburn Factor, Lp is the louver pitch of the louver fins, and Re_{Lp} is the Reynolds number with the louver pitch as the characteristic length. See Nomenclature for clarification of other symbols.

3.4.5 Thermal Resistance by Radiation

The thermal resistance of radiation is generally high and does not contribute much to the heat transfer or the radiation as long as the temperatures of the radiating surface and the surroundings are relatively low ($T_s \geq 5000 K$). Nevertheless, the radiation resistance may be included in the calculation for the sake of accuracy and is defined as follows:

$$R_{rad} = \frac{1}{A_{rad} \epsilon \sigma (T_s + T_{surr})(T_s^2 + T_{surr}^2)} \quad (20)$$

where A_{rad} is the applicable radiative surface area, T_s is the surface temperature of the tube, and T_{surr} is the surrounding air and surface temperature.

3.5 Heat Transfer Analysis Comparison

Another approach that can be used to compare the heat transfer characteristics is using the Log Mean Temperature Difference (LMTD) Method. This method uses the inlet and outlet temperatures of the air and coolant to find the total heat transfer thermal resistance. The procedure is as follows:

The resistance of a radiator can be found using the equation

$$R_{LMTD} = \frac{LMTD}{Q_{Engine}} \quad (21)$$

$$Q_{Engine} = \dot{m}_c c_{p,c}(T_{in} - T_{out}) \quad (22)$$

Where $LMTD$ is the Log Meat Temperature Difference defined by the equation

$$LMTD = F \frac{(T_{in} - T_{exit}) - (T_{out} - T_{enter})}{\ln[(T_{in} - T_{exit})/(T_{out} - T_{enter})]} \quad (23)$$

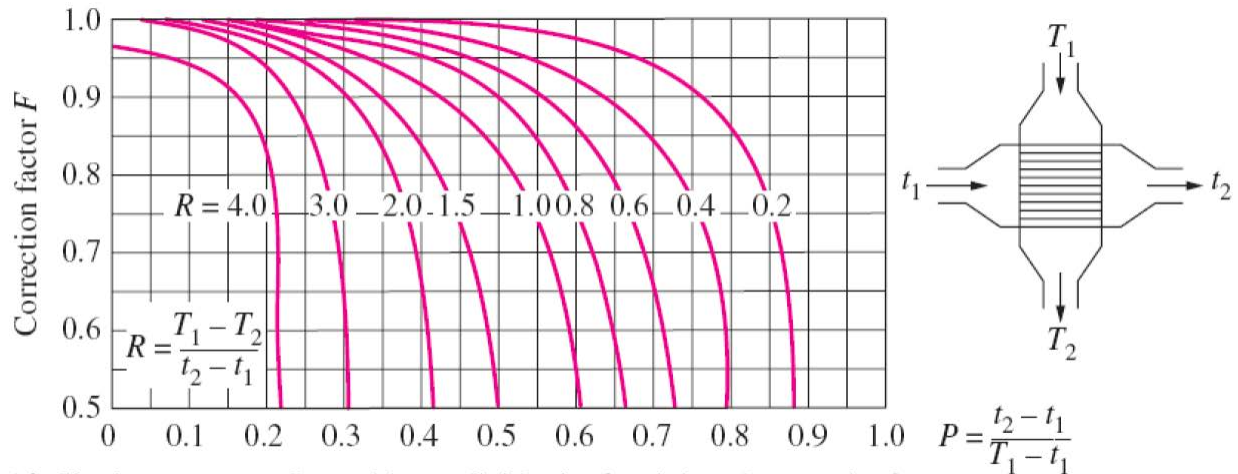
And F can be found using Figure 5.1 where

$T_1 = T_{in}$ The temperature of the coolant going into the radiator in Kelvin

$T_2 = T_{out}$ The temperature of the coolant going out of the radiator in Kelvin

$t_1 = T_{enter}$ The temperature of the air entering the radiator in Kelvin

$t_2 = T_{exit}$ The temperature of the air exiting the radiator in Kelvin



(d) Single-pass cross-flow with one fluid *mixed* and the other *unmixed*

Figure 3.4: F Correction factor for LMTD method as a function of P and R [48].

This method can be used and compared with the total calculated thermal resistance method. If the two agree, one can with confidence assume that the calculated method is correct.

3.6 Fluid Flow Characteristics

3.6.1 Pressure Drop through Tubes

The pressure drop through the radiator tubes is dependent on the geometry of the tube,

the surface finish of the tube, the volumetric flow rate of the fluid, the type (density and viscosity) of fluid, and the remaining configuration of the radiator system. The total pressure drop of the radiator system may be significantly impacted on the configuration of the system beyond the radiator itself including connections, turns, and the loop through the engine block. It is nearly impossible to determine the pressure drop through the entire radiator system numerically. Such a study would require years of testing physical models and collecting real data to determine all the effecting parameters of pressure drop. However, in comparing radiators against one another, a parametric approach to determine the pressure drop only across the radiator may be used. This study will only consider the pressure drop across the tubes of the radiator in order to effectively compare for pumping power required. The pressure drop through the tubes is determined by the Darcy Equation defined as

$$\Delta p = f \frac{L}{2D_h} \frac{G^2}{\rho} \quad (24)$$

where f is the friction factor and can be solved numerically for turbulent flow using the Colebrook Equation,

$$\frac{1}{\sqrt{f}} = -2.0 \log_{10} \left[\frac{\epsilon_f/D_h}{3.7} + \frac{2.51}{Re_D \sqrt{f}} \right] \quad (25)$$

and G is the mass velocity defined by

$$G = \frac{\dot{m}_{pipe}}{A_c} \quad (26)$$

Using this approach for the pressure drop through the radiator tubes can be used to compare any geometry against another and allows for a simple analysis for minimum pumping power which may be defined as

$$P_{pump} = \Delta p \frac{\dot{m}}{\rho} \quad (27)$$

As was aforementioned this pressure drop may not represent the total pressure drop through the entire radiator but may be used only to compare one tube geometry against another. The total pressure drop is needed to accurately determine the pumping power of the coolant system which must be physically measured or calculated using a more advanced and comprehensive method.

3.6.2 Pressure Drop on Air Side

In calculating the required fan power for a specific radiator, one must know the pressure drop and the required air velocity of the radiator as defined by

$$P_{fan} = \Delta p_{air} \dot{V}_{air} \quad (28)$$

The air velocity should be similar to the optimal driving velocity for the vehicle which allows one to model the radiator as being stationary while forced air is being blown across it. The volumetric flow rate for the radiator may be assumed to be

$$\dot{V}_{air} = V_{air} A_{fr} \quad (29)$$

where V_{air} is the air velocity and A_{fr} is the frontal area of the radiator. The pressure drop of the air over the radiator is highly dependent on the geometry and configuration of the air side. For this study a flat tube louvered serpentine fin geometry is considered and a method of calculating pressure drop is presented as follows.

$$\Delta p_{air} = f_{air} \left(\frac{A}{A_o} \right) \frac{G_{air}^2}{2\rho_{air}} \quad (30)$$

Similar to the pressure drop through the tubes, the pressure drop of the air is a function of friction factor, mass velocity, air density at $T_{m,air}$, and the ratio of total surface area (A) to free flow area (A_o). The friction factor is the most difficult variable to determine and the method proposed by Chang et al is used for this geometry [16].

$$f_{air} = f1 * f2 + f3 \quad (31)$$

$$\left. \begin{aligned}
 f1 &= 14.39 Re_{Lp}^{(-0.805 \frac{Fp}{Fl})} \left(\ln \left[1. + \left(\frac{Fp}{Lp} \right) \right] \right)^{3.04} \\
 f2 &= \left(\ln \left[\left(\frac{Fl}{Fp} \right)^{0.48} + 0.9 \right] \right)^{-1.435} \left(\frac{Dh_{air}}{Lp} \right)^{-3.01} (\ln[0.5 Re_{Lp}])^{-3.01} \\
 f3 &= \left(\frac{Fp}{Ll} \right)^{-0.308} \left(\frac{Td}{Ll} \right)^{-0.308} \left(\text{Exp} \left[-0.1167 \frac{Tp}{Dm} \right] \right) \theta^{0.35}
 \end{aligned} \right\} Re_{Lp} < 150 \quad (32)$$

$$\left. \begin{aligned}
 f1 &= 4.97 Re_{Lp}^{(0.6049 - \frac{1.064}{\theta^{0.2}})} \left(\ln \left[\left(\frac{\delta f}{Fp} \right)^{0.5} + 0.9 \right] \right)^{-0.527} \\
 f2 &= \left(\left(\frac{Dh_{air}}{Lp} \right) \ln[0.3 Re_{Lp}] \right)^{-2.966} \left(\frac{Fp}{Ll} \right)^{-0.7931 \left(\frac{Tp}{Tp - Dm} \right)} \\
 f3 &= \left(\frac{Tp}{Dm} \right)^{-0.0446} \ln \left[\left(1.2 + \left(\frac{Lp}{Fp} \right)^{1.4} \right) \right]^{-3.553} \theta^{-0.477}
 \end{aligned} \right\} 150 < Re_{Lp} < 5000$$

$$G_{air} = \frac{V_{air} A_{fr} \rho_{air}}{A_o} \quad (33)$$

CHAPTER 4

TOPICS OF RESEARCH AND EXPERIMENTAL PROCEDURES

4.1 Design Study

Once the existing radiator has been analyzed and its performance criteria identified, it will now be required to identify what improvements can be made to the existing radiator. In particular it is the goal of the author to identify if microchannels can be used to achieve the overall goal of reducing the frontal area of the radiator without sacrificing the heat transfer abilities or increasing the auxiliary power (fan power and pumping power) required to operate the radiator.

As the design of the current radiator is one of the most advanced designs of its kind, the approach to changing the radiator will be taken gradually. First the effects of tube diameter will be investigated followed by tube wall thickness and radiator depth. A secondary study will be conducted on the fins, specifically investigating fin length, fin pitch, and louver pitch. A tertiary study will involve the varying of flow rates of air and coolant. A final study will involve the replacement of materials of the tubes, fins, and coolant.

4.2 Study of Microchannel Tubes

4.2.1 Tube Diameter

The purpose of this study is to identify the possibility of using microchannels to improve the performance and reduce the size of a radiator. The current radiator configuration consists of flat tubes. It was therefore thought that by replacing the flat tubes directly with an array of microchannels would be an easy and cost effective approach.

In this study, a single flat tube was replaced by an array of round tubes which has the potential to increase the external surface area and thus reduce the thermal resistance on the air

side while simultaneously decreasing the thermal resistance on the coolant side with the use of microchannels. To prevent the flow from becoming turbulent or have high velocities, which greatly increases the pressure drop, the number of pipettes or tubes through which the coolant flows must be increased significantly so that the total cross sectional area of the pipettes is similar to the cross section of the original pipe.

Figure 4.1a depicts the original fin and tube geometry. If the single tube were to be replaced by an array of tubes as is seen in Figure 4.1b, the result may have a greater heat transfer rate. In each figure, section A-A represents the cross section of the radiator with the tube array depicted with louvered fins on either side of the tube array. The study continues by decreasing the size of the tubes and by so doing, increasing the number of tubes possible. Following a parametric design of experiments the designs were simulated mathematically and compared for heat transfer and pressure drop improvements.

It was found that as the tube diameter decreased, the pressure drop will increase unless there are a sufficient number of tubes or equivalent cross sectional area to balance the heat transfer and pressure drop. Numerous iterations (60+) were performed to find the right balance of heat transfer, pressure drop, and geometric and manufacturability constraints.

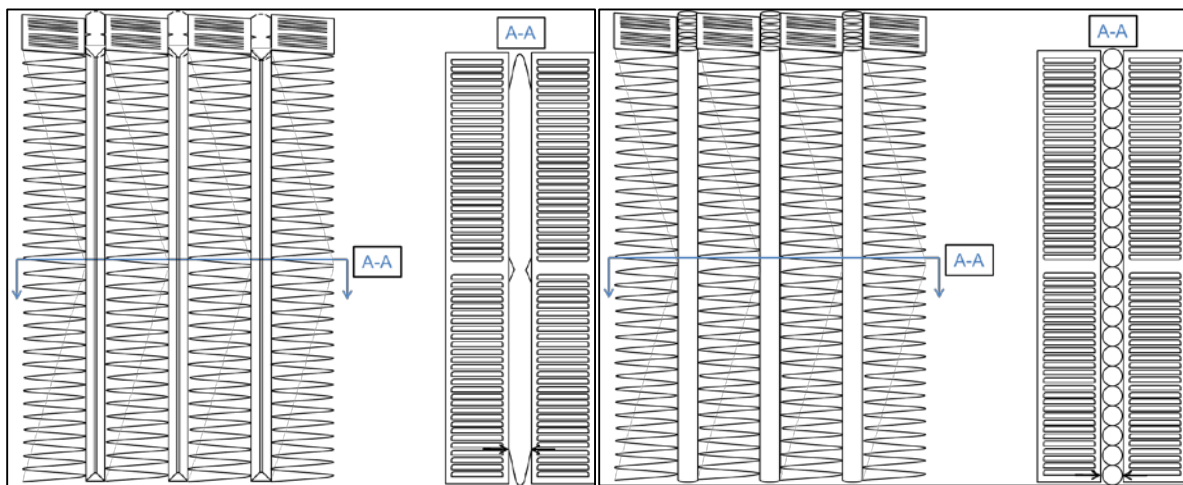


Figure 4.1a&b: Original tube and fin configuration and proposed tube and fin configuration

4.2.2 Tube Thickness

The tube thickness was varied since the thinner tube wall would conduct heat more quickly. It was discovered in the study that the tube wall thickness had less effect on the total resistance because of thermal conductivity. The thermal resistance through the tube wall is the lowest of all thermal resistances in the model. It was discovered however that by decreasing the tube wall thickness, an increase in internal diameter and thus surface area was achieved with the same outer wall diameter. Thus the size of the radiator could be reduced and the pressure drop across the tubes will not be so severe.

Literature was reviewed to identify the smallest tube thickness that could be manufactured and still hold pressure without failure. An outreach to the Microproducts Breakthrough Institute yielded that using diffusion bonded surface manufacturing, both hydraulic diameters and wall thicknesses less than 0.002 in (0.051 mm) could be achieved. These diffusion bonded surfaces can be leak tight at pressures greater than 20,000 psi (137.8 MPa) [54]. Thus, fabrication processes of tube wall thicknesses show that the thickness can be reduced significantly.

After considering manufacturing of microchannel tubes and reviewing literature, it was investigated whether a flat microchannel slab with hollow ports may be a better than an array of tubes. The original thought was that each tube could be laid up with other tubes into an array and then the array could be brazed together but manufacturing experience says that that would require too much labor to produce high-quality parts, especially if there were many microchannel tubes. Thus a microchannel slab may be a better alternative. The external surface area of the slab is slightly less than the tube array design but manufacturability, decreased cost, and structural integrity would be added benefits.

4.2.3 Radiator Depth

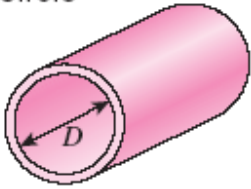
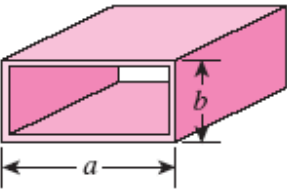
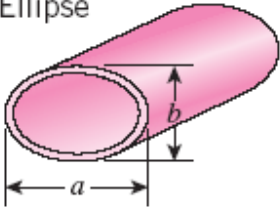
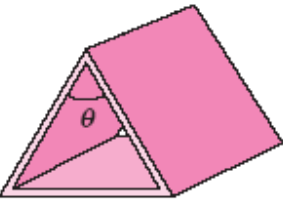
A study of radiator depth was conducted to determine if that would be a feasible alternative to reducing frontal area. By reducing the height of the radiator, the number of tubes remains but surface area on both the tube side and air side is decreased. By reducing width, the number of tube and fin arrays is decreased. By increasing depth the number of tubes may be increased along with surface area of both coolant-side and air-side, thus reducing the thermal resistance while simultaneously decreasing the frontal area. One discovery that was made was that by increasing the tube depth, the air-side convection coefficient and the air-side pressure drop were negatively affected. Thus many iterations were conducted to find the optimal design of the heat exchanger.

4.2.4 Tube Shape

A small study of the tube shape was carried out to see how square microchannels compared to circular microchannels. Many studies have been conducted using various geometries. Khan reviewed various geometries and chose circular ports over rectangular because there was less studies on circular channels and he claimed that they “offer overall best thermo-hydrodynamic performance for a MCHX among various other shapes.” [24] From observation, there is greater internal surface area in rectangular cross-sections than that of circular cross sections and manufacturability may be more cost effective for rectangular for Micro-multiport extrusion tube manufacturing [24] [55]. In addition to having more surface area, the rectangular channels will have thinner walls in a microchannel slab than a slab with circular channels. This could decrease the thermal resistance of the tube walls. However, according to conventional theory, the Nusselt Number for laminar flow through a smooth pipe with a square cross-section is less than that of a round tube. Kim et al. studied the effect of flattened round tubes of varying

aspect ratio and found that a round tube with an aspect ratio of 1 has a higher heat transfer coefficient than a slightly flattened tube with an aspect ratio of 2 but lower than a more flattened tube with an aspect ratio of 4 [50]. This was for an evaporator with phase change at $1400 \leq Re_{Dh} \leq 4200$. Observing Table 4.1 one can see that a rectangular tube with a large aspect ratio offers the highest Nusselt Number but also potentially the highest friction factor which lead to high pressure drop.

Table 4.1: Nusselt number and friction factor for laminar flow through smooth tubes of various cross-sectional geometry [10, p. 437].

Tube Geometry	a/b or θ°	Nusselt Number		Friction Factor f
		$T_s = \text{Const.}$	$\dot{q}_s = \text{Const.}$	
Circle 	—	3.66	4.36	64.00/Re
Rectangle 	a/b 1 2 3 4 6 8 ∞	2.98 3.39 3.96 4.44 5.14 5.60 7.54	3.61 4.12 4.79 5.33 6.05 6.49 8.24	56.92/Re 62.20/Re 68.36/Re 72.92/Re 78.80/Re 82.32/Re 96.00/Re
Ellipse 	a/b 1 2 4 8 16	3.66 3.74 3.79 3.72 3.65	4.36 4.56 4.88 5.09 5.18	64.00/Re 67.28/Re 72.96/Re 76.60/Re 78.16/Re
Isosceles Triangle 	θ 10° 30° 60° 90° 120°	1.61 2.26 2.47 2.34 2.00	2.45 2.91 3.11 2.98 2.68	50.80/Re 52.28/Re 53.32/Re 52.60/Re 50.96/Re

In this study microchannel slabs with round and square microchannel ports were compared with the current flat tube and other flat tube designs to determine the optimal tube shape for enhance heat transfer and limited pressure drop.

4.3 Study of Fins

The serpentine louver fins were studied in depth to identify the heat transfer convection coefficient relationships and solutions were found through literature. Major findings of the louver fins included the significant surface area to fin ratio that existed along with the louvers actually directing the air to increase heat transfer. While investigating louver fins, it was realized that the geometric dimensions of fin length, fin pitch, louver pitch, and tube depth were affected the heat transfer and pressure drop significantly. All of these parameters also contribute to the total convective surface area which will help to reduce the resistance. The air-side resistance of the radiator is the dominant resistance which means that even if the thermal resistance of the tube wall and the thermal resistance of the fluid flow were significantly reduced, the overall heat transfer might not be greatly improved. Thus numerous iterations were performed to determine the best configuration of the fin geometry.

4.3.1 Fin Length

The fin length determines the spacing between the tubes which affects both the convective heat transfer coefficient, h_{air} , and the pressure drop across the radiator, ΔP_{air} . As the fin width is increased, it allows for the extended surface from the tube to reach a cooler free stream temperature as well as increases the surface area and thus increases the heat transfer while simultaneously increasing the flow passage of air thus decreasing the pressure drop.

Unfortunately the constraint involved is that by increasing the fin length, the width of the radiator is also increase unless there are fewer tube and fin arrays which will increase the

pressure drop in the tubes. Thus a balance must be kept and optimized to identify the best possible design.

4.3.2 Fin Pitch

The fin pitch is the space between one fin to the next fin and it also has an effect on both h_{air} and ΔP_{air} . As the fin pitch is decreased, the fin spacing becomes denser. This increases the number of fins which increases the potential for more heat to be transferred as well as increasing surface area which causes R_{fin} to decrease. Unfortunately as the spacing gets tighter, the pressure required to enter those spaces increases thus a balance between h_{air} and ΔP_{air} must be found to improve the current design.

4.3.3 Louver Pitch

The louver pitch has a surprisingly substantial effect on h_{air} . The relationship derived by Chang and Wang related every dimensional parameter to the louver pitch as it is the main contributing difference from other tube geometries [16]. It is found that as the louver pitch is decreased, the number of louver fins is increased and h_{air} is increased because there is more mixing and turbulence created through the air channels. The surface area is also increase slightly which will decrease R_{fin} and allow for better heat transfer. The pressure drop is not significantly affected by the louver pitch which is also good. The restriction on decreasing the louver pitch lies in the manufacturability. The louver pitch is already less than 1mm and decreasing the fin pitch further may not be beneficial in regards to cost and possible structural integrity of the already fragile fins.

4.4 Operating Conditions

Apart from the geometry of the radiator, there are other parameters that should be investigated such as the flow rate of the coolant, the flow rate of the air, the material of the heat

exchanger and the coolant type. Improvements in any of these parameters could help in reducing the size, weight, and energy consumption of the radiator and are thus worth investigating.

4.4.1 Mass Flow Rate of Coolant

According to microchannel theory, the decreased size in microchannels allows for higher heat transfer even at laminar flows. A decrease in the overall cross sectional area means that less flow can be forced through the tubes without an increase in velocity which will increase the pressure drop through the tubes. The flow rate can thus be decreased to maintain laminar flow while still having high heat transfer. A decrease in flow rate also means a decrease in needed coolant and pump size. Using less coolant, which is usually ethylene-glycol-water mixture, is considered more “green” since ethylene-glycol is toxic and a petroleum-based product.

It was observed in this study that depending on the theory utilized in calculating the Nusselt Number ($Nu_D = 3.66$ if $Re_D \leq 2300$ [10] versus Equation (5), where $Nu_D \propto Re_D$) the heat transfer coefficient will be greatly affected. If the Nusselt Number is proportional to the Reynolds number which is proportional to the fluid velocity, as would seem logical, then at higher Reynolds numbers, there will be more heat transferred than at lower Reynolds numbers although both flows may be laminar ($Re_D \leq 2300$). If the other theory hold true and the Nusselt number remains the same for all Reynolds numbers below 2300 then the fluid velocity may be near creeping flow $Re_D < 10$ and still have similar heat transfer as one with $Re_D < 1000$. This is a critical point to observe.

In this study, the theory of Nusselt number correlated to Reynolds number was used. This resulted in the realization that at higher flow velocities $Re_D > 1000$, the convection coefficient, h_c , was higher than flows with $Re_D > 800$ utilizing smaller microchannels. Thus an

investigative study was conducted to determine the ideal trade-off of microchannel hydraulic diameter, number of channels, flow rate, and pressure drop optimization.

4.4.2 Mass Flow Rate of Air

As the goal of this study is to reduce the frontal area of the radiator, a study of the air flow is beneficial. With a smaller radiator, there may be reduced pressure drop and a smaller and less powerful fan would be more attractive. If, however, the depth of the unit is increased thus causing an increased amount of pressure drop, a more powerful fan may be required, but with smaller dimensions. The increased velocity of the air also increases h_{air} which can also help reduce R_{fin} especially since the total surface area may be reduced as the frontal area is reduced. Thus a study and investigation of air flow rate will be conducted to determine the best possible design. Several iterations were performed to determine the best geometric configuration, heat transfer, and pressure drop possible while trying not to increase fan power.

4.4.3 Material of Heat Exchanger

The current design of the radiator is composed entirely of aluminum. Aluminum has many benefits including light weight, high thermal conductivity, easy manufacturability, relatively low cost, galvanic-corrosion and oxidation resistant, and 100% recyclability.

Copper has the potential to be 95% more conductive than aluminum. With the decrease in material by using microchannels, the cost and weight could be comparable if the material of the heat exchanger was changed to copper. With the decrease in available surface area, higher efficiency heat transfer is required which may be made possible by utilizing the more conductive material of copper.

As was mentioned previously, there is a developing material called Carbon Foam being investigated at which has large potential to increase thermal conductivity and reduce weight.

Thus a study of the material of the heat exchanger would be beneficial to determine what possibilities exist [12].

4.4.4 Material of Coolant

Traditionally the coolant used in automotive radiator has been a mixture of ethylene glycol (antifreeze) and water. Water has a fairly good thermal conductivity as is seen in Table 4.1. In the cooling process, it is the water that does the majority of the cooling. Antifreeze is added to the water to decrease the freezing point of the fluid and increase the boiling point as is seen in Table 4.2, as well as preventing corrosion and fouling that would be caused by water. Unfortunately the adding of the antifreeze decreases the desired thermal properties of water.

The thermal conductivity, viscosity, and specific heat of the transfer fluid are all important. As can be seen in the equation, $h_c = Nu_D k/D_h$, the thermal conductivity of the fluid is directly related to the convective coefficient and an increase in the thermal conductivity of the fluid would also increase the heat transfer possible. The equation for potential heat removal, $Q_{Engine} = \dot{m}_c c_{p,c}(T_{in} - T_{out})$, reveals that an increase in the specific heat of the coolant would result in a higher capacity for heat removal. The Reynolds number associated with the coolant flow is directly related to the kinematic viscosity of the fluid by $Re_D = V D_h/\nu$. Thus a decrease in viscosity will increase the Reynolds number which affects the Nusselt number and heat transfer coefficient. This may affect the pressure drop as well since the pressure drop is related to the friction factor and the density of the fluid.

As can be seen in Table 4.1, the lower concentration of 30% Ethylene Glycol has more desirable thermal-fluid properties and might be used to replace the 50% concentration. The caution here would be that if temperatures ever reached 2°F or below, the radiator runs the risk of freezing which could have devastating effects. For large trucks that travel all over the country

all year round, this would be a risk in only using 30% ethylene glycol solution. It may be feasible to use the 30% mixture for warmer parts of the year, then increase the concentration to 50% during the winter months. Propylene glycol is another alternative which may be an attractive substitute since Propylene is non-toxic and therefore more environmentally safe.

Table 4.2: Material properties of different fluids at T=20°C [53] [54]

Fluid	Thermal Conductivity (W/m·K)	Kinematic Viscosity (m ² /s)	Specific Heat (J/kg·K)
Water	0.60475	9.7937×10^{-7}	4.0764×10^3
Air	0.025596	1.5111×10^{-5}	1.0061×10^3
Ethylene Glycol	0.24998	1.9119×10^{-5}	2.3865×10^3
30% Ethylene Glycol-Water	0.48418	2.0885×10^{-6}	3.7141×10^3
50% Ethylene Glycol-Water	0.42568	3.6604×10^{-6}	3.2875×10^3
30% Propylene Glycol-Water	0.47000	2.7000×10^{-5}	3.8500×10^3
50% Propylene Glycol-Water	0.39200	5.7000×10^{-5}	3.6000×10^3

Table 4.3: Freezing and boiling points of commonly used coolants [55]

Working Fluid	Freezing Point		Boiling Point	
	°F	°C	°F	°C
Water	32	0	212	100
30% Ethylene Glycol-Water	2	-13.7	220	104.4
50% Ethylene Glycol-Water	-36.8	-36	225	107.2
30% Propylene Glycol-Water	7	-14	216	102.2
50% Propylene Glycol-Water	-29	-34	222	105.6

Therefore, a study of the coolant type would be beneficial to determine the effects of the coolant on the heat transfer, pressure drop, and other benefits or consequences. A study of coolant type is therefore considered in this work.

CHAPTER 5

CALCULATIONS, TEST METHODS AND RESULTS

With all the parameters of the study were selected, it is necessary to determine the impact of each of the parameters. For the majority of the parameters, established theories and equations were used to derive the desired information. This was compared to literature to verify the probabilistic resulting affects. Further verification may be needed for particular results such as a modified fin design and flow rate.

5.1 Simulation and Calculations

Preliminary calculations for this study were performed using Microsoft Excel to modify and simulate the appropriate geometric dimensions that were affected by the proposed modifications to the design. The geometric parameters were then entered into a programmed code written by the author using Wolfram Mathematica that utilized traditional heat transfer mathematical models to output performance data for comparison against other designs into a Microsoft Excel spreadsheet to compare the various simulations. Using Microsoft Excel, various figures were produced to show the performance of the various parameters under investigation. These figures were analyzed to determine the characteristics and effects of design changes to determine the optimal tube and fin configurations.

In order to verify the results of the calculations, CFD models were created and analyzed to simulate the thermo-hydraulic characteristics of the current design of flat tube as well as a microchannel slab having round-tube geometry and a microchannel tube with square-tube geometry.

5.1.1 Heat Transfer and Thermal Resistance

The heat transfer and thermal resistance model as described previously was applied to the

original heat exchanger. Using both the Total Thermal Resistance method and the LMTD method, a deviation of 13.6% was noted and deemed acceptable with the greater resistance resulting from the Total Thermal Resistance Method. For the remainder of the investigations, the Total Thermal Resistance method was used to determine the highest heat transfer possible.

Figure 5.1 shows the results of all the iterations performed to determine the best possible heat transfer design. The total resistance, R_{total} , is a primarily a function of the internal (or coolant-side) convective resistance, R_c , and the external (or air-side) convective resistance, R_{fin} as is seen in the equation, $R_{total} = R_c + R_{pipe} + (1/R_{fin} + 1/R_{rad})^{-1}$.

Although the thermal radiation, R_{rad} , and the thermal conduction resistance through the pipe wall, R_{pipe} are included in the calculation, the resistances are negligible by comparison. The thermal conduction resistance, R_{pipe} , is generally two orders of magnitude less than R_c and R_{fin} and since R_{rad} and R_{fin} are inverse additive functions, the affects from R_{rad} are negligible. Thus the total resistance, R_{total} , can almost be considered an additive function of R_{fin} and R_c . This can be seen in Figure 5.1. If R_{fin} and R_c are high, R_{total} is also high and if R_{fin} and R_c are low, R_{total} is also low.

As is seen in Figure 5.1, many iterations produced resistances which were both less than the original radiator resistance and, in some circumstances, greater than the existing radiator. It can also be seen that R_c and R_{fin} were reduced from the original design. The extremely low R_c resistances were achieved using microchannels. The low values of R_{fin} were achieved mainly by increasing the surface area, A . There were many other contributions and factors involved in each of the iterations and these affects will be discussed hereafter.

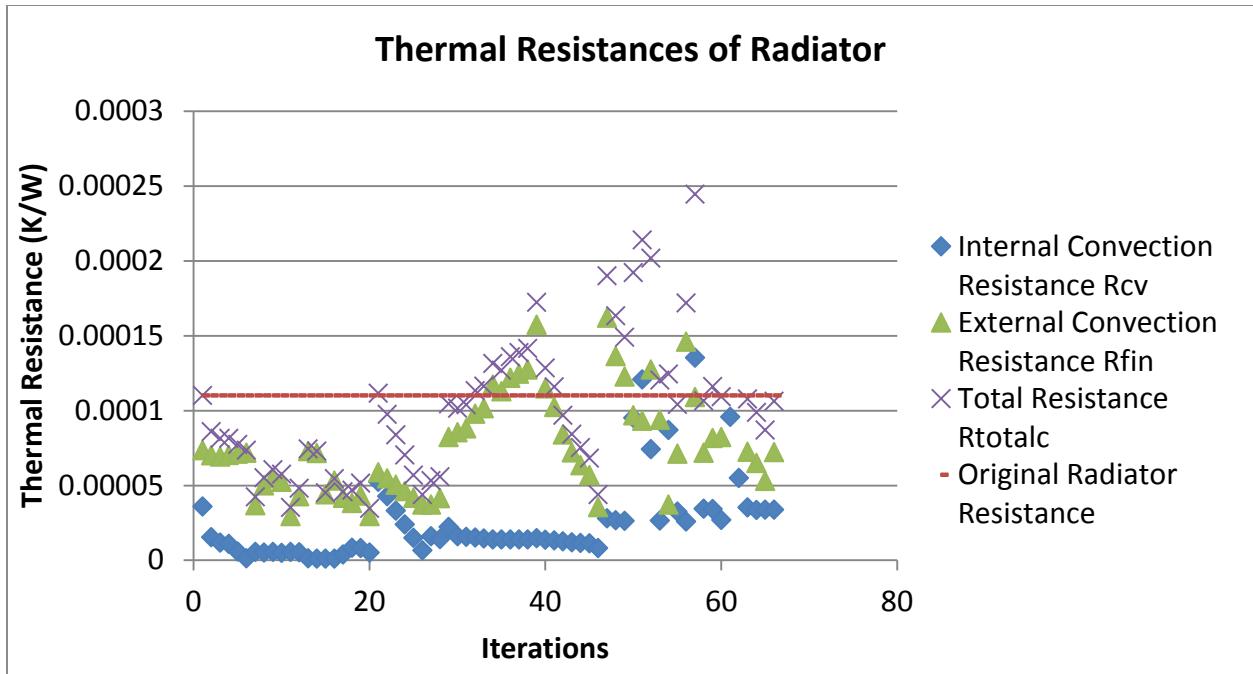


Figure 5.1: Total thermal resistance calculated, showing air-side convective resistance, coolant-side convective resistance, and total thermal resistance.

5.1.2 Results of Tube Diameter on Heat Transfer and Pressure Drop

A hypothetical study was conducted to identify the relationships between the hydraulic diameter and the convective heat transfer coefficient, Reynolds number, and pressure drop. Within this study, the mass flow rate and other parameters were held constant while varying the diameter and the number of total tubes. Figures 5.2-5.5 show the effects of the microchannel hydraulic diameter and number of total tubes against the Reynolds number, the internal convection coefficient, the internal thermal convection resistance, and the pressure drop across the tubes.

As can be seen in Figure 5.2, the Reynolds number decreases with increasing hydraulic diameter but this is dependent on the flow rate and the number of tubes. As the number of tubes increase the flow is able to be dispersed into more tubes allowing the flow velocity in each tube to be decreased thus decreasing the Reynolds number.

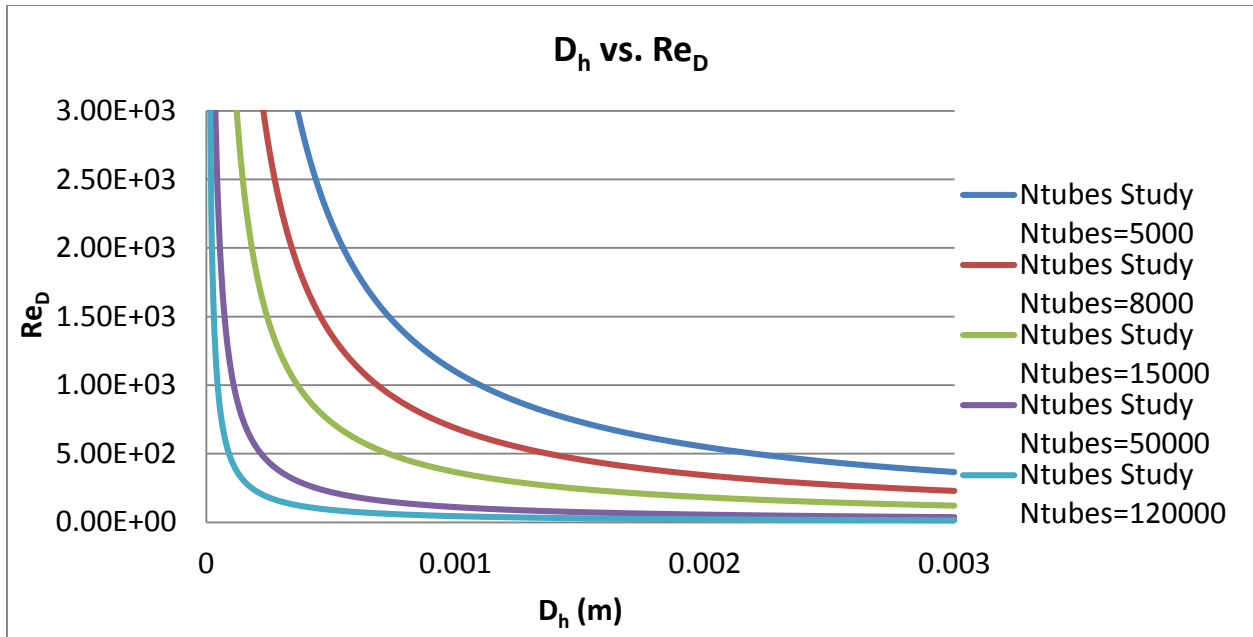


Figure 5.2: Hydraulic diameter vs. Reynolds number

In Figure 5.3, one can see that the effect of the hydraulic diameter on the internal convection coefficient which is a function of the Reynolds number and the hydraulic diameter. As the hydraulic diameter is enlarged, the Reynolds number is decrease and the flow becomes laminar. At laminar flow, the convection coefficient is a function of hydraulic diameter only as $h_c = Nu k/D_h$ and the magnitude of the flow velocity or flow rate has no effect while the flow is laminar as is seen in Table 4.1. The large stair-step characteristic is because of this fact. Thus, for any flow rate or number of tubes, the hydraulic diameter will have the greatest effect on the heat transfer coefficient at laminar flow.

The internal thermal convection resistance can be seen in Figure 5.4 as a function of the internal convection coefficient and the internal surface area as $R_c = 1/(h_c A_i)$. Because at laminar flow the convection coefficient is a function of D_h only, the convection thermal resistance suffers for round or square tubes since the surface area is also a function of D_h and the resulting resistance is $R_c = 1/(Nu k N_{pipe} \pi L)$ for round tubes or $R_c = 1/(Nu k N_{pipe} 4 L)$ for square tubes.

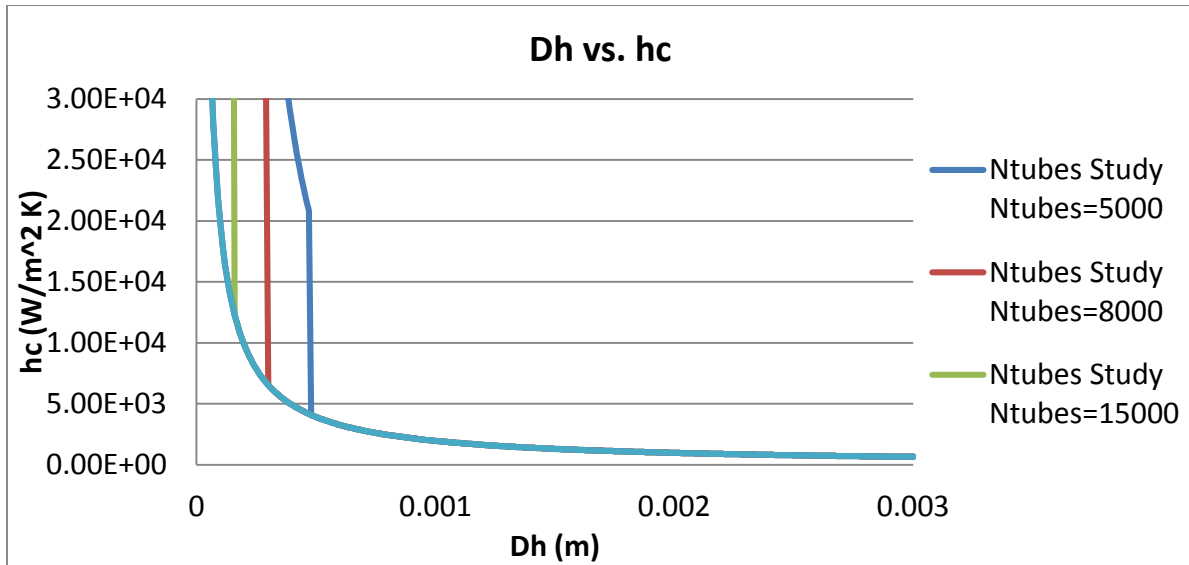


Figure 5.3: Hydraulic diameter vs. internal convection coefficient

The performance cost of microchannels can be seen in Figure 5.5 as the pressure drop significantly increases as the hydraulic diameter is decreased. This can be slightly offset by increasing the number of tubes which enlarges the total cross sectional area of the configuration and decreases the Reynolds number but this is still a challenge. When the hydraulic diameter is enlarged, the pressure drop is relaxed and this challenge is quickly diminished but the benefits of microchannel tubes are also lost.

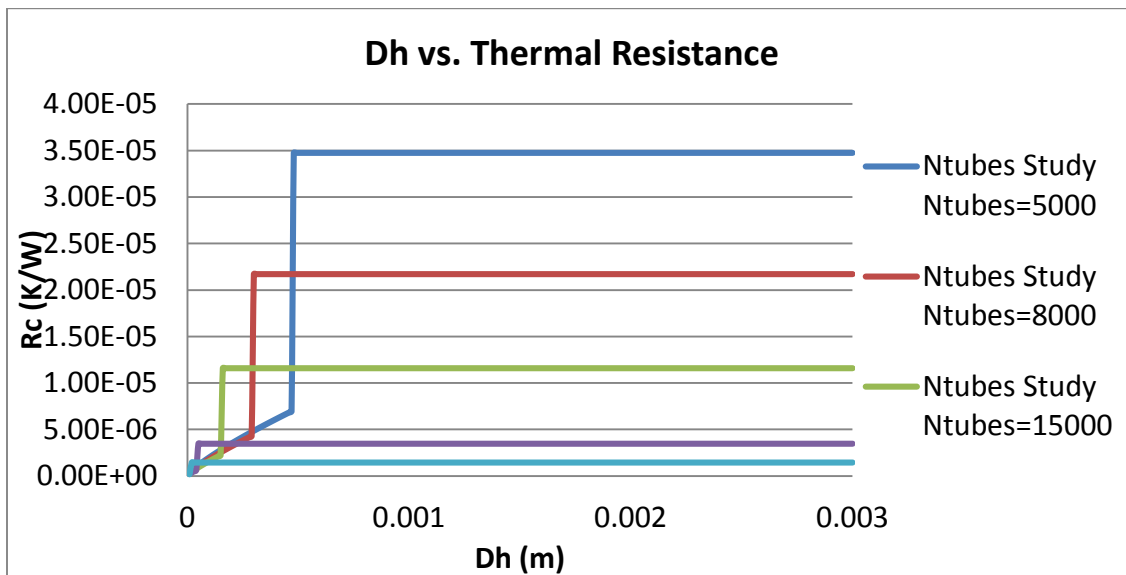


Figure 5.4: Hydraulic diameter vs. internal thermal convection resistance

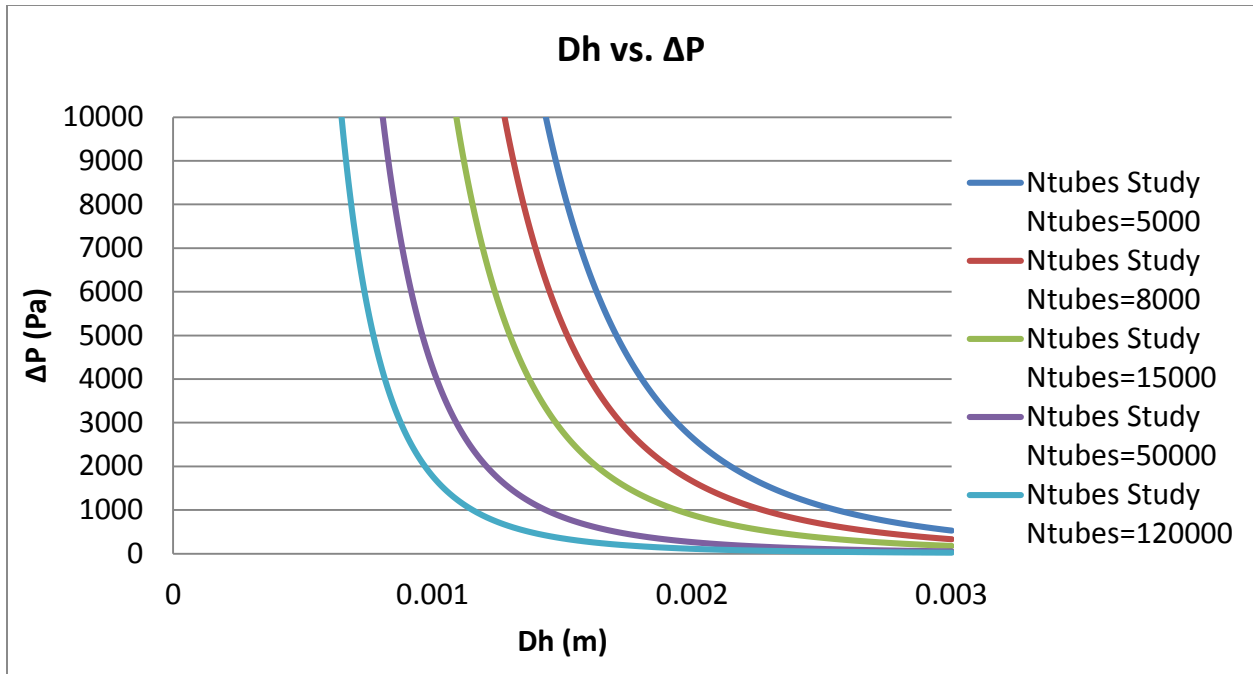


Figure 5.5: Hydraulic diameter vs. pressure drop

An additional hypothetical study was conducted varying the flow rate and comparing the maximum available heat transfer rate and pressure drop for a series of different hydraulic diameters. This study is based on the NTU- ϵ method for a mixed/unmixed cross flow heat exchanger holding the air side resistance and conditions constant while varying the flow rate and hydraulic diameter of the system. This was done for a system having 1100 tubes (Figures 5.6-5.9) and then for a system of 1500 tubes (Figures 5.11-5.12).

As is seen in Figure 5.6, the maximum heat transfer rate increases with the increase of flow rate since this increases the Reynolds number and the NTU coefficient. The laminar flow in the tubes significantly limits the maximum amount of heat that can be transferred but once the flow becomes turbulent, the heat transfer is significantly improved. As is also noted, for smaller hydraulic diameter tubes, the shift to turbulent flow occurs much sooner at comparative flow rates.

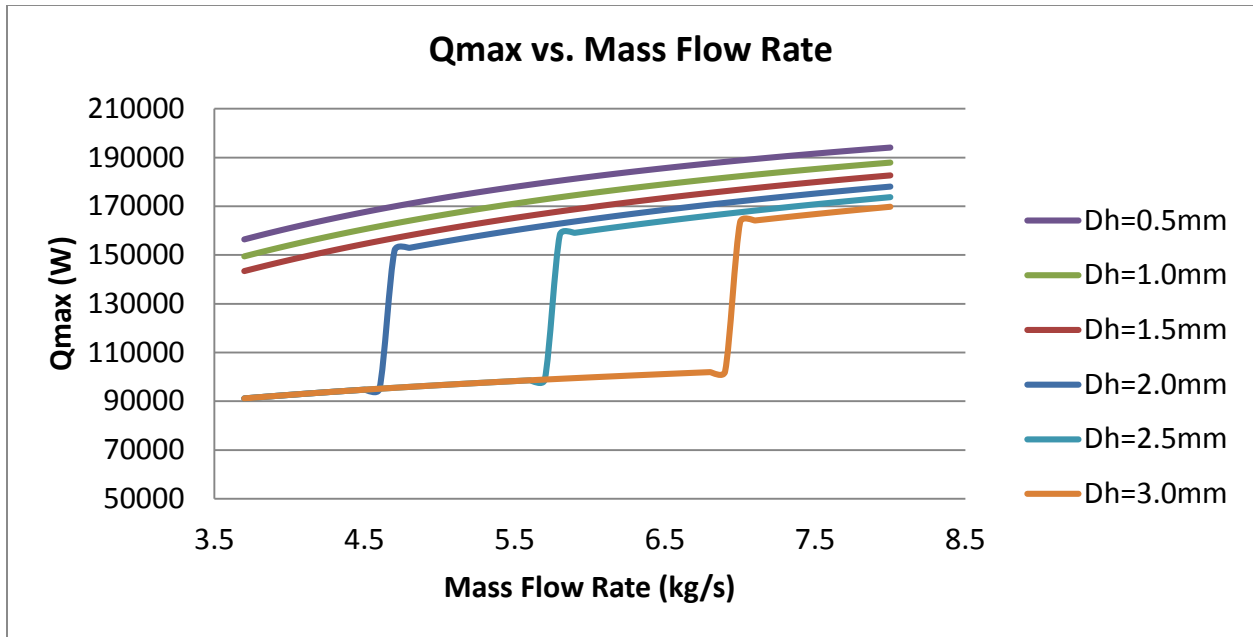


Figure 5.6: Mass flow rate vs. maximum heat transfer for an array of 1100 tubes of varying hydraulic diameters

Figure 5.7 demonstrates the cost of microchannel performance somewhat more clearly than does Figure 5.5. The pressure drop is severely dependent on the hydraulic diameter or the total amount of cross-sectional area or flow area is available. Even at varying flow rates, the pressure drop is not as severely affected by flow rate as by hydraulic diameter. The scale for Figure 5.10 is logarithmic to accurately portray the cost of microchannel performance. The stair-step effect is caused by the shift from laminar to turbulent flow. This effect is not as comparably significant for pressure drop as it is for heat transfer performance.

Figures 5.8 and 5.9 demonstrate the same characteristics as Figures 5.6 and 5.7. The difference is the increase in the total number of tubes in the system for Figures 5.8 and 5.9. This increase is the number of tubes increases the total internal surface area which allows for an increase in maximum heat transfer. It also reduces the flow velocity through each tube which causes the flow to become laminar. But the rate of heat transfer at laminar flow is even increased and causes a decrease in pressure drop as is seen in Figure 5.9.

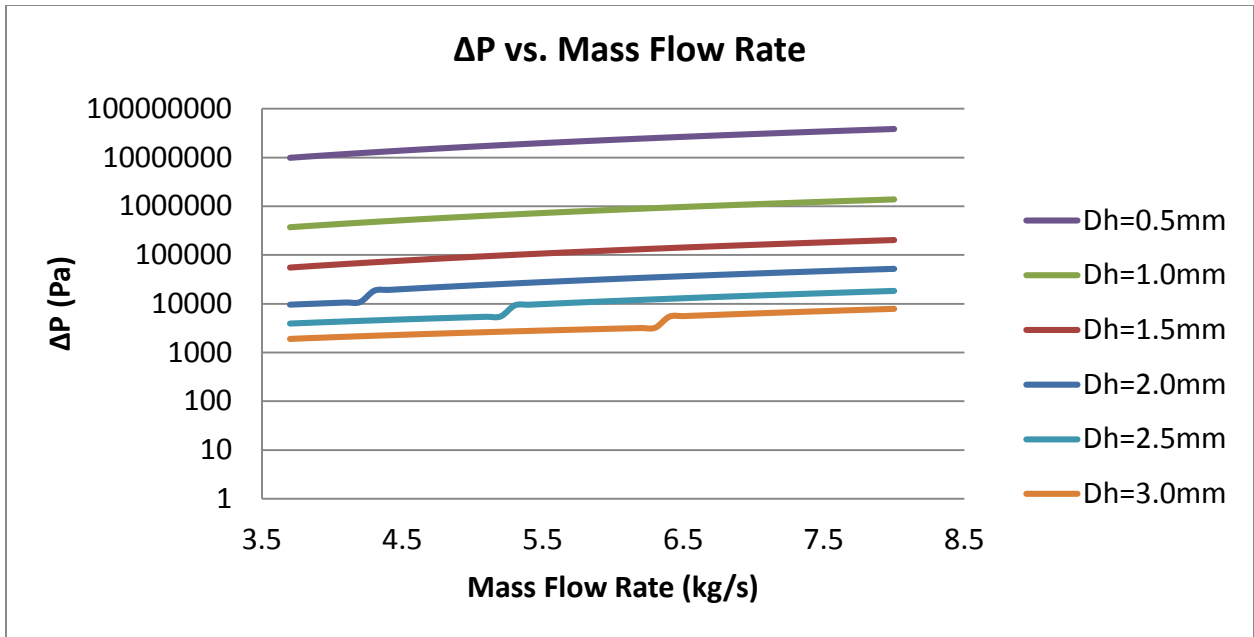


Figure 5.7: Mass flow rate vs. pressure drop for an array of 1100 tubes of varying hydraulic diameters

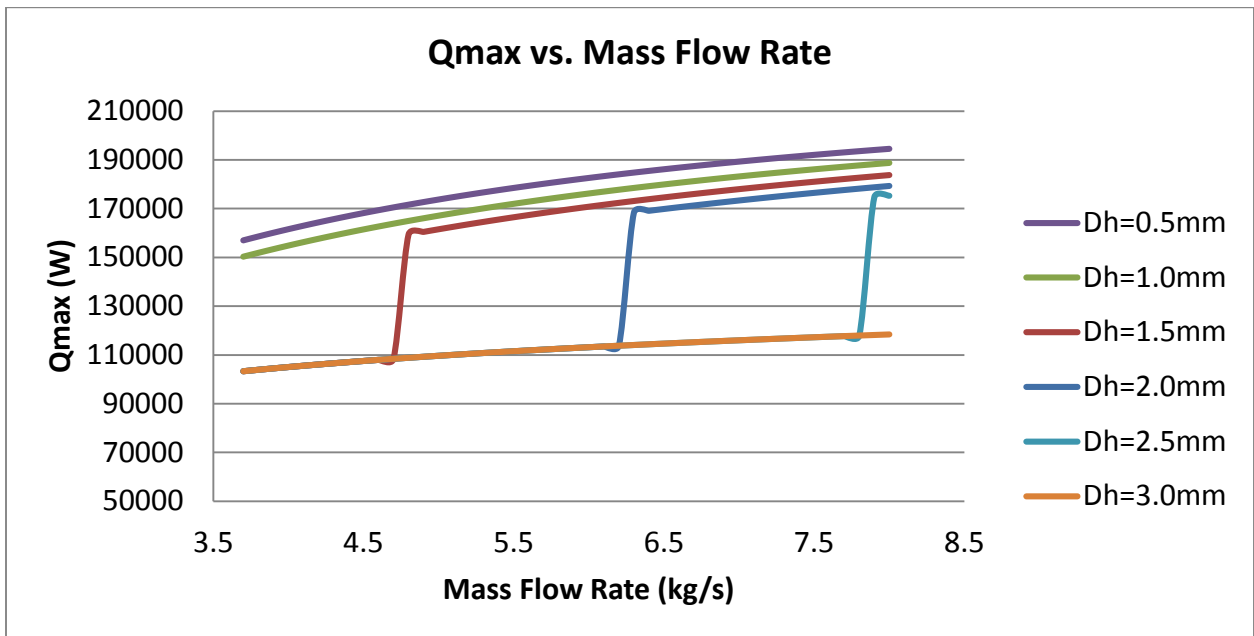


Figure 5.8: Mass flow rate vs. maximum heat transfer for an array of 1500 tubes of varying hydraulic diameters

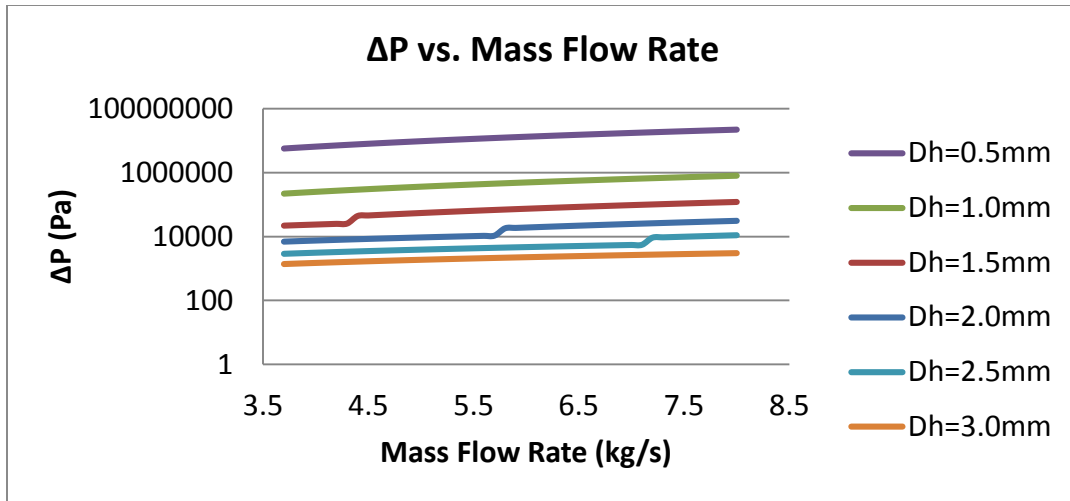


Figure 5.9: Mass flow rate vs. pressure drop for an array of 1500 tubes of varying hydraulic diameters

5.1.3 Results of Tube Thickness

The tube thickness was investigated to determine the effects on the overall heat transfer and total thermal resistance. Because the tube walls were already thin and the material was highly conductive, the resulting thermal conductive resistance, R_{pipe} was significantly lower than R_c or R_{fin} and for the majority of the studies, R_{pipe} was not considered a contributor to the overall heat transfer resistance. However, a quick study shows that the microchannel design does decrease the thermal conductivity resistance substantially as is seen in Figure 5.10.

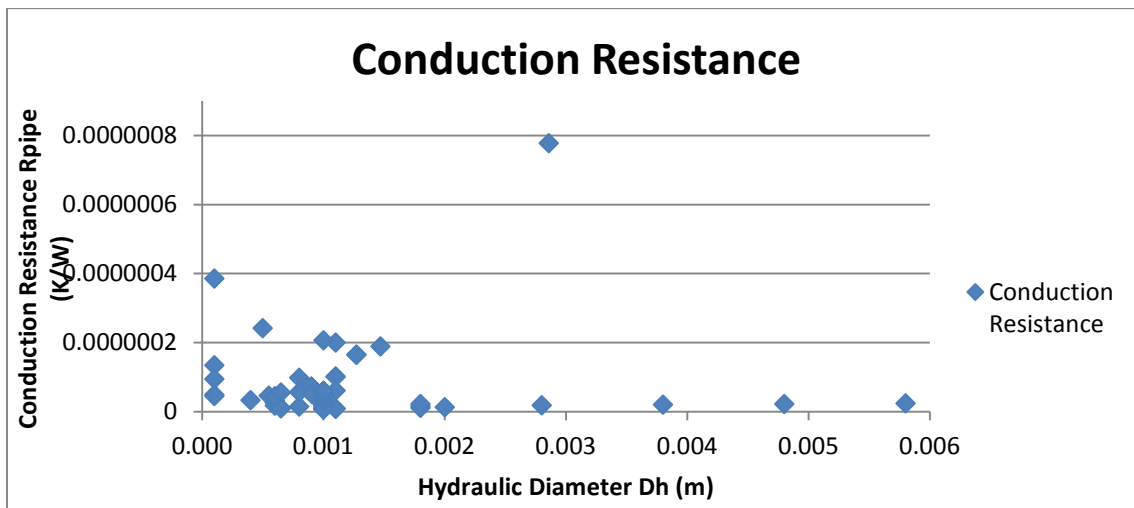


Figure 5.10: Effects of hydraulic diameter on R_{pipe} . The highest resistance value corresponds to the original radiator (flat tube) design.

5.1.4 Air-Side Heat Transfer Results

An intensive study was conducted on improving the air-side heat transfer since it was the dominant thermal resistance in the thermal resistance model. It was first noticed that the total contribution to the external convection resistance, R_{fin} is a function of the external convection coefficient, h_{air} , and the total convective surface area, A , which is a combination of the fin surface area and the tube wall external surface area. It was noticed that the surface area contribution of the tube walls was minor in comparison to the surface area of the fins. It is also noted that for louver fin and flat tube geometry, the external convection coefficient, h_{air} , is governed mainly by the fin geometry with little contribution from the tube pitch. Thus a study of the fins is most beneficial to improve the air-side heat transfer.

5.1.4.1 External Convection Coefficient

A hypothetical study was also performed on the fin geometry parameters of fin length, louver pitch, fin pitch, and tube depth to determine the overall effects on the heat transfer coefficient. In addition to the geometric effects on the external convection coefficient, the air velocity and fin material will also have an effect. A study of each of these parameters is given as follows.

In Figure 5.11 it is observed that the Louver Length (related to fin length by $Ll = Fl - w_{edge}$, where w_{edge} is the width of the un-louvered part of the fin) has a significant effect on h_{air} . Thus, as the louver length is increased by only a few millimeters, the capacity to remove heat from the tubes is increased.

The Tube Depth also has an effect on h_{air} as seen in Figure 5.11, such that as the tube depth increases, the heat transfer is not as effective since the front part of the fins will be cooled fastest and h_{air} will thus not be as significant. If the tube depth can be decreased, h_{air} will

increase or another alternative is to increase the fan speed for a higher convection coefficient. This will, however, increase the required fan power which is not desirable but should be considered.

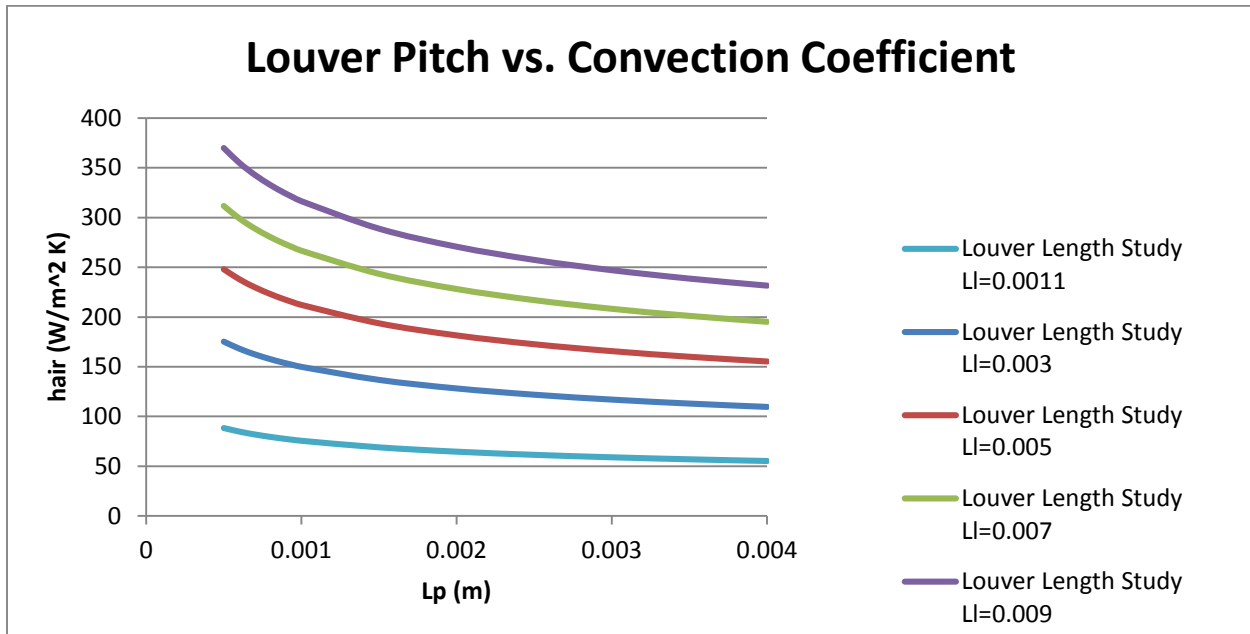


Figure 5.11: Effects of louver length (fin length) on the external convection coefficient comparing against louver pitch

The fin pitch (see Figure 5.12) also has a slight impact on h_{air} and as the fin pitch is decreased, meaning the packing of the fins is tighter, the convective heat transfer coefficient is increased since the louver fins will direct the air through the louvers more effectively and increase h_{air} . This effect is not nearly so significant as fin length or tube depth and due to manufacturing requirements, it may be more worthwhile to keep the fin pitch unaltered.

The air velocity provided by the fan or by the velocity of the vehicle moving as the air flows through the radiator, has a substantial effect on the external convection coefficient. As is seen in Figure 5.13, as the velocity of the frontal air is increased, so also is the convection coefficient. However, it is worth noting that the effect of a significant increase in air velocity does not have as large an effect as the fin length. Thus to improve efficiency without

significantly increasing the fan power requirement, the fin geometry may be a better option to investigate.

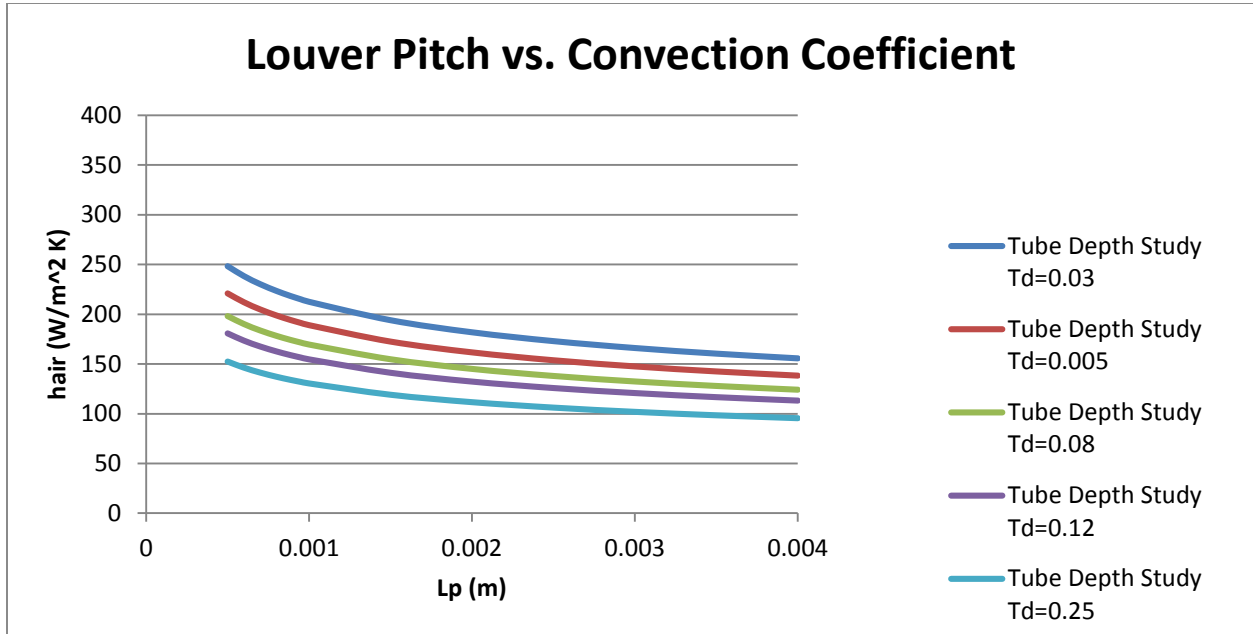


Figure 5.12: Effects of tube depth on the external convection coefficient comparing against louver pitch

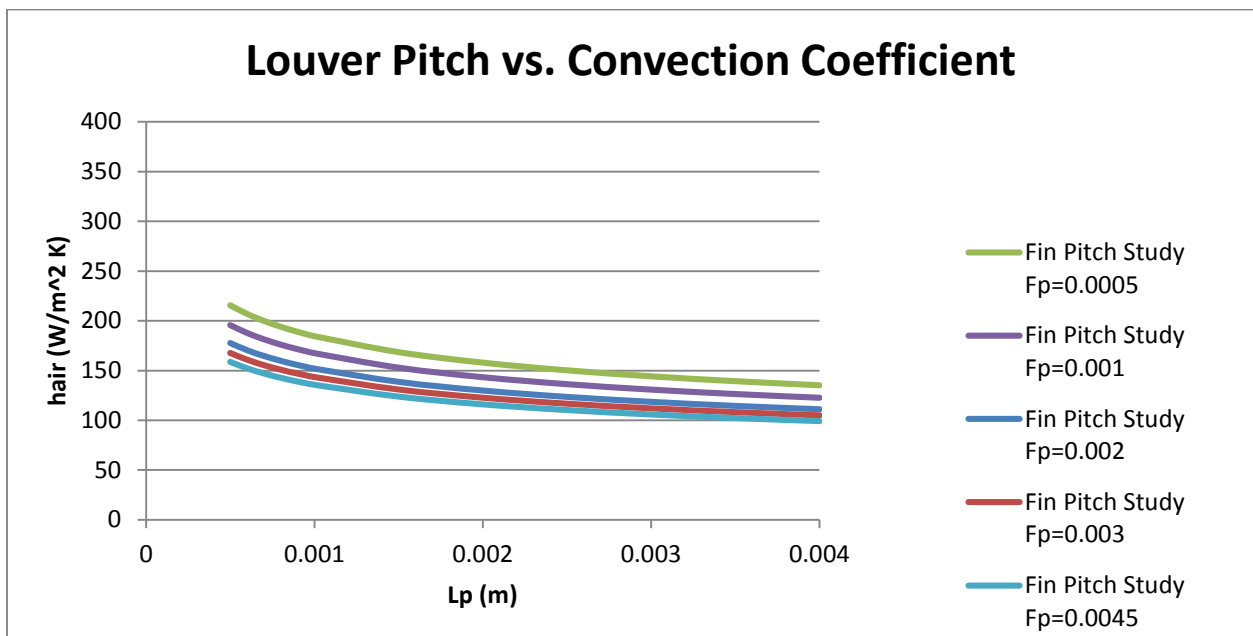


Figure 5.13: Effects of fin pitch on the external convection coefficient comparing against louver pitch

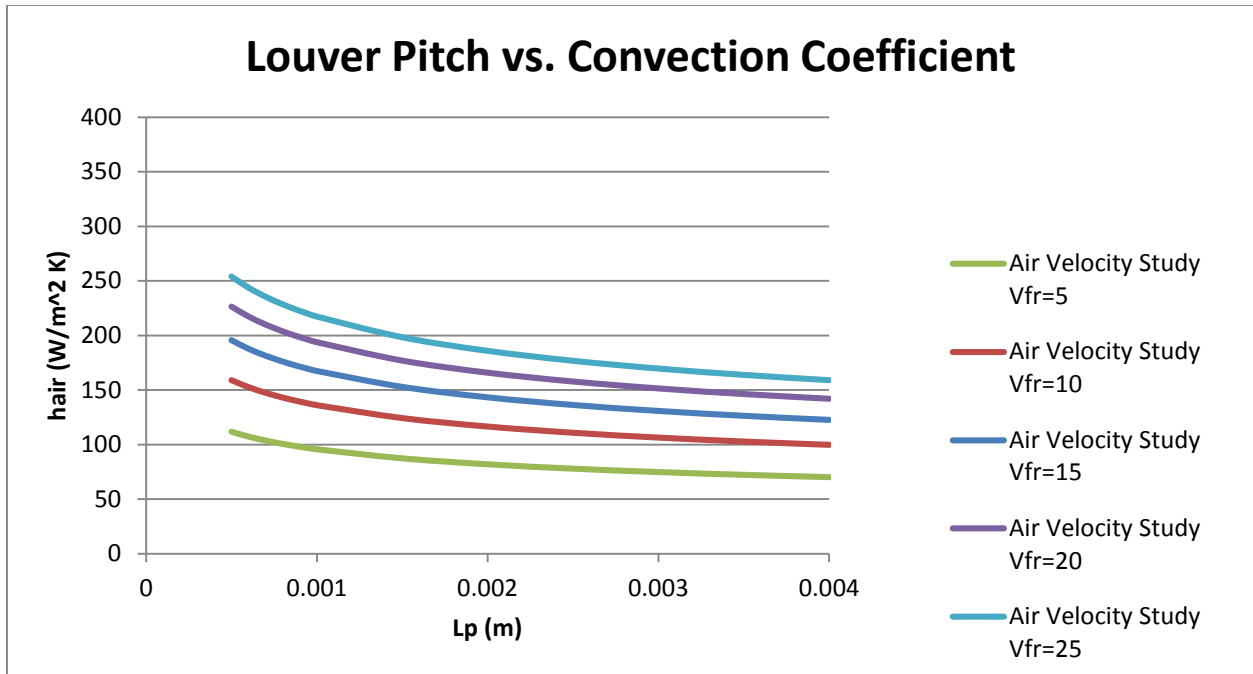


Figure 5.14: Effects of air frontal velocity (from fan) on the external convection coefficient comparing against louver pitch

A quick study on the fin material changing the material from copper to aluminum showed 0.17% increase in fin efficiency, 0.16% increase in fin effectiveness, and 0.11% decrease in total thermal resistance. Thus, a change of fin material would not be beneficial for reducing weight, cost, or improving thermal performance.

5.1.4.2 External Surface Area and External Convection Resistance

The total external convective surface area was found to have a significant (nearly dominant) effect on the external convection resistance. As this is the greatest thermal resistance in the thermal resistance model, the relationship is critical to understand to reduce the total thermal resistance of the unit. As the fins contribute the grand majority of surface area to the total convective surface area, the louver fin geometry becomes increasingly significant. It would be fairly simple to increase the total convective surface area if space were not an issue, however, since the goal of this work is to reduce the size of the radiator, this becomes a significant challenge.

Throughout this study, it was observed that unless h_{air} was significantly increased, a decrease in A would result in a dramatic increase in R_{fin} . As seen in Figure 5.15, the dependence of R_{fin} on A cannot be neglected. This is due to the fact that the original radiator design had a substantial amount of surface area which resulted in a low thermal resistance. In order to decrease the surface area and still maintain a low resistance, h_{air} must be significantly increased.

Figure 5.16 demonstrates the dependency of the external thermal convection resistance, R_{fin} , on h_{air} and the total external surface area, A . Even when h_{air} is high, the dependence on A is significantly greater causing the thermal resistance to decrease if the surface area is sufficiently large. The factors affecting total surface area are largely dependent on the dimensions of the louver fins including Tube Depth, Fin Length, and Fin Pitch. Various studies of the effects of these parameters were performed to determine the optimal configuration.

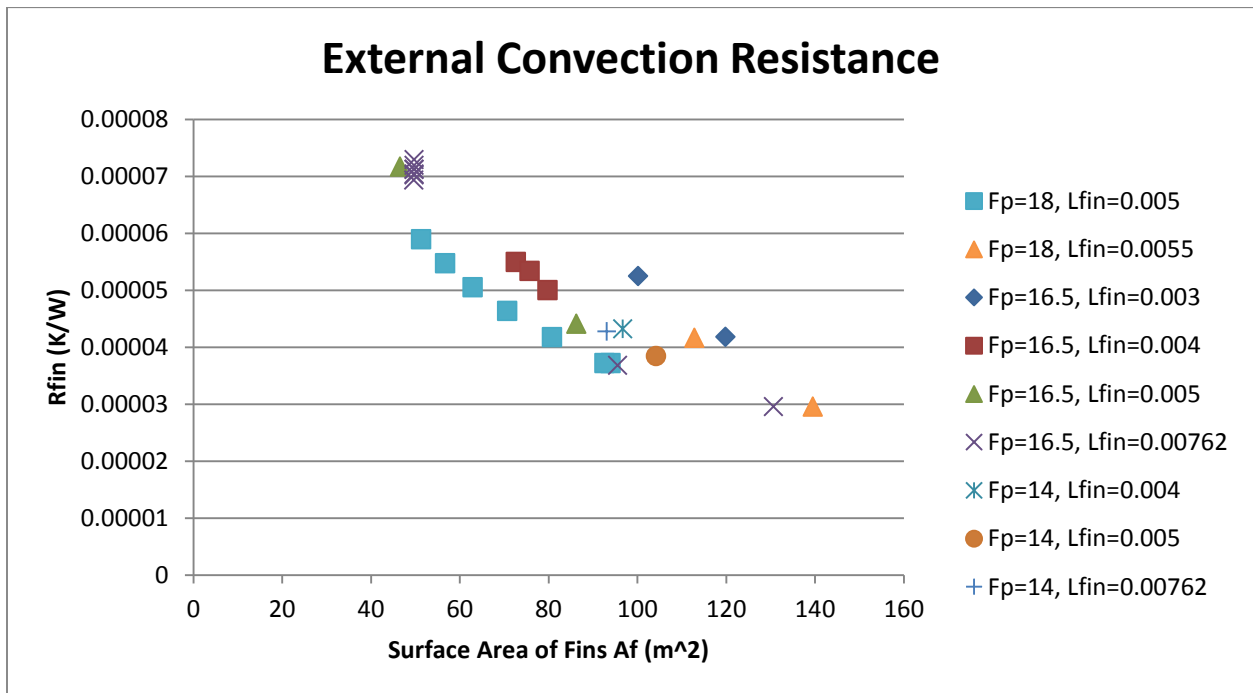


Figure 5.15: Effects of fin surface area on external convection resistance

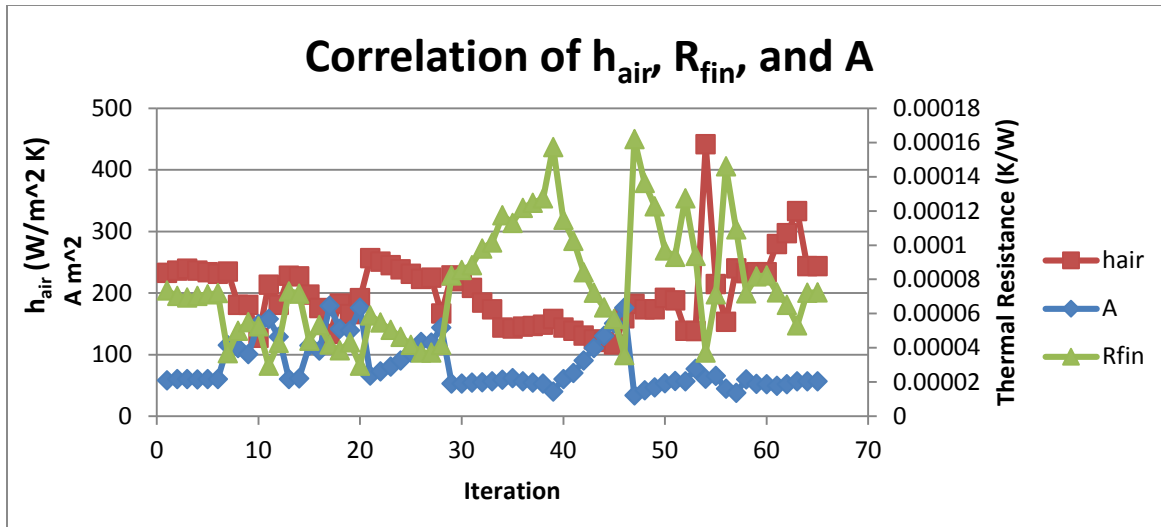


Figure 5.16: Comparison of h_{air} and A to R_{fin}

5.1.5 Air-Side Pressure Drop

A study was performed to see the effects of the fin dimensions and configurations to determine the maximum heat transfer possible with the lowest pressure drop. Due to the complex dependency of pressure drop on the geometric configuration of the radiator, a hypothetical study was not considered. The study was performed on the iterations of the designs to establish the relationships between the different geometrical parameters and the pressure drop. The following are the results of the study.

The fin length was believed to have some effect on the pressure drop as is shown in Figure 5.17. However, the relationship seems to go counter of what intuition would say. Intuitively the pressure drop should decrease if the fin length increased because there would be more free flow area. This is indeed verified with observing Equation (26) and observing that the pressure drop is dependent on the ratio, A/A_0 , or the ratio of total convective surface area to total free flow area. For the fin length, the total surface area increases more significantly than the free flow area causing an increase in pressure. A normalized relationship of A/A_0 against pressure drop is shown in Figure 5.18.

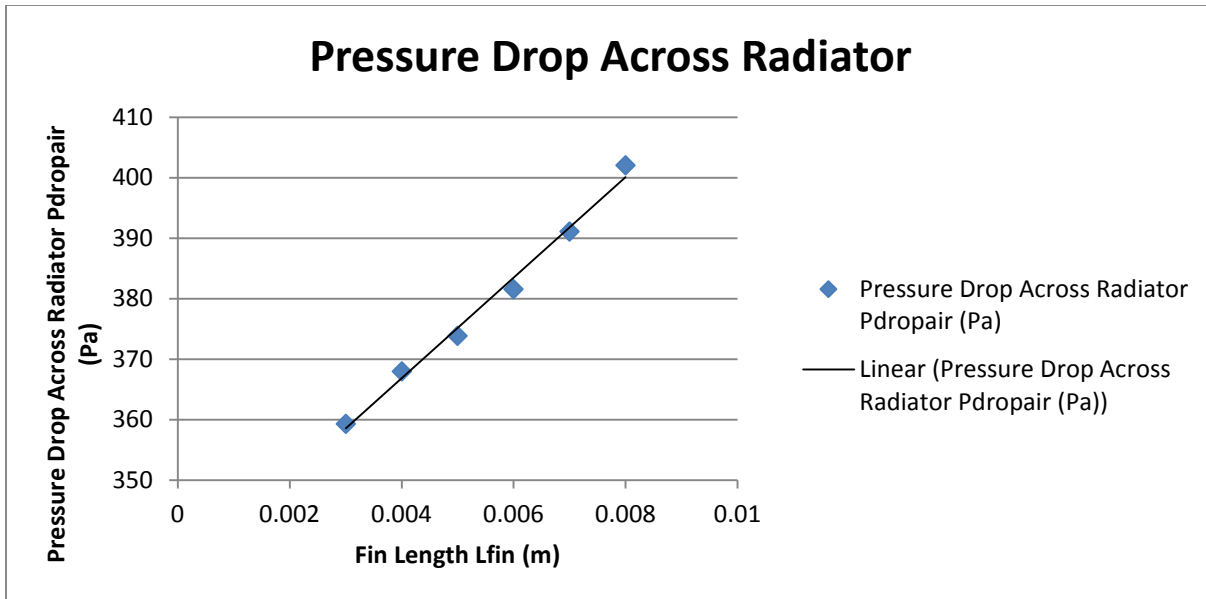


Figure 5.17: Effects of fin length on air-side pressure drop

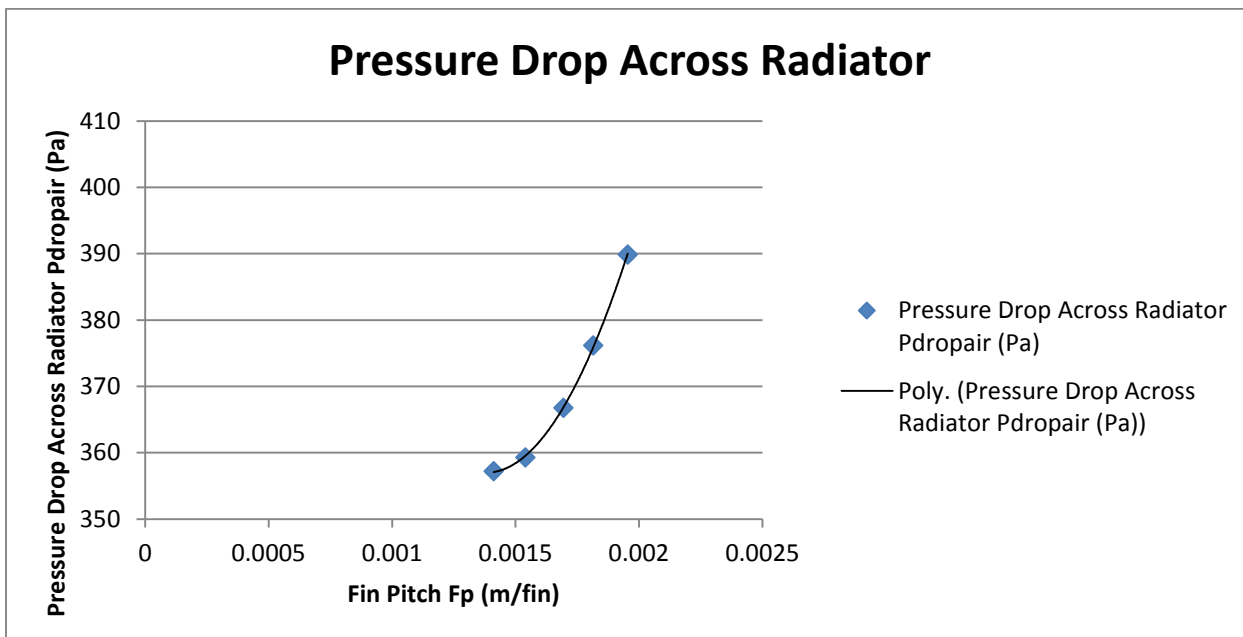


Figure 5.18: Effects of fin pitch on pressure drop

Figure 5.19 is similar to Figure 5.17 in that the relationship seems counter-intuitive. As the fin pitch (the space between fins) decreases, the pressure drop should increase. Once again, Figure 5.20 shows that this is the case with the normalized relationship.

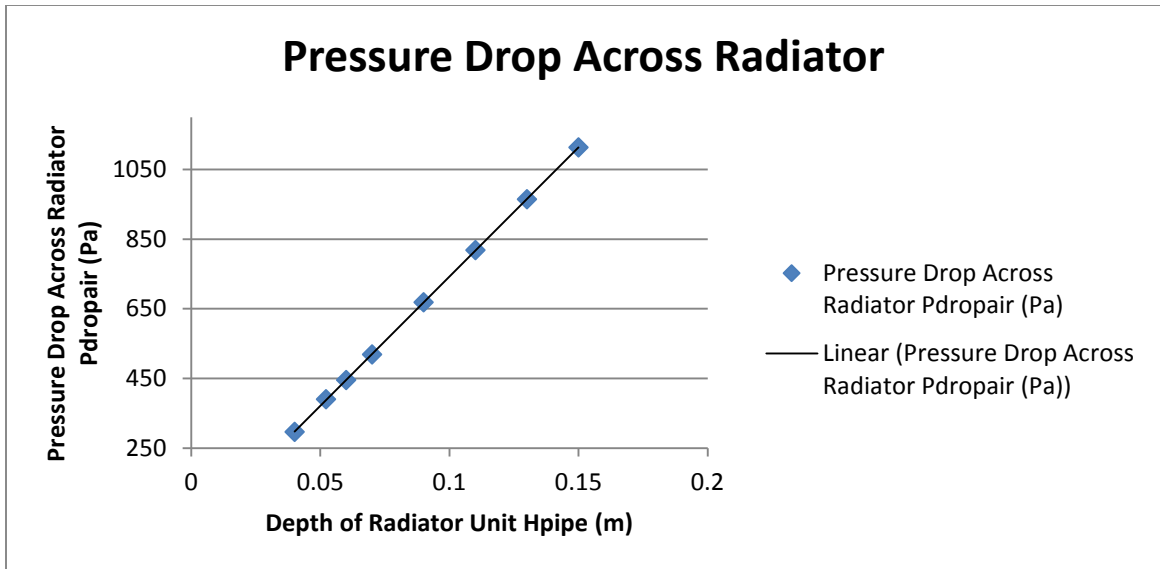


Figure 5.19: Effects on tube depth on pressure drop

Figure 5.20 shows that there is a strong relationship between the tube depth and the pressure drop. This was again verified in the normalized relationship found in Figure 5.22. To reduce the frontal area, the tube depth could be an alternate dimension to increase to retain total surface area. However, with a sharp pressure drop increase, the increase in tube depth may be too costly in terms of fan power requirements. Thus more iterations were performed to determine the optimal design of the relationship between pressure drop and heat transfer for the air-side conditions.

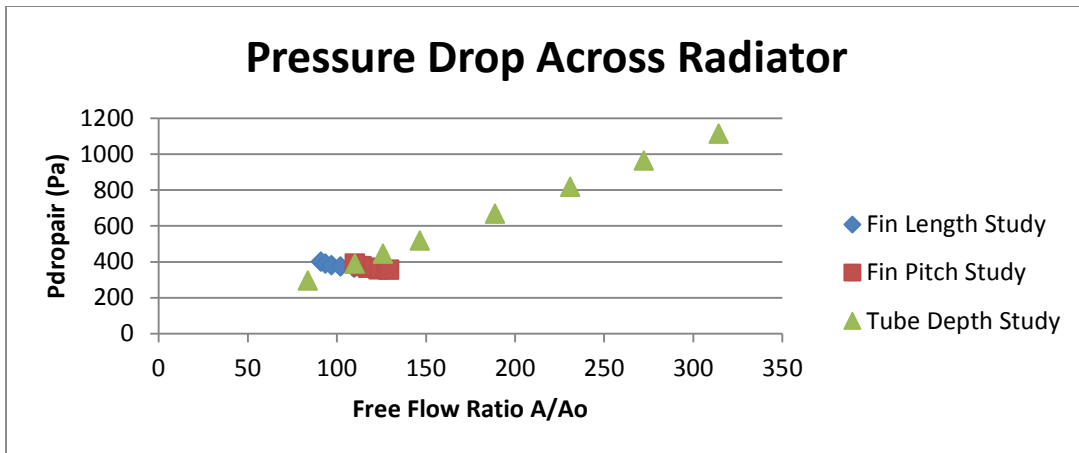


Figure 5.20: Effects of fin pitch, fin length, and tube depth on pressure drop using normalized relationship

5.1.6 Auxiliary Power and Heat Transfer

In order to accurately identify a valid solution or an improvement to the design, certain criteria need to be considered. These criteria include the overall heat transfer of the radiator, the pumping power required for the coolant, and the fan power needed to cool the radiator. The fan is an auxiliary that is regulated by a thermostat on the radiator unit. Although the fan will not always be running (the design intent), the study will consider the maximum operating conditions to over-design against failure possibilities.

By considering the fan power and pumping power to be a combined auxiliary power, this parameter can be used in finding a critical relationship. The total heat transfer possible is characterized by the following equation:

$$Q_{max} = \epsilon C_{min}(T_{in} - T_{enter}) \quad (34)$$

Where ϵ is the heat exchanger effectiveness defined by

$$\epsilon = 1 - \exp\left\{-\frac{1}{c}[1 - \exp(-c NTU)]\right\} \quad C_{max} \text{ unmixed}, C_{min} \text{ mixed} \quad (35)$$

where $c = C_{min}/C_{max}$ and $C_{min} = C_c = \dot{m}_{air} c_{p,air}$ and $C_{max} = C_h = \dot{m} c_p$. NTU represents the number of transfer units and is defined as

$$NTU = \frac{UA}{C_{min}} = \frac{1}{C_{min} R_{total}} \quad (36)$$

The result provides the maximum amount of heat possible. These parameters can be compared against each other forming a powerful comparison as is seen in Figure 5.23. In this figure, it is easy to discern that the desirable range of values would be those with greater heat transfer abilities and less than or equal auxiliary power than the original radiator design. As can

be seen, there are several options that fit both these criteria. However, the other goal is to decrease the frontal area as much as possible. Comparing the charts next to each other, one can determine which design is most preferable is that with the lowest frontal area that still meets the auxiliary power and heat transfer requirements.

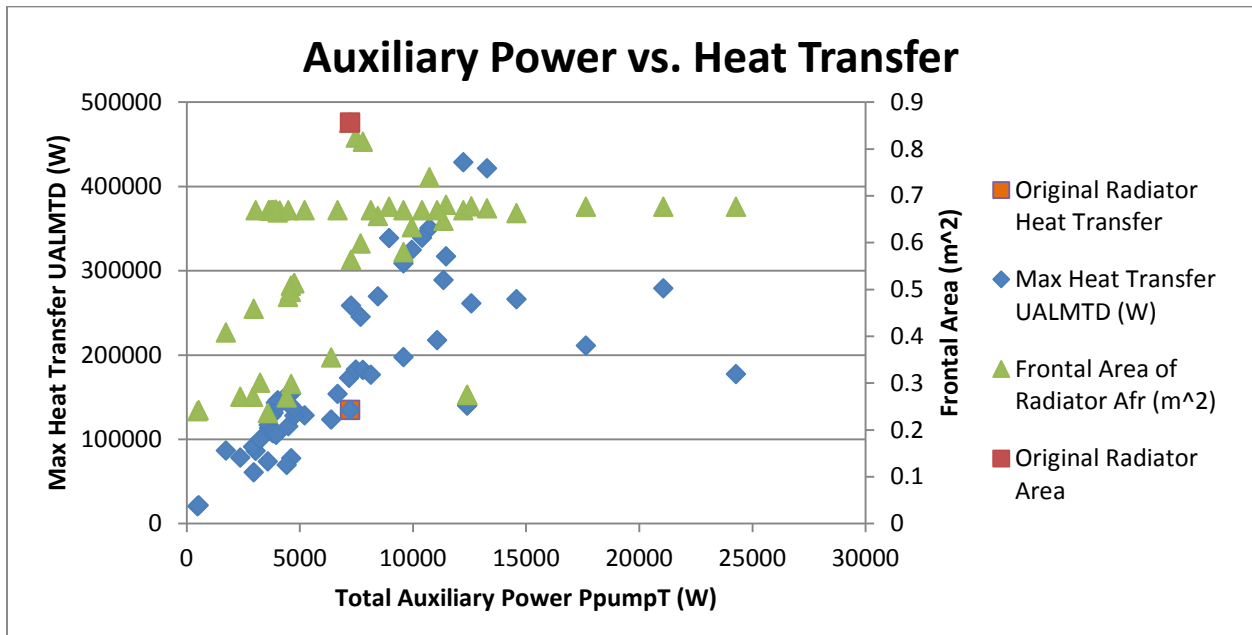


Figure 5.21: Comparison of total heat transfer and auxiliary power. Also, a comparison to the frontal area and auxiliary power is given to determine the optimal solution.

5.1.7 Energy Cost/Benefit Analysis

One interesting discovery is that the fan power is generally greater than the pumping power for the radiator. This is because the fan is required to operate with a higher mass flow rate than is the pump. Thus, in order to decrease the auxiliary power, decreasing the fan power is most beneficial. A fortunate correlation is that a decrease in frontal area also means a decrease in fan size. So long as the pressure drop across the air-side of the radiator is not significantly greater than the original design, a simple reduction in frontal area equates to a decrease in fan power needed. If the pressure drop can also be reduced by varying the geometry and maintaining the needed heat transfer, the auxiliary power will be reduced.

With a smaller frontal area, the drag on the vehicle may also be reduced. If this is in addition to a decrease in auxiliary power and an increase in heat transfer ability, the overall re-design process of the radiator will have been successful. A study of the aerodynamic drag reduction associated with the frontal area is outside the scope of this research. This is due to the fact that the overall geometry of the vehicle will determine the actual drag and the size of the radiator may have little effect on the drag depending on the geometry and aerodynamics of the vehicle. A reduction of frontal area simply allows for the aerodynamics drag to possibly be decreased.

5.2 Optimization of Model

With the goals of the research defined and the parameters of variability selected, an optimization of the radiator design is required. By utilizing the relationships found in the various aforementioned studies, an optimization of the geometry may unfold. Each iteration considered the effects of the changes and compared them to the theoretical predictions. The results were then analyzed and used again for an additional iteration. In total there were over 70 iterations to determine the optimal design of the heat exchanger based on the parameters of Maximum Heat Transfer Possible, the Auxiliary Power, and the frontal area. Several potential solutions were identified and then analyzed further.

5.2.1 Geometry

The solutions found through the optimization process led to a number of different geometric configurations. These designs were then filtered by first observing all the designs that complied with the heat transfer and auxiliary power requirements. Then the designs were compared against each other for frontal area. Finally, by looking at the decrease in height and maximum heat transfer, the following designs were selected as possibilities.

Table 5.1: Comparison of radiator designs

Parameter Name	Symbol	Units	Original Radiator	Design Flat 3.0	Design Square 1.0
Tube Type	<i>Type</i>		Flat	Flat	Square
Height of Radiator Unit	<i>L</i>	mm	933.45	680	700
Width of Radiator Unit	<i>W</i>	mm	917.62	634	721.62
Depth of Radiator Unit	<i>Td</i>	mm	52.44	100	76.7
Mean Diameter	<i>Dm</i>	mm	2.38	1.50	1.90
Hydraulic Diameter	<i>Dh</i>	mm	2.90	2.19	1.50
Tube Thickness	<i>t</i>	mm	0.45	0.20	0.20
Perimeter of Tube	<i>P</i>	mm	101.94	198.71	6.00
Number of tubes	<i>Npipe</i>		91	40	75
Louver Fin Length	<i>Lf</i>	mm	7.77	14.00	7.62
Louver Fin Pitch	<i>Fp</i>	mm	1.54	1.54	1.49
Louver Length	<i>Ll</i>	mm	5.77	13.00	6.62
Louver Pitch	<i>Lp</i>	mm	0.861	0.857	0.865
Fin Thickness	δf	mm	0.10	0.10	0.10
Louver Angle	θ	°	30	30	30
Tube Pitch	<i>Tp</i>	mm	10.00	15.50	9.52
Total Surface Area	<i>A</i>	m ²	68.877	63.782	60.304
Free-Flow Area	<i>Ao</i>	m ²	0.57397	0.39144	0.40665
Frontal Area	<i>Afr</i>	m ²	0.85655	0.43112	0.50513

5.2.2 Design Improvements

The radiator design was improved in some parameters such as the maximum heat transfer and the frontal area. However, there was difficulty in reducing the frontal area of the radiator without losing the heat transfer benefits. Since the radiator has a substantial amount of surface area, reducing the frontal area without reducing the surface area required that the radiator depth be increase or the fin pitch tightened. These parameters increase the flow resistance of air across the radiator. Thus, in order to improve heat transfer and reduce frontal area, higher flow rate of air is required and this results in an increase in pressure drop and pumping power.

Table 5.2: Results of design improvements made

Parameter Name	Symbol	Units	Original Radiator	Design Flat 3.0	Design Square 1.0
Total Resistance	R_{totalc}	K/W	1.15E-04	-23%	-2%
Height of Radiator Unit	L	mm	933.45	-30%	-30%
Width of Radiator Unit	W	mm	917.62	-31%	-21%
Depth of Radiator Unit	Td	mm	52.44	129%	62%
Frontal Area of Radiator	A_{fr}	m ²	0.857	-52%	-45%
Pressure Drop	Δp	Pa	8563	41%	40%
Pumping Power	P_{pump}	W	59.4	38%	40%
Pressure Drop Across Radiator	Δp_{air}	Pa	564	402%	439%
Fan Power	P_{fan}	W	7153	299%	525%
Number of Transfer Units	NTU		0.684	64%	-12%
Heat Exchanger Effectiveness	ϵ_o		0.437	35%	-9%
Max Heat Transfer/Pumping Power	$Q_{max}/P_{auxiliary}$	W/K/W	19.40	-73%	-83%
Max Heat Transfer	Q_{max}	W	139940	7%	5%
Total Pumping Power	$P_{auxiliary}$	W	7212	296%	521%
Total Fluid Volume in Pipes	V_{pipe}	m ³	0.006211	-45%	-22%
Exit Coolant Temperature	T_{out}	K	323.17	0%	0%
Exit Air Temperature	T_{exit}	K	314.81	-1%	0%
Drag Power	P_{Drag}	W	32.27	-60%	53%
Volumetric Heat Transfer	Q_{max}/V_{pipe}	W/m ³	3115473	-3%	17%

The results of Table 5.2 suggest that the reduction of frontal area can be achieved up to 52%. This is also with an heat transfer enhancement of 7% but the cost to this gain is 296% increase in auxiliary power. This is compared to the 60% reduction in drag-related power but for a 500hp engine with an initial auxiliary power of 7212 W (9.7 hp) a 60% reduction in drag power (0.04 hp) is not worth a 296% increase (29.0 hp) in auxiliary power. More fuel would be spent running the cooling module than what would be saved with the reduction of frontal area.

5.3 CFD Verification

In order to confirm the findings from the calculations, (that heat transfer can be improved with microchannels but not without an increase in pressure drop) some kind of experiment is

required. Although the computational method has demonstrated that there is a theoretical improvement, the method of performing the iterations is subject to error. Therefore, a further validation of the design is necessary. This can be made possible in two ways: physical testing of the model or computational fluid dynamic (CFD) modeling verification. The more preferable and accurate method is to test the physical model at simulated operating conditions. This however, requires many resources such as a testing facility, the manufactured model for testing, and long hours of logging data. This can be expensive in terms of time, costs, and resources. The alternative is to construct several simplified CFD models to demonstrate that the design changes do in fact improve the current design.

5.3.1 Microchannel Tubes

Three CFD models were created to directly compare the performance of the original flat tube against a multiport extrusion microchannel slab with round channels and a multiport extrusion microchannel slab with square channels. The three models are equal in length and in external surface area and are subject to the same boundary conditions with are seen in figures 29-31. The models were designed for the same total mass flow rate through the tube geometry. A constant temperature wall boundary was applied to one of the thin faces to simulate the leading edge of the heat exchanger in the free stream. A convective wall boundary condition was applied to one face with the same coefficient defined for each model which was derived from testing of the actual model. The models were created for only half of each tube, applying a symmetry plane to the filled-channel face. The original flat tube, as is seen in Figure 5.22, was modeled only as a fluid body with wall boundary conditions surrounding the geometry with a conductive shell of 0.45 mm. For the microchannel models, both fluid and the microchannel slab were modeled together in order to see conductive effects through the microchannels. Each model was simulated

with a fine and a coarse mesh in order to verify results by means of a mesh-independent study.

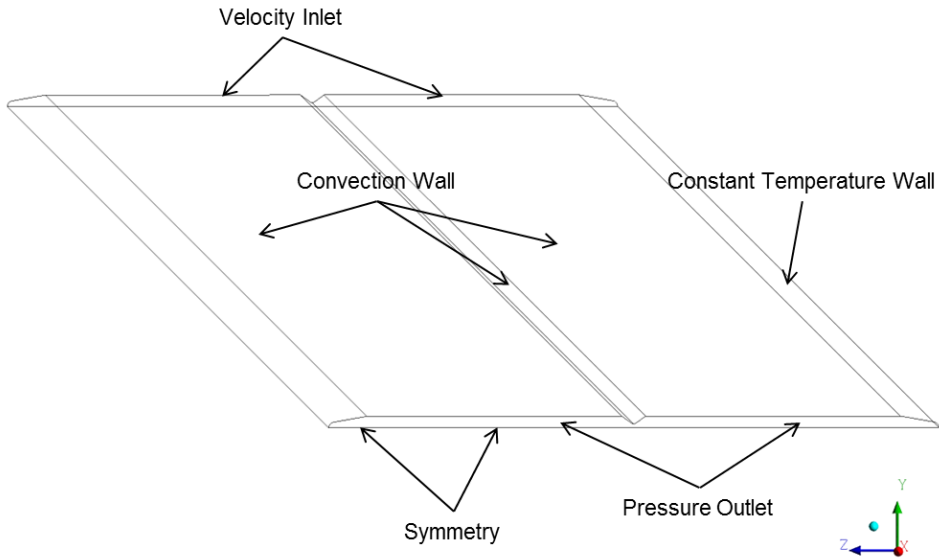


Figure 5.22: CFD model and boundary conditions for original flat tube, round microchannel slab and a square microchannel slab

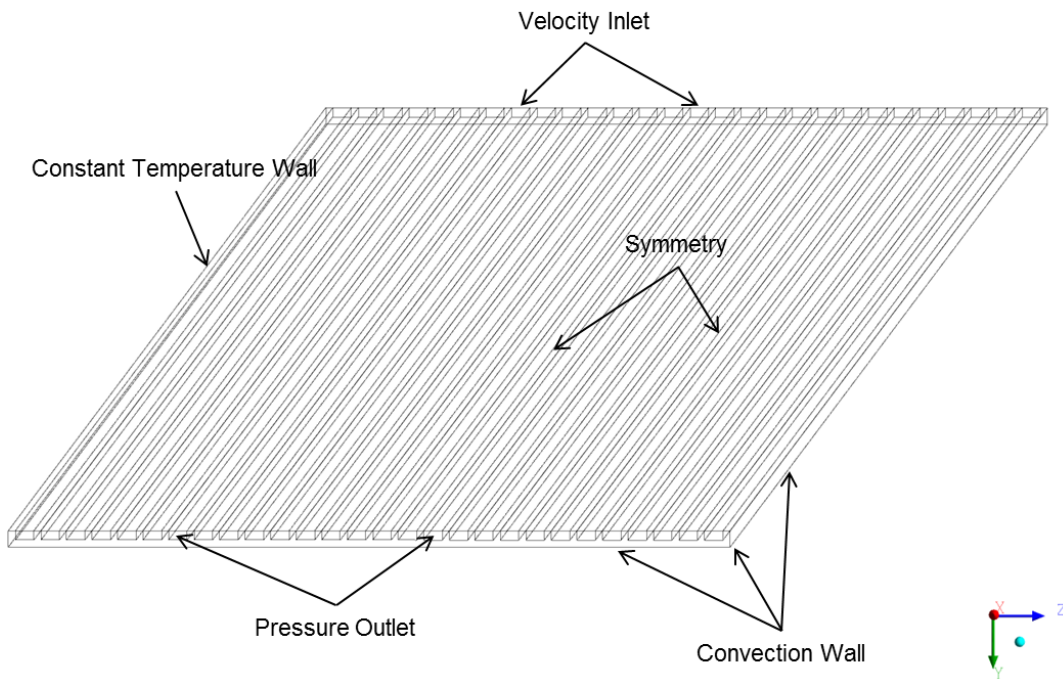


Figure 5.23: CFD model with boundary conditions for microchannel square tube slab

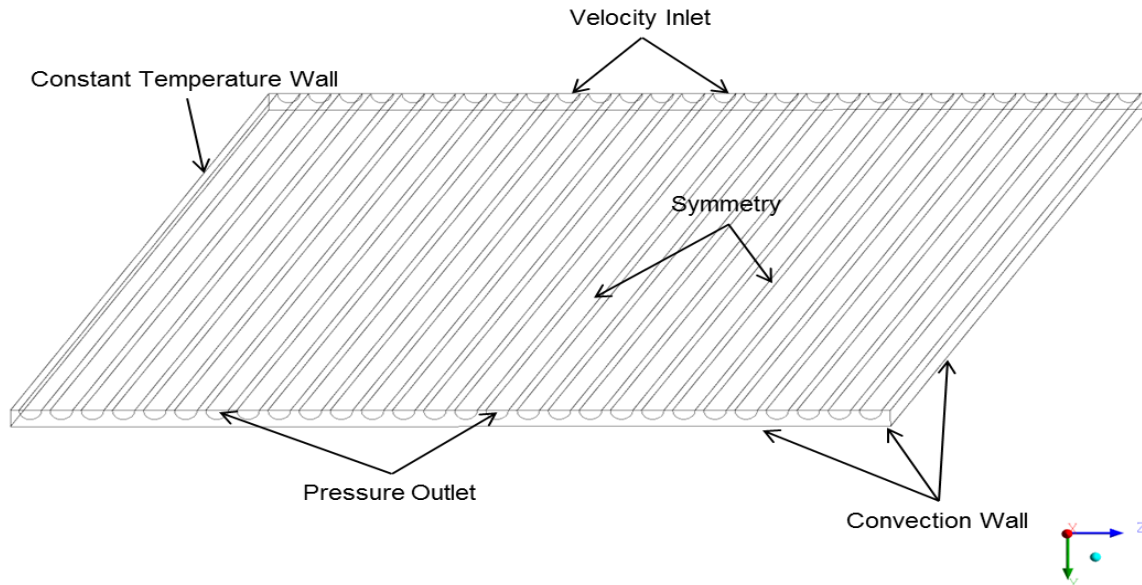


Figure 5.24: CFD model with boundary conditions for microchannel round tube slab

The results of the simulation show that microchannels can enhance the heat transfer as is characterized by the outlet temperature of the tube, but the pressure drop is significant.

Table 5.3: Results of CFD simulation for mass flow average temperature at outlet

Test	CFD (K)	Calc (K)	% Diff (CFD-Cal)/CFD	% Diff (CFDF-CFDC)/CFDF
Original Tube Coarse	325.461	323.414	0.633	0.110
Original Tube Fine	325.102	323.414	0.522	
Square MC Tube Coarse	323.472	321.958	0.470	0.029
Square MC Tube Fine	323.377	321.958	0.441	
Round MC Tube Coarse	322.958	321.692	0.393	0.768
Round MC Tube Fine	320.495	321.692	0.373	

Table 5.4: Results of CFD simulation for pressure drop across tubes

Test	CFD (Pa)	Calc (Pa)	% Diff (CFD-Cal)/CFD	% Diff (CFDF-CFDC)/CFDF
Original Tube Coarse	6357	8563	34.7	4.7
Original Tube Fine	6673	8563	28.3	
Square MC Tube Coarse	49760	38209	23.2	21.2
Square MC Tube Fine	63110	38209	39.5	
Round MC Tube Coarse	10550	61942	48.7	47.2
Round MC Tube Fine	19990	61942	210	

Table 5.5: Results of simulation for convection heat transfer coefficient

Case Name	h_{CFD} (W/m ² K)	h_{calc} (W/m ² K)	%difference
Original Flat Coarse	5814.625	6631.17	14%
Original Flat Fine	5734.478	6631.17	16%
Square Microchannel Coarse	6242.607	7546.652	21%
Square Microchannel Fine	7546.652	1823.76	76%
Round Microchannel Coarse	12038.64	9148.21	24%
Round Microchannel Fine	10019.42	9148.21	9%
Louver Fin Original	274.0524	249.393	9%

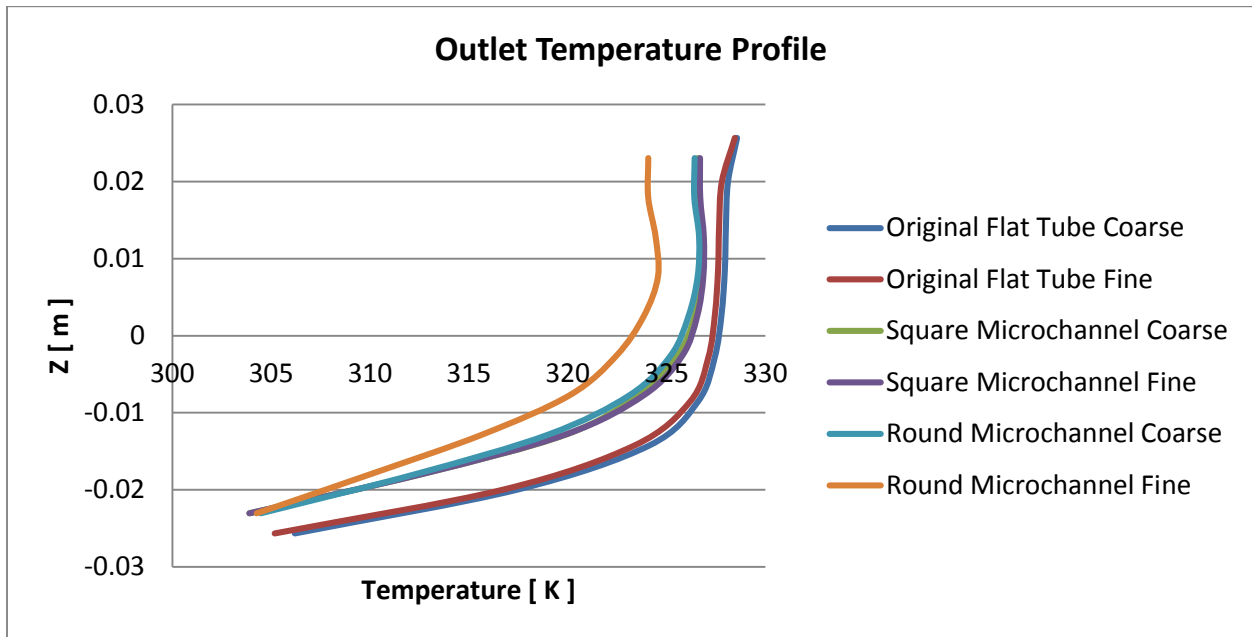


Figure 5.25: Temperature profile at the tube outlet

The study conducted using computational fluid dynamics verified the theory that the heat transfer may be enhanced with microchannels. The study also verified that the pressure drop through the microchannel tubes is significantly higher than the flat tube design. Therefore, it is not recommended to use the microchannels since the pressure drop will have an adverse effect on power consumption and little gain with heat transfer. Further results of CFD simulation can be seen in Appendix B.

5.3.2 Fin Geometry

A CFD verification model for the fin geometry is proposed in order to demonstrate that the new geometry does in fact improve the heat transfer of the unit. This will be done by first creating a model to simulate the original design. This is done to accurately compare the results of the CFD simulations as the results of the simulation may not match the results of the calculations.

The CFD model will consist of two louver fins inside of a 3-dimensional control volume with applied boundary conditions as follows: vertical side planes are walls with a constant temperature applied, the top and bottom planes are symmetric boundary conditions, the front face is a velocity inlet, while the rear face is a pressure outlet. This can be seen in Figure 5.26.

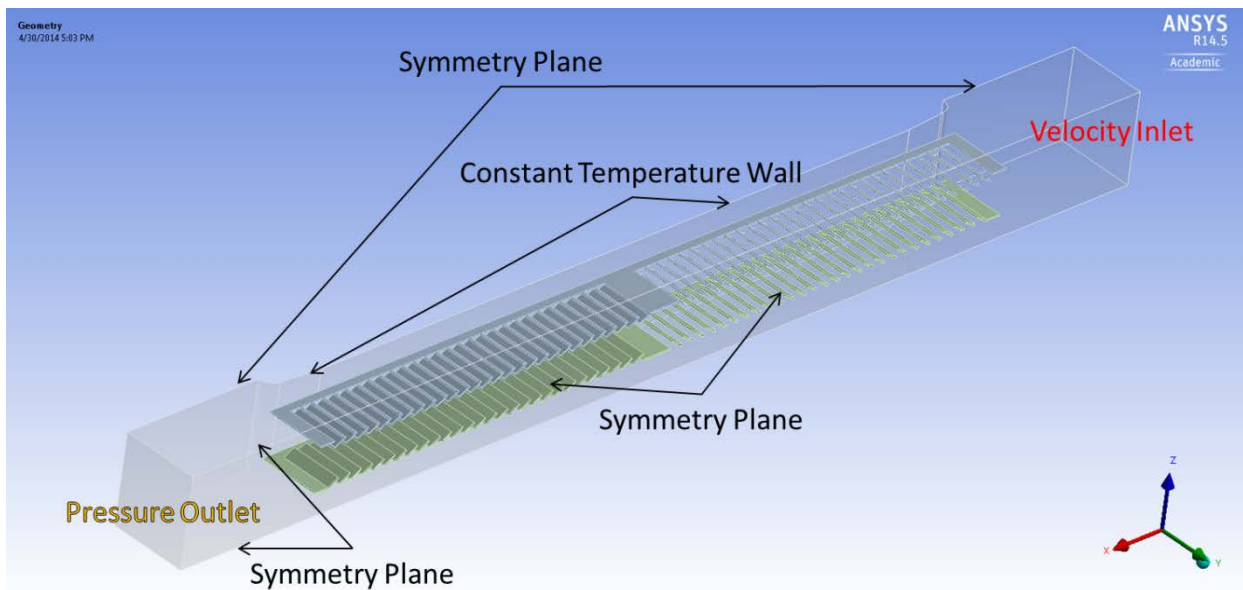


Figure 5.26: CFD model of original fin geometry

The CFD model was used to compare the heat transfer and pressure drop of two different fin geometries. The original fin geometry barely meets the length criteria for the correlation presented by Chang and Wang [16] on louver fin geometry. The proposed fin design is well outside of the range for the specified conditions, however, extrapolating the relationship to a

longer fin suggests that a wider and longer fin is capable of providing sufficient heat transfer to extend the radiator depth-wise without causing a significant pressure drop. Thus a CFD simulation can be utilized to verify this fact. Figure 5.27 demonstrates the new fin design as it is longer and slightly wider than the original fin.

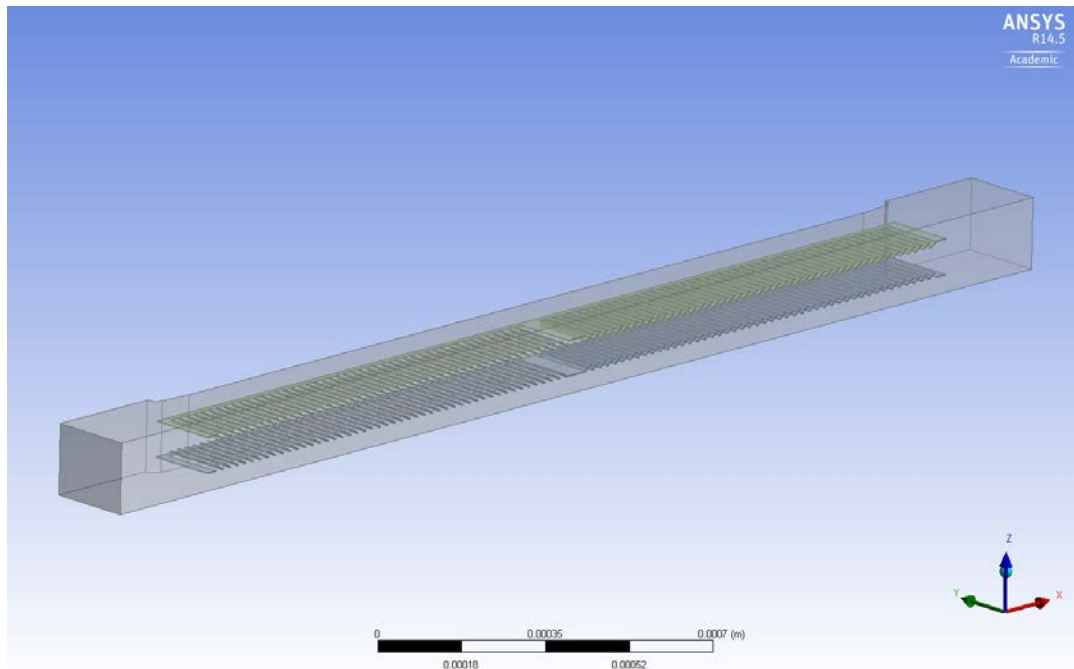


Figure 5.27: CFD model of proposed new fin geometry

The results of the model of the original fin can be seen in the volume rendering below in Figure 5.28. The results of the louver fin case agreed with the theoretical predictions within 9% for the heat transfer. Due to the simplification of the model the pressure drop is severely under-predicted by the CFD model. This is due mainly to the geometrical configuration of the CFD model and the fact that the stagnation pressure at the tube tip is not fully captured by the model.

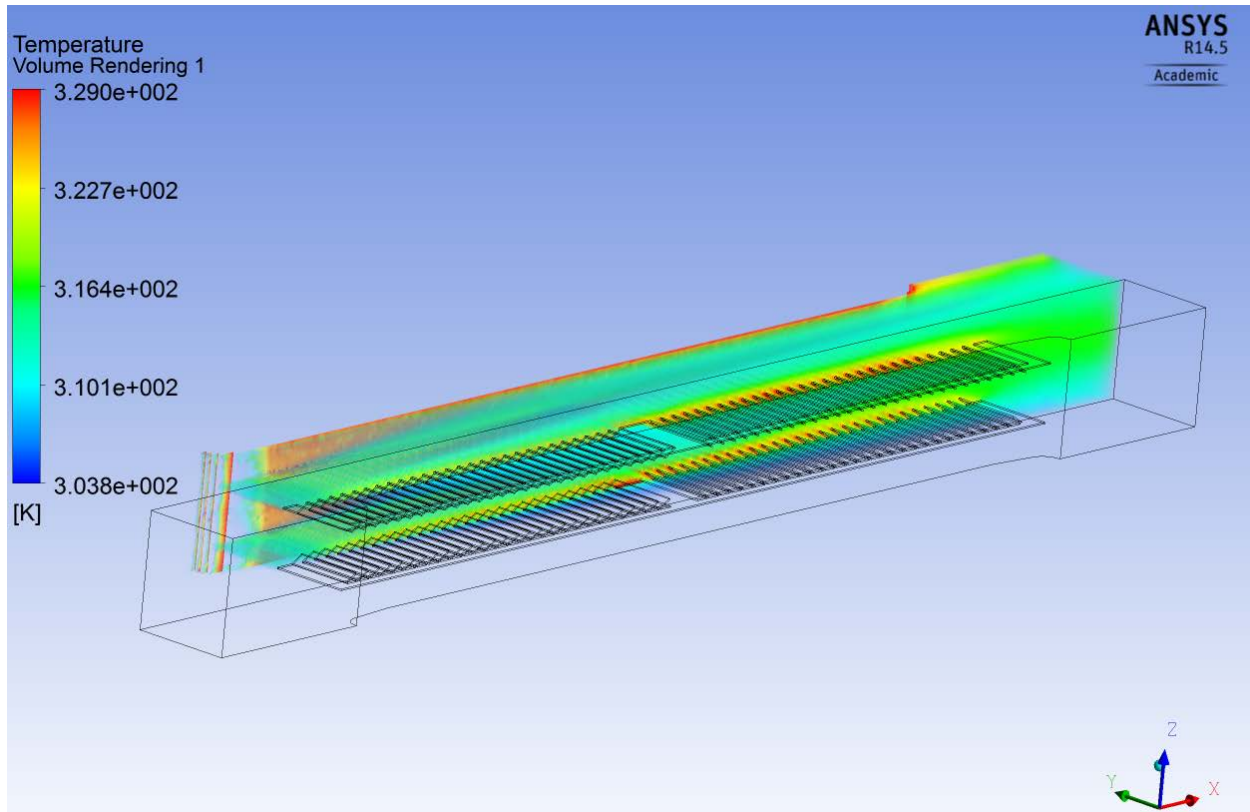


Figure 5.28: Volume rendering of fluid temperature of the original fin as a result of heat transfer from the wall through the fin and into the free stream air.

The new fin was modeled and the results can be seen in Figure 5.29. As can be seen, a wider fin does in fact allow more heat to transfer and reduces the fin temperature by transferring more heat to the air.

Table 5.6: Dimensions of fin geometry

Symbol	Dimension Description	Original Fin	New Fin	Units
L	Axial length of tube. In this study the length is the height of the radiator	933.45	933.45	mm
W	Total width of the radiator	907.62	903.56	mm
T_d	Tube depth. For this study the tube depth is the same as the fin depth and the depth of the radiator	52.24	85.0	mm
D_m	Mean diameter or Tube width	2.38	2.38	mm
A_c	Cross sectional area of tube	73.116	122.665	mm ²
F_L	Fin length	8.45806	12.0	mm
t	Tube thickness	0.45	0.45	mm
P	Internal tube perimeter	102.30	168.20	mm

N_{pipe}	Number of tubes	91	62	tubes
F_p	Fin pitch	1.539	1.539	mm
L_l	Louver length	7.26	11.0	mm
L_p	Louver pitch	0.861	0.861	mm
δ_f	Fin thickness	0.080	0.080	mm
θ	Louver angle	30	30	°
T_p	Tube pitch (Fin Length + Dm)	10.838	14.38	mm
N_{LFin}	Number of louver fins per fin	56	94	
A	Total air side convective heat transfer surface area (fins and tubes)	58.406	95.111	m ²
A_i	Internal surface area of tubes	8.690	9.734	m ²
A_o	Total free flow area for air	0.6514	0.7076	m ²
A_{fr}	Frontal area of radiator ($L \times W$)	0.857	0.843	m ²
D_h	Hydraulic diameter of tubes $D_h = (4A_c)/P$	2.86	2.92	mm

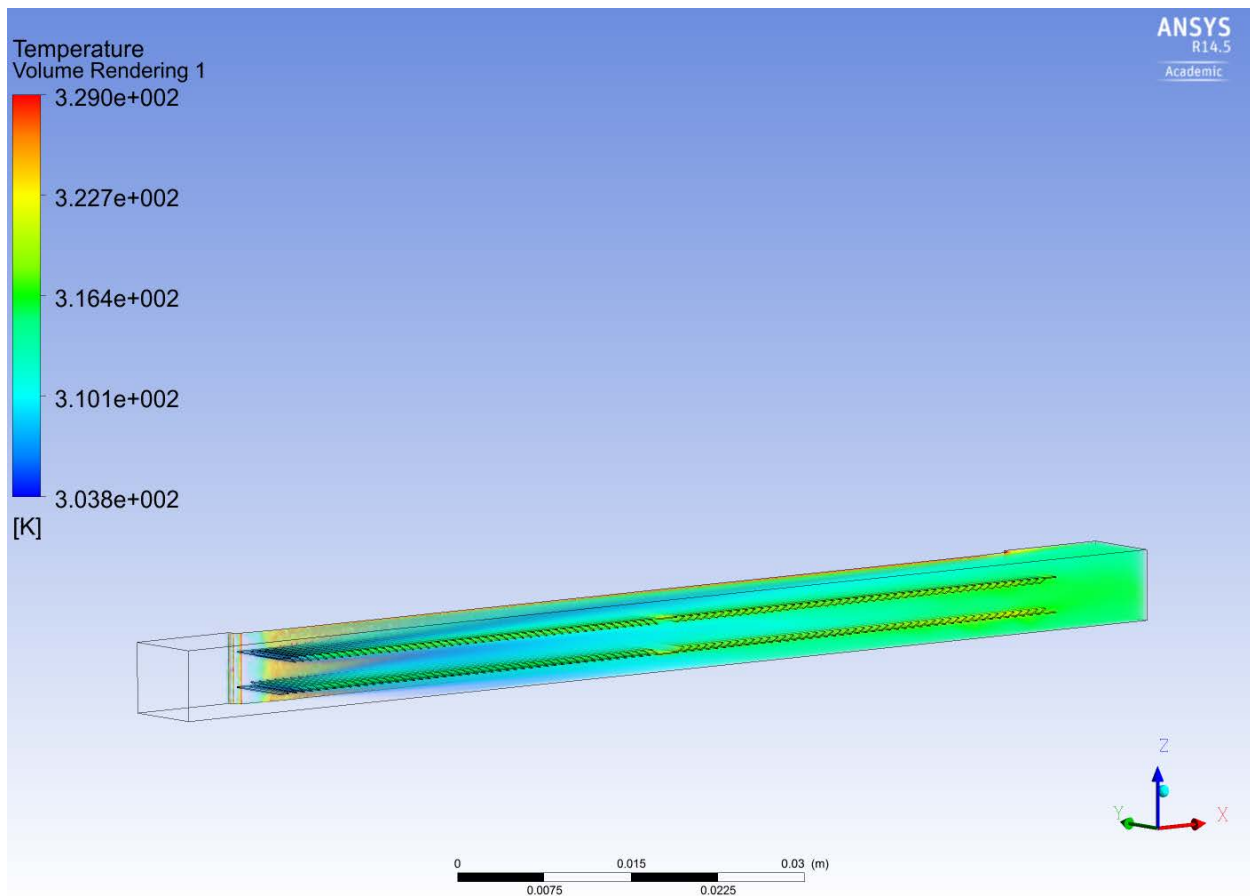


Figure 5.29: Volume rendering of new fin

The pressure drop for the models was measured and compared with calculated values as can be seen in Table 5.7.

Table 5.7: Pressure drop across louver fin geometries

Model	CFD (Pa)	Calc (Pa)	% Diff (CFD-Cal)/CFD
Louver Fin Original	873.78	564.47	35.4%
New Louver Fin	3584	2101	41.4%

Although the heat transfer is improved with the new fin, the material cost, weight, and size can also increase as well as having more pressure drop across the radiator. Therefore, a larger fin would not be beneficial.

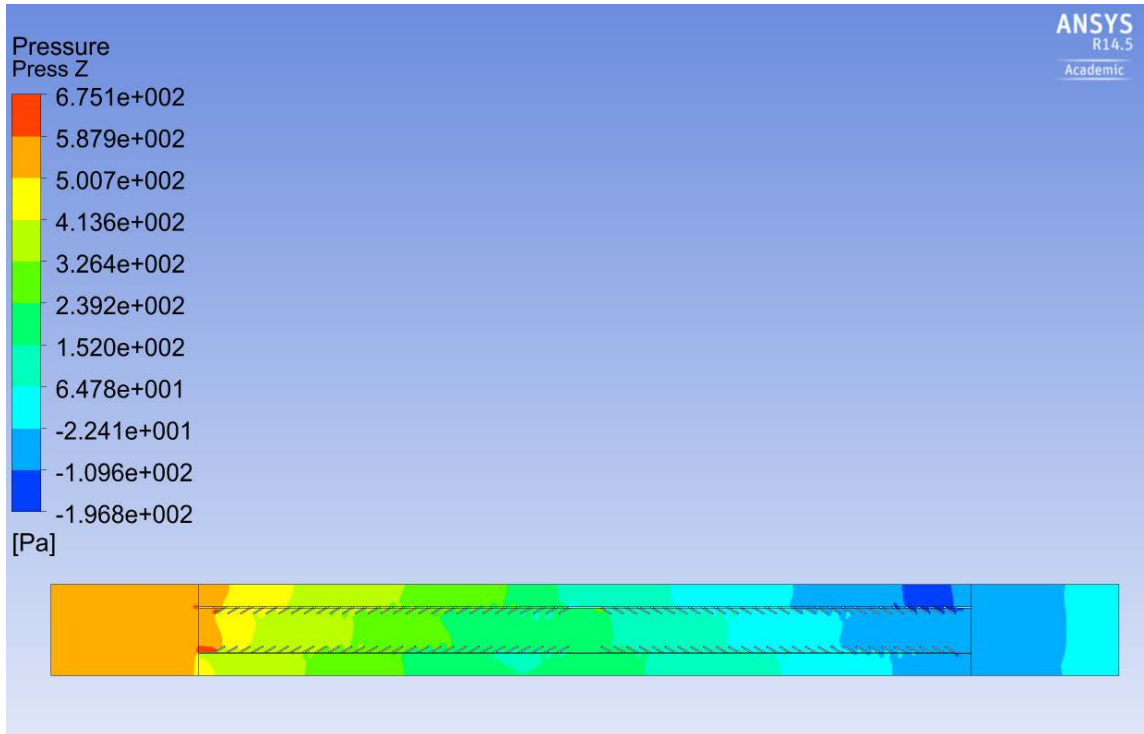


Figure 5.30: Pressure profile of original fin

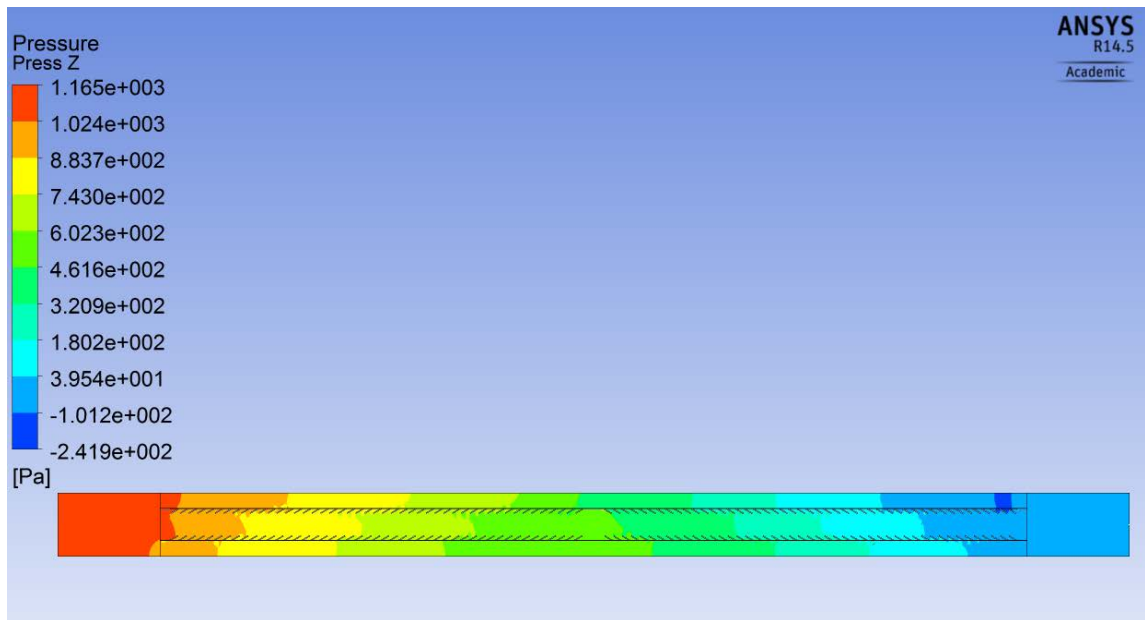


Figure 5.31: Pressure profile of new fin

CHAPTER 6

CONCLUSION

6.1 Design Improvements

This study investigated the application of microchannel technology into an automotive radiator. It was found that microchannels do have the potential to enhance heat transfer but are highly restrictive due to the extreme pressure drop that is developed through the microchannel tubes for almost any flow. It was observed that microchannels containing laminar flowing fluid exhibit a constant thermal resistance that is undesirable for heat transfer. Flat tubes were found to be more successful for heat exchangers needed for transferring large amounts of heat at a rapid rate. Therefore, although microchannels can be used in automotive radiator applications, they are not recommended due to the high pressure drop that results.

The design of the radiator was somewhat improved by focusing on the fin configuration. With the goal being to reduce the frontal area comes the challenge of both a reduction of potential air-flow for cooling and a high restriction on required surface area. The goal of the new heat exchanger design is to transfer more or at least as much heat from the cooling fluid to the air as effectively as possible. If the air flow is significantly increased, the maximum heat transfer rate may still be maintained. This may be done using a fan that is almost constantly running or shuts off at high speeds.

The total auxiliary power can be reduced by careful design of the radiator respecting the total surface area and flow restrictive geometry. The area reduction that resulted from this study can more be seen in Figure 6.1.

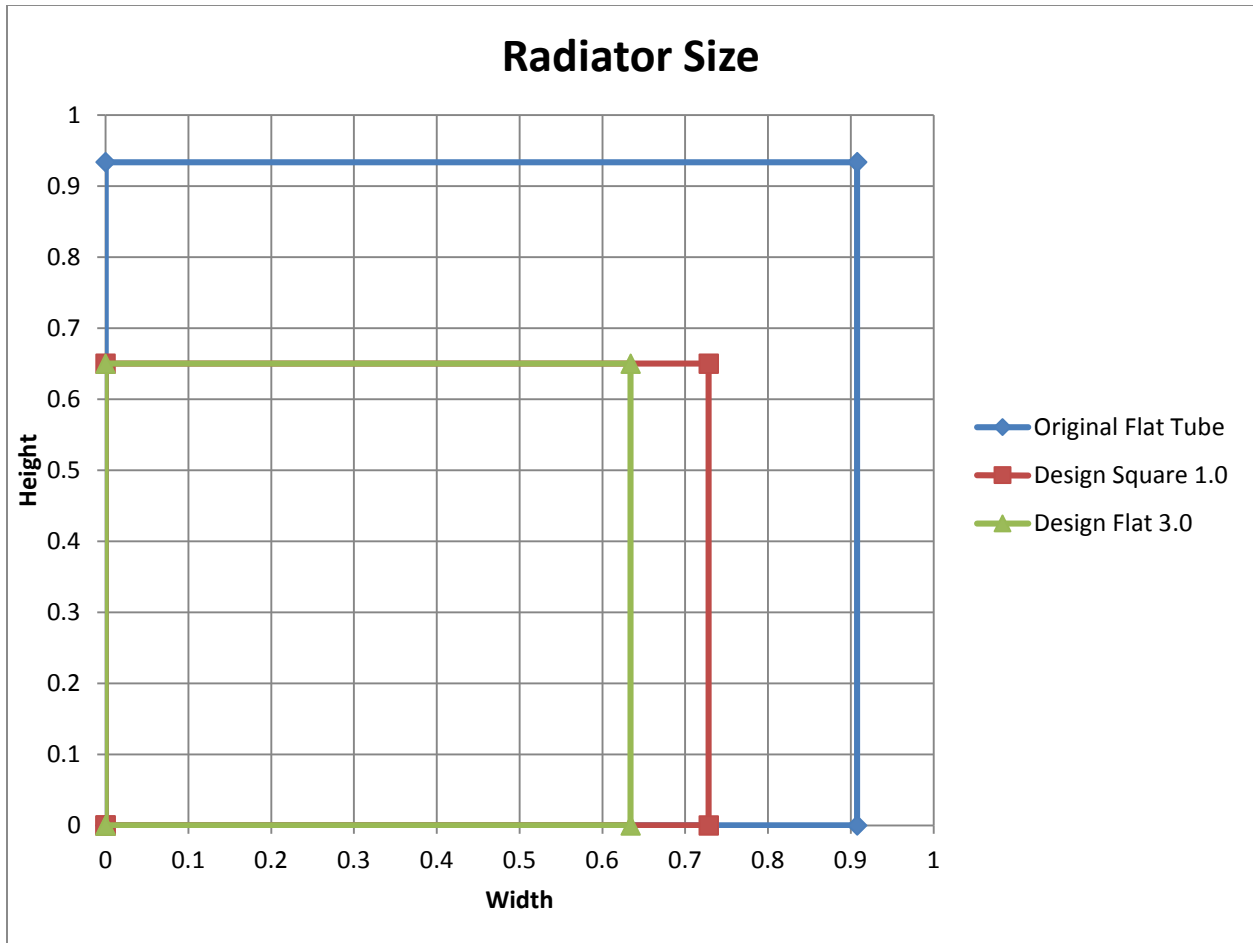


Figure 6.1: Frontal area reduction

6.2 Material Benefits

6.2.1 Fuel Economy

The reduction of frontal area should allow changes to be made to the aerodynamics of heavy duty vehicles, thus allowing for a reduction in aerodynamic drag and an improvement in fuel economy. In addition to the area reduction, the auxiliary power was also reduced which can also increase fuel economy.

6.2.2 Mechanical Performance

The improved radiator design allows for more heat to be transferred with a smaller frontal area. The reduction of frontal area is made possible by increasing the size of the fins but reducing the number of fins while employing flat or wavy tube geometry on the coolant side, thus

increasing the internal convection heat transfer convection coefficient and the external convection heat transfer coefficient reducing the overall thermal resistance of the radiator. With a reduction of size of the radiator, the needed volumetric flow of air is increased in order to remove the same amount of heat in a smaller space.

6.3 Conclusion

The presented research captures the need for the design improvement of radiator heat exchangers in heavy-duty vehicles in order to reduce aerodynamic drag and improve fuel economy. A method for analyzing an existing radiator is set forth including the needed parameters for effective comparisons of alternative designs. An investigation of microchannels was presented and it was determined that microchannels can improve the overall heat transfer of a radiator while decreasing the dimensions of the radiator. Investigations into improving the air-side heat transfer were considered and an improved fin design was found. A procedure of optimization of the radiator design was conducted and an optimal solution was obtained. The overall heat transfer of the design was improved from the original design by 7% in addition to a 52% decrease in frontal area but at the cost of a 300% increase in auxiliary power. The flow rate of the coolant could not be decreased as this would decrease the maximum heat transfer rate.

The predictions of microchannels were verified through a computational fluid dynamic model to demonstrate that microchannels can enhance the heat transfer but also result in a large pressure drop. Predictions of the louver fin geometry correlation extrapolation was verified using CFD and the improvement of the new fin geometry and air-side heat transfer predictions were realized.

It was further found that flat tubes provide more surface area with higher heat transfer characteristics than do microchannels for a given flow rate. Thus, it is not recommended that

microchannels be used to replace flat tubes in automotive radiator heat exchangers.

The results the study suggest that the reduction of frontal area can be achieved up to 52%. This is also with heat transfer enhancement of 7% but the cost to this gain is 296% increase in auxiliary power. This is compared to the 60% reduction in drag-related power but for a 500hp engine with an initial auxiliary power of 7212 W (9.7 hp) a 60% reduction in drag power (0.04 hp) is not worth a 296% increase (29.0 hp) in auxiliary power. More fuel would be spent running the cooling module than what would be saved with the reduction of frontal area. A large reduction of frontal could potentially lead to fuel savings if the auxiliary power is not increased for the vehicle. However, as this study has shown, microchannel technology is not the correct method to use to achieve a reduction of frontal area without an increase in auxiliary power.

6.4 Future Research

Although it was determined that microchannels are not feasible in a radiator application, microchannels could possibly be used to cool the engine directly and could potentially replace the radiator or reduce the needed size by focusing on the direct heat transfer from the engine to the coolant.

Further research may include a study of the feasibility of a water-to-water heat exchanger that can be used as an automotive heat exchanger. According to preliminary calculations, the size of the water-to-water heat exchanger is significantly less than a water-to air heat exchanger. However, the challenge then becomes how to cool the secondary fluid without increasing the size of the radiator significantly. Thus, if a method could be devised to accomplish this challenge, a great improvement in the reduction of radiator size may be made.

Another consideration may be an innovative implementation of evaporative cooling within a radiator possibly using microchannels to cool the module by means of small-scale mass

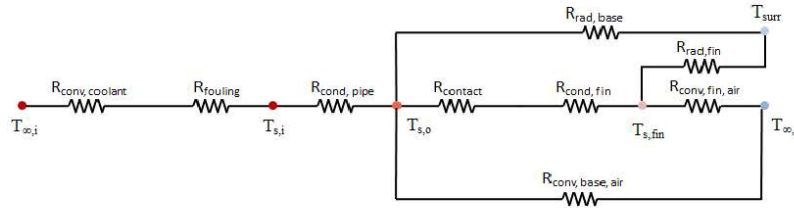
transfer evaporative cooling. If there were material that would increase in porosity with an increase in temperature this could be used to keep the engine from overheating by releasing trace amounts of water or safe coolant which would evaporate and in effect cool the radiator and the engine. Further investigation of this possibility would be required to determine the feasibility of this phenomena.

APPENDIX A
MATHEMATICAL MODELING CODE

Calculations for Peterbilt Radiator

Resistance Model

The resistance of a radiator can be modeled with the following thermal resistance circuit



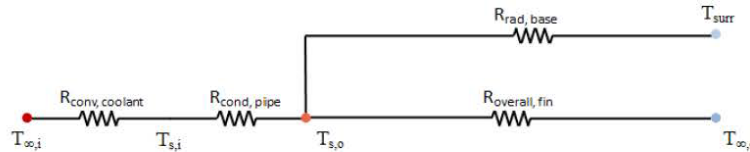
The total thermal resistance is the sum of all the composite resistances and may be found using superposition addition of the thermal resistance of the heat through the convective coolant plus the thermal resistance of the heat through the pipe wall plus the thermal resistance of the heat through the fin array to the convective air with radiation assuming that the temperature of the surroundings is the same as the temperature of the air ($T_{\infty} = T_{surr}$). This may be represented by the following equation:

$$R_{total} = R_{conv,coolant} + R_{fouling} + R_{cond,pipe} + \frac{1}{\left(\frac{1}{R_{contact} + R_{cond,fin} + \frac{1}{\left(\frac{1}{R_{rad,fin}} + \frac{1}{R_{conv,fin,air}} \right)} \right) + \frac{1}{R_{rad,base}} + \frac{1}{R_{conv,base}}} \right)$$

This may be simplified by neglecting the radiation of the fins and condensing the other parts to an overall fin resistance, leaving

$$R_{total} = R_{conv,coolant} + R_{fouling} + R_{cond,pipe} + \frac{1}{\left(\frac{1}{R_{rad,base}} + \frac{1}{R_{overall,fin}} \right)}$$

Which simplifies the model to



With

$$R_{conv,coolant} = 1 / (h_c A_i)$$

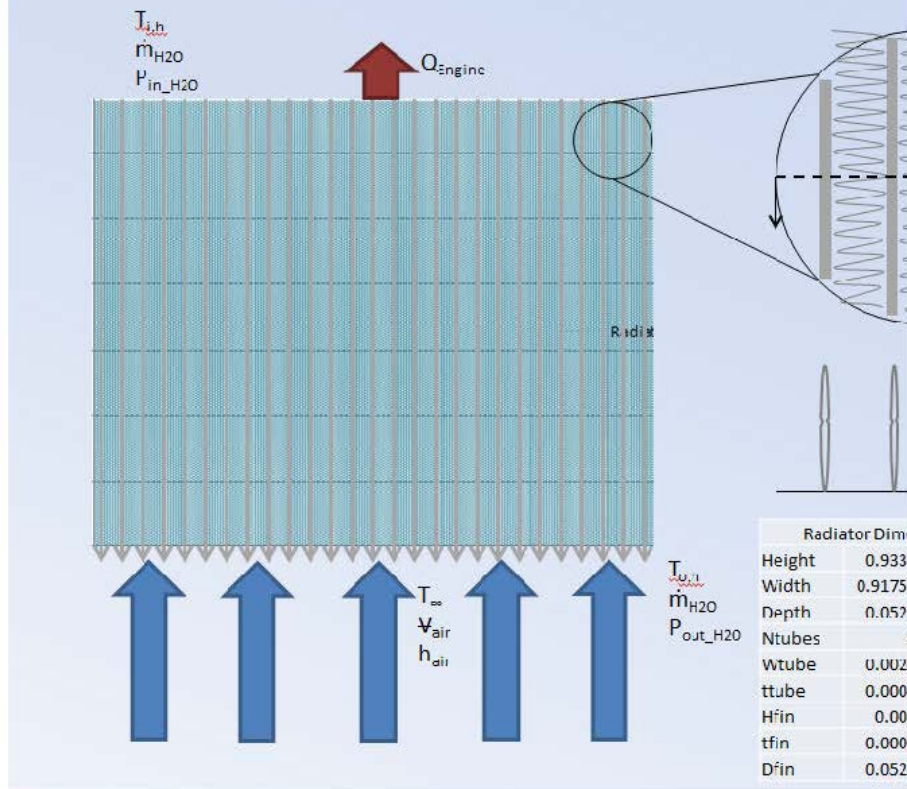
$$R_{fouling} = R_f'' A_i$$

$$R_{cond,pipe} = \ln(D_o / D_i) / (\pi L k_{pipe})$$

$$R_{overall,fin} = 1 - N A_{fin} / A_i \left(1 - (\eta_{fin} / (1 + \eta_{fin} h_{air} A_{fin} (R_{tc}'' / A_{contact,base}))) \right)$$

$$R_{rad,base} = 1 / (A_{base} \epsilon \sigma (T_s + T_{surr}) (T_s^2 + T_{surr}^2))$$

Current Radiator Model



where

h_c is the coefficient of convection for the coolant

A_i is the surface area inside the pipe ($D_i \pi L$)

D_o is the outer diameter of the pipe

D_i is the inner diameter of the pipe

k_{pipe} is the thermal conductivity of the pipe material

A_o is the surface area outside the pipe

Known Values

The total thermal resistance is defined as the change in temperature of a system divided by the total heat removed from the system or

$$R_{\text{total}} = (T_1 - T_2) / q$$

For this specific radiator system, at 380 hp and 1900 RPM, the heat removed from the engine is $q = 199.0 \text{ kW}$, and the temperature delta is $\Delta T_{\text{Engine}} = 67.3 \text{ }^\circ\text{C}$, therefore,

Calculating Total Resistance

$$R_{\text{total}} = R_{\text{conv, coolant}} + R_{\text{cond, pipe}} + \frac{1}{(1/R_{\text{rad, base}} + 1/R_{\text{conv, fin}})}$$

Operating Temperatures

■ Operating Conditions

■ Given

```
Tin = 55.81 + 273.15 (* (K) (from Conditions for Calculations Red) *)
Tout = 49.46 + 273.15 (* (K) (from Conditions for Calculations Red) *)
Tsur = 38 + 273.15 (* 90°F Temperature of Surroundings *) ;
T∞ = Tsur (* 90°F = 32.22°C Free air stream temperature *) ;
Tenter = 30.7 + 273.15 (* Temperature of Air in front
of the radiator (from Conditions for Calculations Red) *) ;
Texit = 43.7 + 273.15 ;
Tm = (Tin + Tout) / 2 ;
Ts = Tm - .5 (* °C + 273.15 K Surface Temperature of pipe wall *) ;
328.96
322.61
```


■ Geometry of Pipe

```
(*  
A 68.87707  
Ai 8.65889  
Ao 0.57397  
Afr 0.85655  
Af 60.14173  
Dh 0.00290  
Deq 0.00971  
Ac 0.00007400  
L 0.93345  
P 0.101936545  
Npipe 91  
NArray 92  
Nfin 55844  
Pfin 1005.187588  
Dhair 0.002286717
```

```
Dimensions  
Fin Pitch 16.5  
Nfin/NArray 607  
Afin 0.00107696  
Apipe 0.095992773  
Ain 0.095152668  
Agap 1.17302E-05  
Pf 0.017999921  
Hpipe 0.05224  
Lfin 0.00762  
Ntubes 1  
tpipe 0.00045  
L 0.93345  
Width 0.90762  
Npipe 90  
NArray 91  
Wpipe 0.00238  
Npipets 90  
*)
```



```

A = 68.87707(*m2 Total Heat Transfer Area by conveciton*);
Ai = 8.65889(*m2 Total internal Surface Area of Tubes*);
Ao = 0.57397(*m2 Free flow area of one side of heat exhcnager*);
Afr = 0.85655(*m2 frontal area (HxW)*);
Af = 60.14173(*m2 Surface Area of Fins exposed to heat transfer*);
Ac = 0.00007400; (*cross sectional area of pipe*);
P = 0.101936545(*m, Perimeter of single pipe*);
Deq = 0.00971 (*m Equivalent Diameter*);
Npipe = 91 (*number of tubes*);
tpipe = 0.00045;
L = 0.93345(*m, lenth of tube*);
Nfin = 55844 (*fins in total radiator*);
δ = .0001(*m) fin thickness*);
Lfin = 0.00762;
Pair = 1005.187588;
Dhair = 0.002286717(*Hydraulic Diameter of free flow*);
Acontact = Npipe * Nfin * Hpipe * 2 δ
(* (m2) Contact area of fins on base (52.18mmx1mm)*);
Pf = 0.017999921 (*m Perimeter of fin*);
Afin = 0.00107696 (*m2 Surface Area of single fin*);
Hpipe = 0.05244(*length of fin*);
W = 0.91762;
Ntube = 1;
Apipe = 0.095992773;
Abase = Apipe * Npipe;
Type = "Flat";(*Round, Square, Flat*)
(*Output A and Ai and Dh

```

■ Geometry of Fin

Table 6.1 Heat Exchanger Correlations: Flat Tube			
Fin type	Surface condition	Author (year)	Correlations
Plain	Dry		N/A
Plain	Wet		N/A
Plain	Frosted		N/A
Louver	Dry	Chang & Wang (1997)	<p><u>j-factor correlation</u></p> $j = Re_{Lp}^{-0.49} \left(\frac{\theta}{90}\right)^{0.27} \left(\frac{F_p}{L_p}\right)^{-0.14} \left(\frac{F_l}{L_p}\right)^{-0.29} \left(\frac{T_d}{L_p}\right)^{-0.23} \times \left(\frac{L_l}{L_p}\right)^{0.68} \left(\frac{T_p}{L_p}\right)^{-0.28} \left(\frac{\delta_f}{L_p}\right)^{-0.05}$ <p>where, F_l: fin length, L_p: louver pitch, L_l: louver length T_d: tube depth, T_p: tube pitch, θ: louver angle</p>

θ	30	Louver angle		
Td	0.05224 m	Tube Depth	Td=Hpipe	0.05224
Lp	0.000861429 m	Louver Pitch	LP=(Td/2-Endgap-Midgap/2)/(Nlfins)	
Ll	0.005773939 m	Louver length	Ll=c-2*0.001	
Fl	0.007773939	Fin Length	Fl=c	
Fp	0.001539394 m/fin	Fin Pitch		
δ_f	0.0001 m	Fin Thickness		
Tp	0.01 m	Tube Pitch	Tp=Lfin+Dout	
Nlfins	28 fins/side	Number of Louver fins on one array (2 arrays per fin)		
Midgap	0.002 m	Gap in middle of louver fin array		
Endgap	0.001 m	Gap on ends of fin		
Dm	0.00238 m	Dm=Dout Major Diameter		
Re _{Lp}	$Re_{Lp} = \frac{V_{air} L_p \rho_{air}}{\mu_{air}}$	Reynolds number based on louver spacing		
Alouver	6.46681E-05 m ²	Alouver=4*Nlfins*(Ll* δ_f)		

$F_l = 0.007773939;$
 $L_p = 0.000861429;$
 $L_l = 0.005773939;$
 $T_d = 0.05224;$
 $T_p = 0.01;$

```

F = .98(* Function of PF and RF as seen in above figure*);
LMTD = F * (Tin - Texit) - (Tout - Tenter) / Log[(Tin - Texit) / (Tout - Tenter)]
(*Temperature used to calculate fluid properties*)
(*Output Ts and Tlm K _____ *)
14.8894

```

Internal Convection Resistance

■ Thermal Resistance of Convection of Coolant

To find $R_{\text{conv, coolant}}$ we will use the equation

$$R_{\text{conv, coolant}} = \frac{1}{h_c A_i}$$

To find Nu we must first determine the characteristics of the flow with Re and Pr which are defined as

$$\text{Re}_D = 4 \frac{\dot{m}}{P \mu} \text{ and } \text{Pr} = c_p \frac{\mu}{k} \text{ where}$$

■ Operating Conditions

```

mdot = 7.65(*kg/s coolant mass flow according to case 1*);
(Ts - 273.15) "°C"
(Tm - 273.15) "°C"
(*Output Ts and Tm _____ *)

```

52.135 °C

52.635 °C

0.07912087912087913

0.0791209

■ Properties of Fluid

$$T_m = \frac{(T_s + T_o)}{2} = 52.635 \text{ °C}$$

```

Hyperlink["Physical Properties Calculator",
"http://www.mhtl.uwaterloo.ca/old/onlinetools/airprop/airprop.html"]

```

Physical Properties Calculator

Input Values		Results	
Fluid:	Ethylene Glycol 50% ▾	Density:	1.0378E+3 (kg/m ³)
Temperature:	52.635 (degrees C) ▾	Dynamic Viscosity:	1.6180E-3 (kg/m.s)
Digits:	5 ▾	Kinematic Viscosity:	1.5591E-6 (m ² /s)
Calculate		Specific Heat: c _p	3.3574E+3 (J/kg K)
		Conductivity: k	0.45037 (W/m.K)
		Prandtl number:	12.062
		Thermal Diffusivity:	1.2926E-7 (m ² /s)
		Thermal Expansion Coefficient:	3.0695E-3 (1/K)

$\mu = 1.16180 \times 10^{-3}$ (*dynamic viscosity of engine coolant, 50:50 water-ethelyne-glycol mixture at T_m*);
 $\mu_s = 1.6385 \times 10^{-3}$ (*dynamic viscosity of engine coolant, 50:50 water-ethelyne-glycol mixture at T_s*);
 $\rho = 1.0378 \times 10^3$ (*density of engine coolant, possibly water-glycerol mixture at T_m=(T_i+T_o)/2*);
 $c_p = 3.3574 \times 10^3$ (* (J/kg K) Specific heat of 50: 50 ethylene-glycol-water coolant @T_m=389 K =8.37 $\frac{kJ}{kg K}$ *);
 $k = 0.45037$ (*(W/m K) thermal conductivity of coolant*);

■ Calculations

$$D_h = \frac{4 \bar{A}_c}{P} \text{ (*m Hydraulic Diameter*)}$$

$$\dot{m}_{pipe} = \dot{m} / N_{pipe}$$

$$v = \frac{\dot{m}_{pipe}}{(\bar{A}_c) \rho}$$

$$Re_D = \frac{\dot{m}_{pipe} D_h}{\mu \bar{A}_c}$$

$$Pr = c_p \frac{\mu}{k}$$

$$L / Deq \geq 10$$

(* Display ReD and Pr and if L/Dh ≥ 10 _____ *)

0.00290377

0.0840659

1.09465

2839.35

8.66094

True

■ Finding Nu

Nu is based on Re and Pr and using equations from page 536 in HT textbook

```
ef = 0.0000015;
ef / Dh
ef / Deg
f1c := If [ReD < 3000, 64 / ReD,
  If [3000 ≤ ReD ≤ 5 × 106, f = (0.790 Log[ReD] - 1.64)-2, 0.05]]];
(*for f see figure 8.3 on page 495*)
f2c := NSolve[ $\frac{1}{\sqrt{fs}} == -2.0 \text{Log}10\left[\frac{ef / Dh}{3.7} + \frac{2.51}{ReD \sqrt{fs}}\right]$ , fs] // Flatten;
(*Colebrook Equation*)
f3c = 1 /  $\left[-1.8 \text{Log}10\left[\left(\frac{ef / Dh}{3.7}\right)^{1.1} + \frac{6.9}{ReD}\right]\right]^2$ ; (*Haaland Equation*)
f4c = 96 / ReD; (*Friction factor for flow between parallel plates for a/b>8,
see page 437 of "Heat Transfer a Practical Approach" by Cengel*)
```

Non - Circular Pipes: $f = \frac{k}{Re}$, $48 \leq k \leq 96$

Geometry Factor k

Square	56.91
2:1 Rectangle	62.19
5:1 Rectangle	76.28
Parallel Plates	96.00

f1c

f2c

f3c

f4c

0.00051657

0.00015448

0.0225404

NSolve::ifun : Inverse functions are being used by NSolve, so

some solutions may not be found; use Reduce for complete solution information. >>

{fs → 0.0447156}

0.0455093

0.0338106

6.3.2 Analytic and Numerical Solutions: Laminar Flow

(1) Hydrodynamic Entrance Length L_h .

- Results for L_h :

$$\frac{L_h}{D_e} = C_h Re_{D_e} \quad (6.5)$$

- Table 6.1 gives C_h
- Compare with scaling:

$$\left(\frac{L_h / D}{Re_D}\right)^{1/2} \sim 1 \quad (6.2)$$

Rewrite (6.5)

$$\left(\frac{L_h / D_e}{Re_{D_e}}\right)^{1/2} = (C_h)^{1/2} \quad (a)$$

Example: Rectangular channel, aspect ratio 2, Table 6.1 gives $C_h = 0.085$. Substituting this value into (a), gives

$$\frac{Nu_D}{\left(\frac{Pr Re_D}{x/D}\right)^{1/2}} \sim 1 ;$$

The hydraulic entrance length and thermal entrance length

Ch = 0.011;

Ct = 0.012;

Lx = NSolve[(Lh/Dh)/ReD]^1/2 == (Ch)^1/2, Lh] // Flatten

Lxt = NSolve[(Lt/Dh)/ReD Pr]^1/2 == (Ct)^1/2, Lt] // Flatten

{Lh → 0.0906929}



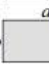
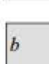

{Lt → 0.0114234}

$$\left(\frac{L - (Lh / Lx)}{L}\right)$$

NuLx = NSolve[Nux / (Pr ReD / ((Lh / Lx) / Dh))^1/2 == (Ch)^1/2, Nux] // Flatten

0.902841

{Nux → 2.94295}

geometry	C_h	C_t	
		uniform surface flux	uniform surface temperature
	0.056	0.043	0.033
 $a/b = 1$	0.09	0.066	0.044
 $a/b = 2$	0.085	0.057	0.043
 $a/b = 4$	0.075	0.042	0.053
	0.011	0.012	0.008

```

f = f3c; (*Define f based on calculations*)
n := If[Ts > Tm, 0.4, 0.3];
xfd = 0.05 ReD Pr Dh (*Entrance length*)
ReL = V  $\frac{Dh \rho}{\mu}$ 
L
L / Dh
xfd / L
(L - xfd) / L
NuCaseC1 :=
  If[0.6 ≤ Pr ≤ 160 && ReD ≥ 10000 && L / Dh ≥ 10, Nu = 0.023 ReD4/5 Prn, Text["N/A"]]
  (*n=0.4 for Ts>Tm and n=0.3 for Ts<Tm, see pg. 536*);
NuCaseC2 := If[0.7 ≤ Pr ≤ 16700 && ReD ≥ 10000 && L / Dh ≥ 10,
  Nu = 0.027 ReD4/5 Pr1/3  $\left(\frac{\mu}{\mu_s}\right)$ , Text["N/A"]]
  (*μs is evaluated at the surface temperature instead of Tm*);
NuCaseC3 := If[0.5 ≤ Pr ≤ 2000 && 3000 ≤ ReD ≤ 5 × 106 && L / Dh ≥ 10,
  Nu =  $\frac{(f/8)(ReD-1000)Pr}{1+12.7(f/8)^{1/2}(Pr^{2/3}-1)}$ , Text["N/A"]] (*Dependant on f*);
NuCaseC4 := If[2300 ≤ ReD ≤ 3100 && L / Dh ≥ 10,
  Nu = 3.5239  $\left(\frac{ReD}{1000}\right)^4 - 45.148 \left(\frac{ReD}{1000}\right)^3 + 212.13 \left(\frac{ReD}{1000}\right)^2 - 427.45 \left(\frac{ReD}{1000}\right) + 316.08$ ,
  Text["N/A"]] (*For transitional flow 2300<ReD<3100*);
NuCaseA1 := If[ReD < 3000, Nu = 4.36, Text["N/A"]] (*For Laminar,
  Fully-Developed Flow and uniform qs**);
NuCaseA2 := If[ReD < 3000 || Pr ≥ 5, Nu = 3.66 +  $\frac{0.065 (Dh/L) * ReD * Pr}{1 + 0.04 ((Dh/L) * ReD * Pr)^{2/3}}$ ,
  Text["N/A"]] (*For Laminar, Fully-Developed Flow and uniform qs**);
NuCaseA3 := If[ReD < 3000, Nu = 7.54 +  $\frac{0.03 (Dh/L) ReD Pr}{1 + 0.016 ((Dh/L) ReD Pr)^{2/3}}$ , Text["N/A"]]
  (*For developing Laminar flow between Parallel plates*);
NuCaseA4 := If[ReD > 2300, Nu = 0.012 (ReD0.87 - 280) Pr0.4  $\left(1 + \left(\frac{Dh}{L}\right)^{2/3}\right)$ , Text["N/A"]]
  (*For Fully Developed Turbulent Flow in a flat
  pipe. See "Heat transfer and pressure drop correlations for
  the wavy fin and flat tube heat exchangers" by Dong et al*)
NuCaseA5 := If[ReD < 2300 && Pr > 0.6, Nu = 0.332 ReD0.5 Pr1/3, Text["N/A"]]
  (*For Laminar flow over a flat plate*)
NuCaseA6 := Nux /. NuLx
(* Display Ai and f _____*)

```

3.57039

2839.35

0.93345


```
321.462
3.82494
-2.82494
NuCaseC1
NuCaseC2
NuCaseC3
NuCaseC4
NuCaseA1
NuCaseA2
NuCaseA3
NuCaseA4
NuCaseA5
NuCaseA6
(*Display results for Nu based on the different cases and NuAve _____
*)
N/A
N/A
N/A
8.14223
4.36
6.54956
9.32135
21.2158
N/A
2.94295
```

321.462														
3.82494														
-2.82494														
NuCaseC1														
NuCaseC2														
NuCaseC3														
NuCaseC4														
NuCaseA1														
NuCaseA2														
NuCaseA3														
NuCaseA4														
NuCaseA5														
NuCaseA6														
(*Display results for Nu based on the different cases and NuAve _____														
*)														
N/A														
N/A														
N/A														
8.14223														
4.36														
6.54956														
9.32135														
21.2158														
N/A														
2.94295														

■ Calculating hc and Rcv from Nu

$$NuD = (NuCaseA6) \left(\frac{(Lh / . Lx)}{L} \right) + NuCaseA4 \left(\frac{L - (Lh / . Lx)}{L} \right)$$

(*Define NuD from the previous cases*)

Ri (*m²*)

$$hc = NuD \frac{k}{Dh}$$

$$Rcv = \frac{1}{hc Ri}$$

$$hq = \frac{(m \cdot pipe \cdot cp (Tin - Tout))}{Ri / Npipe (Tin - Tout)}$$

$$Nuq = hq \frac{Dh}{k}$$

(* Display the hc (W/m²K) for the coolant and the Rcv (K/W) _____ *)

19.4404
 8.65889
 3015.18
 0.0000383023
 2966.21
 19.1247

■ Pressure Calculations

According to the publication, "Analysis of effectiveness and pressure drop in micro cross-flow heat exchanger" by Kang and T seng the pressure drop is a function of the mass velocity which is the mass flow rate through the pipe divided by the cross sectional area. The pressure drop is also a function of the hydraulic diameter and the darcy friction factor that is based on the Reynolds number derived from the hydraulic diameter

the mass velocity is

$$G_1 = \dot{m}_1 / A_{c1} \tag{29}$$

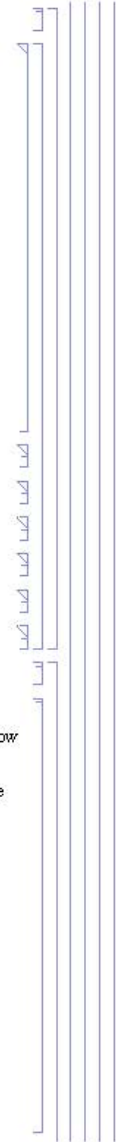
$$G_2 = \dot{m}_2 / A_{c2} \tag{30}$$

where \dot{m} is mass flow rate. Therefore the pressure drops of the hot and cold flow sides are

$$\Delta P_1 = \frac{f_1 G_1^2 Y}{D_h (2g_c) \rho_1} \tag{31}$$

$$\Delta P_2 = \frac{f_2 G_2^2 X}{D_h (2g_c) \rho_2} \tag{32}$$

where $g_c = 1$.



```

G =  $\frac{\text{mdotpipe}}{A_c}$ ;
ef = 0.0000015;
NSolve[ $\frac{1}{\sqrt{fs}} == -2.0 \text{Log}10\left[\frac{ef/Dh}{3.7} + \frac{2.51}{\text{Re}D\sqrt{fs}}\right]$ , fs] // Flatten
NSolve::ifun: Inverse functions are being used by NSolve, so
some solutions may not be found; use Reduce for complete solution information. >>
{fs -> 0.0447156}
f
0.0455093
PdropRad =  $f \frac{L \rho}{2 Dh} v^2$  (*Darcy equation*)
PdropRadm = 88520 (*Pa, taken from given data*)
 $\frac{\text{PdropRadm} - \text{PdropRad}}{\text{PdropRadm}} * 100$ 
9096.25
88520
89.7241
PumpPower = PdropRad *  $\frac{\text{mdot}}{\rho}$  (*Pa*m3/s=W*)
PumpPowerMax = PdropRadm *  $\frac{\text{mdot}}{\rho}$ 
PumpPowerhp = 0.00134102209 * PumpPower (*HorsePower*)
67.0517
652.513
0.0899178

```

Fouling Resistance in Pipe

The fouling resistance is defined as

$$R_{\text{fouling}} = R_f'' A_i$$

And R_f'' may be found on page 675 of Heat Transfer textbook or in literature.

$R_f = 0.000002$; (*For riverwater below 50°C 0.0002-0.001*)

$R_{\text{foul}} = R_f N_{\text{pipe}} A_i$

0.00157592

Thermal Conductive Resistance

The conductive resistance through the pipe wall is defined as

```

Rcond,pipe =  $\frac{\ln(r_o/r_i)}{2 \pi L k_{pipe}}$ 
Deq
L
ri = Deq / 2
ro = Deq / 2 + tpipe
kpipe = 215 (*thermal conductivity of aluminum is 205  $\frac{kW}{m K}$  at 25°C,
215  $\frac{kW}{m K}$  at 125°C, and 250  $\frac{kW}{m K}$  at 225°C according to Engineering Toolbox*);
Rcond =  $\frac{\text{Log}\left[\frac{r_o}{r_i}\right]}{Npipe 2 \pi L kpipe}$ 
0.00971
0.93345
0.004855
0.005305
7.72471  $\times 10^{-7}$ 

```

Thermal Resistance of Fins

The overall resistance of the fins can be modeled as

$$R_{\text{overall, fin}} = 1 - N_{\text{fin}} \frac{A_{\text{fin}}}{A_t} \left(1 - \left(\frac{\eta_{\text{fin}}}{1 + \eta_{\text{fin}} h_{\text{air}} A_{\text{fin}} \left(\frac{R_{t'}}{A_{\text{conv},\text{base}}} \right)} \right) \right)$$

Which includes the convection resistance and the conductive resistance through the fins. The fin efficiency is define as

- **Operating Conditions**

- **Air Properties**

Hyperlink["Physical Properties Calculator",
"http://www.mhtl.uwaterloo.ca/old/onlinetools/airprop/airprop.html"]

Physical Properties Calculator

Properties Evaluated at Film Temperature T_{film}

```

Tfilm = (Ts + T∞) / 2 - 273.15 (*film temperature*)
Vfr = 13.333 (* (m/s) Velocity of air for mass flow ≈30 MPH or 48 kmh *);
Aradiator = Afr (*m² area of Radiator*);
ρair = 1.1096 (*kg/m³ at T∞=(Tenter+Texit)/2*);
cpair = 1.0072 × 10³ (*J/kg K at T∞*);
μa = 1.9381 × 10⁻⁵ (*kg/m*s at T∞*);
kair = 0.027444 (* m²/s at T∞*);
mdotair = Vfr Aradiator ρair (*kg/s*)

Vair =  $\frac{\text{mdotair}}{\rho_{\text{air}} A_0}$ 
(*Display Tfilm and mdotair _____
_____*)

45.0675
12.6721
19.8972

θb = Ts - T∞
14.135

■ Fin Geometry
kfin = kpipe (* same thermal conductivity as aluminum pipe *);
Dhair
Hpipe (*Height of fin*)
(* Output Dhair (hydraulic diameter of the air intake) and
Hpipe _____ *)

0.00228672
0.05244

■ Air Calculations
See http://www.wlv.com/products/databook/db3/data/db3ch6.pdf for theory on air-side calculations for air-cooled heat exchanger with louvered fins

```



```

Prair = cpair  $\frac{\mu a}{kair}$ 
ReA = Vair  $\frac{Dhair \rho air}{\mu a}$ 
Pe = ReA Prair (*Peclet Number = Re Pr*)
x = Hpipe
 $\frac{Dhair}{x}$  (*Use this value when choosing NuDair. Small value-use NuD2 or NuD3,
Large value-→ NuD4 or NuD5*)
NuT = Pe  $\frac{Dhair}{x}$ 
0.711286
2604.92
1852.84
0.05244
0.0436064
80.7957

```

■ Nusselt Number for Convection Coefficient

```

NuD1 = 0.3 +  $\frac{0.62 ReA^{1/2} Prair^{1/3}}{(1 + (0.4 / Prair)^{2/3})^{1/4}} (1 + (ReA / 282000)^{5/8})^{4/5}$ 
(*for all ReA*Prair≥0.2, eq. 7.46 pg 438 of Heat Transfer Book*)
NuD2 = (3.66^2 + 0.7 + (1.077 (NuT)^{1/3} - 0.7)^3)^{1/3} (*for 10<NuT<100,
Heat Exchanger Design Handbook 1.5.1-3 eq 12*)
NuD3 = (3.66^3 + 0.7^3 + (1.077 (NuT)^{1/3} - 0.7)^3)^{1/3} (*for 10<NuT<∞,
Heat Exchanger Design Handbook 1.5.1-3 eq 15*)
NuD4 = 0.332 Prair^{1/3}  $\left( ReA \frac{Dhair}{x} \right)^{1/2}$  (*for local Nusselt Number good for Pr>0.1*)
26.1625
4.81509
4.80995
3.15858
NuDair = NuD1;

```

■ Different Method Considering Louver fins

```

j = ReLp^{-0.49}  $\left( \frac{\theta}{90} \right)^{0.27} \left( \frac{Fp}{Lp} \right)^{-0.14} \left( \frac{Fl}{Lp} \right)^{-0.29} \left( \frac{Td}{Lp} \right)^{-0.23} \left( \frac{Ll}{Lp} \right)^{0.68} \left( \frac{Tp}{Lp} \right)^{-0.28} \left( \frac{\delta f}{Lp} \right)^{-0.005}$ 
0.00893662
hjair = j  $\frac{mdotair cpair}{Ao Prair^{2/3}}$  (*convective heat transfer coefficient W/m²*)
249.393

```

■ Convection Coefficient

```

h1 =  $\frac{0.174 \text{ mdotair cpair}}{((\text{ReA})^{0.383}) \text{ Ao } (\text{Prair})^{2/3}}$  (*from literature
      "Performance evaluation of a radiator in a diesel engine"*)
h2 =  $\frac{\text{NuDair kair}}{\text{Dhair}}$  (*from heat transfer book*)
hjair
(* Output NuDair, h1, h2, and hjair (W/m²K) _____
      _____ *)

```

238.787

313.989

249.393

hair = hjair (*select Nussult Number*)

249.393

```

hmes =  $\frac{\text{mdotair cpair } (\text{Texit} - \text{Tenter})}{\text{A } (\text{Tm} - \text{Tenter})}$ 

```

109.823

■ Fin Calculations

```

m =  $\left( \frac{\text{Pf hair}}{\text{kfin Afin}} \right)^{1/2}$ 
ηf = Tanh[m Lfin] / (m Lfin) // N
4.4031
0.999625

```

■ Fin Effectiveness

```

εfin =  $\frac{\text{Afin}}{\text{Abase}} \eta_f$ 
efin =  $\frac{\text{Af}}{\text{Abase}} \eta_f$ 
6.88229

```

■ Contact Resistance

```

Lflux = 0.00005;
kflux = 180; (*  $\frac{\text{W}}{\text{m K}}$  Brazing flux:http://
      www.superiorflux.com/aluminum_brazing_flux.html;
      Assuming 90% Aluminum and 10% Silicon .9*200 +.1*83.6=188*)
Rtc =  $\frac{\text{Lflux}}{\text{kflux Acontact}}$ 
      (*Contact resistance of brazed aluminum. From HE Book pg 119,
      Aluminum/Aluminum with metallic (Pb) coating 0.01-0.1 m²K/W*)
5.21179 × 10-9

```



■ Fin Efficiency

$$Cl = 1 + \eta f_{\text{hair}} Af (R_{tc} / A_{\text{contact}});$$

$$\eta_{\text{over}} = 1 - \frac{Af}{A} \left(1 - \frac{\eta f}{Cl} \right) \quad (*\text{Eq 3.110a from ch3} *)$$

0.999671

■ Fin Resistance

$$R_{\text{fin}} = \frac{1}{\eta_{\text{over}} \text{hair } A}$$

0.000058235

Pressure Drop

From given measured conditions

In many cases that expectation will be met; however, as seen later, it is overly simplistic. The friction factor can be related to flow rate and pressure drop through

$$f = \frac{A_{\text{min}} \bar{\rho}}{A_T \rho_i} \left[\frac{2 \rho_i \Delta p}{G^2} - (K_c + 1 - \sigma^2) - 2 \left(\frac{\rho_i}{\rho_o} - 1 \right) + (1 - \sigma^2 - K_c) \frac{\rho_i}{\rho_o} \right] \quad [6.1.13]$$

where $\bar{\rho} = (\rho_i + \rho_o) / 2$, and the entrance and exit coefficients K_c and K_e are geometry dependent (see Kays and London, 1984). For air-side flows it is common that entrance and exit effects are small and density changes are negligible. For such a case, Eq. [6.1.13] simplifies to

$$f = \frac{A_{\text{min}} \rho}{A_T} \left[\frac{2 \Delta p}{G^2} \right] \quad [6.1.14]$$

The fan power required to move the air flow through the heat exchanger is

$$P = \frac{G A_{\text{min}} \Delta p}{\rho} \quad [6.1.15]$$

A_{min} is the free flow area, A_o , $G = \dot{m}_{\text{air}} / A_{\text{min}}$; A_T is the total heat transfer area, A

By rearranging equation 6.1.14 we find the pressure drop as

$$\Delta p = f \left(\frac{A_T}{A_{\text{min}}} \right) \frac{G}{2 \rho}$$

and, thus doing, equation 6.1.15 becomes

$$P = \frac{G^2 A_T f}{2 \rho^2}$$

To find the friction factor f we refer to the following table

(*See <http://>

www.wlv.com/products/databook/db3/data/db3ch6.pdf page 6-6 for above*)

ReLp

981.299


```

If[ReLp < 150, {f1 = 14.39 ReLp(-0.805  $\frac{Dp}{n}$ ) (Log[1.0 + ( $\frac{Fp}{Lp}$ )])3.04,
  f2 = (Log[( $\frac{F1}{Fp}$ )0.48 + 0.9])-1.435 ( $\frac{Dhair}{Lp}$ )-3.01 (Log[0.5 ReLp])-3.01,
  f3 = ( $\frac{Fp}{L1}$ )-0.308 ( $\frac{Td}{L1}$ )-0.308 (Exp[-0.1167  $\frac{Tp}{Dm}$ ]) e0.35, Text["N/A"]}
If[150 < ReLp < 5000, {f1 = 4.97 ReLp(0.6049 -  $\frac{1.064}{e^{0.1}}$ ) (Log[( $\frac{\delta F}{Fp}$ ) + 0.9])-0.527,
  f2 = (( $\frac{Dhair}{Lp}$ ) Log[0.3 ReLp])-2.966 ( $\frac{Fp}{L1}$ )-0.7931 ( $\frac{Tp}{Tp-Dm}$ ),
  f3 = ( $\frac{Tp}{Dm}$ )-0.0446 Log[(1.2 + ( $\frac{Lp}{Fp}$ )1.4)]-3.553 e-0.477, Text["N/A"]}
fair = f1 * f2 * f3
N/A
{21.7439, 0.00126323, 2.22202}
0.0610337
Gair =  $\frac{m \dot{t} a i r}{A o}$ ;
Pdropair = fair ( $\frac{A}{A o}$ )  $\frac{G a i r^2}{2 \rho a i r}$  (*Pa*)
FanPower = Pdropair * m \dot{t} a i r (*W*)
FanPowerhp = FanPower * 0.00134102209 (*HorsePower*)
1608.7
20385.5
27.3374

```

Radiation Resistance

The resistance from the radiation of the base may be defined as

$$R_{\text{rad, base}} = 1 / (A_{\text{base}} \epsilon \sigma (T_s + T_{\text{sun}}) (T_s^2 + T_{\text{sun}}^2))$$

Arad = .25 * (Afr - Ao) (*Frontal area of tubes Calculated from measurements*)

e = .99; (*Emmissivity of aluminum from

Engineering Toolbox: Roughly Polished@100°C e=0.18,

Commercial sheet @ 100°C e=0.09, Aluminum rough @ 300K=0.07,

Aluminum foil @ 300K=0.04*);

$\sigma = 5.67 \times 10^{-8}$ (* $\frac{W}{m^2 K^4}$ Boltzmanns Constant*);

Ts

Tsurr

0.070645

325.285

311.15

$$R_{rad} = \frac{1}{A_{rad} \epsilon \sigma (T_s + T_{surr}) (T_s^2 + T_{surr}^2)}$$

1.95548

Total Resistance of Radiator

$$R_{total} = R_{conv, coolant} + R_{fouling} + R_{cond, pipe} + \frac{1}{(1/R_{rad, base} + 1/R_{overall, fin})}$$

Rcv
Rcond
Rfin
Rrad

$$R_{totalc} = \left(R_{cv} + R_{cond} + 1 / \left(\frac{1}{R_{fin}} + \frac{1}{R_{rad}} \right) \right) (*K/W*)$$

0.0000383023

7.72471×10^{-7}

0.000058235

1.95548

0.0000973081

Total Resistance

LMTD (*K*)

QEngine = mdot * cp (Tin - Tout) (*"W" Based on Operating Conditions*)

Rtotal = LMTD / (QEngine) (*K/W*)

Atotal = (A) (*total external heat transfer area m²*)

$$U = \frac{1}{R_{total} A_{total}}$$

$$Uc = \frac{1}{R_{totalc} A}$$

14.8894

163.094.

0.000091293

68.8771

159.033

149.203

% Deviation

$$\text{diff} = \frac{R_{\text{total}} - R_{\text{totalc}}}{R_{\text{total}}} * 100 \text{ (*K/W*)}$$

-6.58876

Surface Density of Radiator

$$SD = A_{\text{total}} / (W * L * Td) \text{ (*m}^2/\text{m}^3\text{*)}$$

$$\text{HeatFlux} = Q_{\text{Engine}} / A_i \text{ (*W/m}^2\text{*)}$$

1539.28

18835.5

■ Surface Density of Compact Heat Exchangers vs. Microchannel

and micro-miniaturization techniques have made possible the fabrication of small flow passages or 'microchannels'. Microchannels are broadly characterized by small flow passages of 1 mm in diameter or less, which allows for heat transfer surface densities to be $10\,000\text{ m}^2\text{ m}^{-3}$ or more [7,10,11]; this value contrasts with compact heat exchangers having a density of $700\text{ m}^2\text{ m}^{-3}$. Owing to their higher heat transfer, lower weight, and their space, energy, and materials savings potentials over their traditional tube and enhanced surface heat exchanger counterparts, microchannels can meet all the above-mentioned challenges.

■ Definition of Microchannel

Any flow channel diameter or hydraulic diameter of 1 mm or below is broadly classified in the heat transfer and fluid flow literature as 'microchannel', 'microtube', or 'micro-device' [10,21-28].

■ Heat Transfer Coefficients of Microchannels

Forced-convection heat transfer in a crossflow microchannel heat exchanger (MCHE) experiment. The microchannels on the plates of the MCHE were machined using a che from 0.4-mm-thick stainless steel plates, and the plates were bonded together by vacu. The influence of the aspect ratio of microchannels was analyzed based on MCHEs maximum volumetric heat-transfer coefficient using deionized (DI) water as the work $\text{MW m}^{-3}\text{ K}^{-1}$, with a corresponding pressure drop of <6 kPa when the Reynolds microchannels was ~ 64 . Besides, the maximum volumetric heat-transfer coefficient, us fluid, was $0.67\text{ MW m}^{-3}\text{ K}^{-1}$, with a corresponding pressure drop of ~ 30 kPa when Re of the average Nusselt number (Nu) and Re values were obtained from MCHEs wi validity was confirmed by MCHEs with 2 and 10 plates.

$A_{total} = (A) (*total \text{ external heat transfer area } m^2*)$

$$U = \frac{Q_{Engine}}{LMTD A_{total}} (*\frac{W}{m^2 K}*)$$

68.8771

159.033

U A LMTD

QEngine

163 094.

163 094.

$$U_{rad} = \frac{Q_{Engine}}{A_{total} LMTD} SD (*\frac{W}{m^2 K}*)$$

$U_{rad} / (1\,000\,000) (*MW*)$

244 797.

0.244797

$U_{rad} (1 \text{ "m"}^3 / (100 \text{ "cm"}^3)^3)$

$$\frac{0.244797 \text{ m}^3}{\text{cm}^3}$$

$C_{min} = \text{Min}[\dot{m}c_{p,air}, \dot{m}c_p]$

$C_{max} = \text{Max}[\dot{m}c_{p,air}, \dot{m}c_p]$

$C1 = C_{min} / C_{max}$

12 763.3

25 684.1

0.496933

$$NTU = \frac{1}{R_{total} C_{min}}$$

$$NTU_o = \frac{1}{R_{total}} 1 / C_{min}$$

$UA = \dot{m}c_{p,air} NTU$
 $(NTU - NTU_o) / NTU_o * 100$

0.805171

0.858222

10 276.6

-6.18148

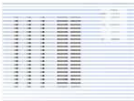
Overall effectiveness for heat exchanger (See page 684 of Heat Transfer, A Practical Approach by Cengel)

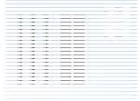
for C_{min} mixed and C_{max} unmixed

$$\epsilon_o = 1 - \text{Exp}\left[\frac{-1}{C1} (1 - \text{Exp}[-C1 NTU])\right]$$

```

eo = If [mdot cp > mdotair cpair,
  1 - Exp [  $\frac{-1}{C1} (1 - \text{Exp}[-C1 NTU])$  ], 1 - Exp [ (1 - C1 (1 - Exp[-NTU])) ] ]
Qmax = eo Cmin (Tin - Tenter)
HeatFluxC = Qmax / Ai
0.484999
155.435.
17.951.

Pic1 =  ;

Pic =  ;

PumpPowerT = PumpPower + FanPower
20.452.6
TotalPower0 = 20.452.55841;

Thout = Tin -  $\frac{Qmax}{mdot cp}$ 
Tout
Tcout = Tenter +  $\frac{Qmax}{mdotair cpair}$ 
Texit
322.908
322.61
316.028
316.85

```

Output Summary

```

Filename = CurrentValue["NotebookFileName"]
Output = TableForm[List [{"Parameter Name", "Symbol", "Value", "Units"},
  {"Case Name", "Filename", Filename, ""},
  {"Resistances"},
  {"Internal Convection Resistance", "Rcv", Rcv, "K/W"},
  {"Conduction Resistance", "Rcond", Rcond, "K/W"},
  {"External Convection Resistance", "Rfin", Rfin, "K/W"},
  {"Radiation Resistance", "Rrad", Rrad, "K/W"},
  {"Total Resistance", "Rtotalc", Rtotalc, "K/W"}, {"LMTD Total Resistance",
  "Rtotal", Rtotal, "K/W"}, {"Percent Difference", "diff", diff, "%"},
  {""},
  {"Dimensions"}],

```

```

{"Height of Radiator Unit", "L", L, "m"}, {"Width of Radiator Unit",
"W", W, "m"}, {"Depth of Radiator Unit", "Hpipe", Hpipe, "m"},
{"Frontal Area of Radiator", "Afr", Afr, "m^2"}, {"Tube Equivelent Diameter",
"Deq", Deq, "m"}, {"Number of Tube Arrays", "Npipe", Npipe, "Arrays"},
{"Number of Tubes Per Array", "Ntube", Ntube, "Tubes"},
{"Fin Length", "Lfin", Lfin, "m"},
{""},
{"Heat Transfer Calculations"},
{"Surface Density", "SD", SD, "m^2/m^3"}, {"Overall Heat Transfer Coefficient",
"U", Uc, "W/m^2"}, {"Heat Flux", "HeatFlux", HeatFluxC, "W/m^2"},
{"Total Heat Transferred", "Urad", Urad, "W/m^3 K"},
{""},
{"Water Side Calculations"},
{"Hydraulic Diameter", "Dh", Dh, "m"},
{"Mass Flow Rate of Coolant", "mdot", mdot, "kg/s"},
{"Reynolds Number", "ReD", ReD, ""}, {"Nusselt Number", "NuD", NuD, ""},
{"Flow Rate Through Each Pipe", "mdotpipe", mdotpipe, "kg/s"},
{"Convection Coefficient", "hc", hc, "W/m^2 K"},
{"Pressure Drop", "PdropRad", PdropRad, "Pa"},
{"Pumping Power", "PumpPower", PumpPower, "W"}, {"Pumping Power",
"PumpPowerhp", PumpPowerhp, "hp"}, {"Fluid Velocity", "V", V, "m/s"},
{""},
{"Air Side Calculations"},
{"Air Velocity", "Vair", Vair, "m"}, {"Mass Flor Rate of Air", "mdotair",
mdotair, "kg/s"}, {"Hydraulic Diameter of Airflow", "Dhair", Dhair, "m"},
{"Fin Length", "Lfin", Lfin, "m"}, {"Fin Efficiency", "etaf", eta_f * 100, "%"},
{"Fin Effectiveness", "efin", efin * 100, "%"},
{"Overall Efficiency", "etaover", eta_over * 100, "%"},
{"Convection Coefficient", "hair", hair, "W/m^2 K"},
{"Reynolds Number Hydraulic Diameter", "ReA", ReA, ""},
{"Reynolds Number Louver Pitch", "ReLp", ReLp, ""},
{"Pressure Drop Across Radiator", "Pdropair", Pdropair, "Pa"},
{"Fan Power", "FanPower", FanPower, "W"},
{"Fan Power", "FanPowerhp", FanPowerhp, "hp"},
{""},
{"Surface Areas"},
{"External Surface Area of Pipes", "Abase", Abase, "m^2"},
{"Surface Area of Fins", "Af", Af, "m^2"},
{"Total Convective Surface Area", "A", A, "m^2"},
{"Internal Surface Area of Pipes", "Ai", Ai, "m"}, {"Free Flow Area", "Ao",
Ao, "m"}, {"Total Cross Sectional Area", "Actot", Ac * Npipe * Ntube, "m^2"},
{""},
{"Summary"},
{"Parameter Name", "Symbol", "Value", "Units"},
{"Case Name", "Filename", Filename, ""},
{"Total Resistance", "Rtotalc", Rtotalc, "K/W"},
{"Height of Radiator Unit", "L", L, "m"}, {"Width of Radiator Unit",
"W", W, "m"}, {"Frontal Area of Radiator", "Afr", Afr, "m^2"},
{"Pressure Drop", "PdropRad", PdropRad, "Pa"}, {"Pumping Power", "PumpPower",
PumpPower, "W"}, {"Pumping Power", "PumpPowerhp", PumpPowerhp, "hp"},
{"Pressure Drop Across Radiator", "Pdropair", Pdropair, "Pa"},
{"Fan Power", "FanPower", FanPower, "W"},

```

```

{"Fan Power", "FanPowerhp", FanPowerhp, "hp"}, {"Number of Transfer Units",
"NTU", NTU, ""}, {"Heat Exchanger Effectiveness", "eo", eo, ""},
{"Max Heat Transfer/Pumping Power", "Qmax/PpumpT", Qmax / PumpPowerT, "W/K/W"},
{"Percent Area Reduction", "RedAfr", ((0.85655 - Afr) / 0.85655), "%"},
{"Percent Energy Savings", "Esave",
((TotalPower0 - (PumpPower + FanPower)) / TotalPower0 * 100), "%"},
{"Fin Pitch", "Fp", Fp, "m"}, {"Max Heat Transfer", "Qmax", Qmax, "W"},
{"Total Pumping Power", "PpumpT", PumpPower + FanPower, "W"},
{"Total Fluid Volume in Pipes", "Actot*L", Ac * Npipe * Ntube * L, "m^3"},
{"Entrance Length for flow", "xfd", 0.05 ReD Pr Dh, "m"},
{"Exit Coolant Temperature", "Thout", Thout, "K"},
{"Exit Air Temperature", "Tcout", Tcout, "K"},
{"Volumetric Heat Transfer", "Qmax/V", Qmax / (L * W * Hpipe), "W/m^3"},
{"Heat Transfer Requirement", "Qtras", mdot cp (Tin - Tout), "W"},
{""},
{"Radiator Dimensions"},
{"Parameter Name", "Symbol", "Value", "Units"},
{"Tube Type", "Type", Type, "m"}, {"Height of Radiator Unit", "L", L, "m"},
{"Width of Radiator Unit", "W", W, "m"},
{"Depth of Radiator Unit", "Td", Hpipe, "m"}, {"Mean Diameter", "Dm", Dm, "m"},
{"Hydraulic Diameter", "Dh", Dh, "m"}, {"Tube Thickness", "t", tpipe, "m"},
{"Perimeter of Tube", "P", P, "m"}, {"Number of tubes", "Npipe", Npipe, "m"},
{"Louver Fin Length", "Lf", Fl, "m"}, {"Louver Fin Pitch", "Fp", Fp, "m"},
{"Louver Length", "Ll", Ll, "m"}, {"Louver Pitch", "Lp", Lp, "m"},
{"Fin Thickness", "df", delta, "m"}, {"Louver Angle", "theta", theta, "deg"},
{"Tube Pitch", "Tp", Tp, "m"}, {"Total Surface Area", "A", A, "m^2"},
{"Free-Flow Area", "Ao", Ao, "m^2"}, {"Frontal Area", "Afr", Afr, "m^2"},
{"Link", "R:\\PACCAR Heat Exchanger\\Microchannel Calculations"}];
SetDirectory[
  "R:\\PACCAR Heat Exchanger\\Microchannel Calculations\\Corrected_files"];
Export["RadiatorResistance_Original.xls", Output, "XLS"]
Speak["Remember to save under a different file name"]

Radiator Resistance_test.nb
RadiatorResistance_Original.xls

```

Table 11: Comparison of Radiator Designs

Symbol	Units	Original Radiator	Design 10.0	Design 10.1
L	mm	933.45	650	650
W	mm	917.62	761.3	761.3
T_d	mm	52.24	80	80
D_m	mm	2.38	0.7	0.7
A_c	mm ²	73.116	49.485	49.485
F_L	mm	7.77	12	12
t	mm	0.45	0.1	0.1
P	mm	102.31	1.57	2
N_{pipe}	tubes	91	53*114	53*114
F_p	mm	1.54	1.54	1.54
L_i	mm	5.77	11	11
L_p	mm	0.861	.861	.861
δ_f	mm	0.1	0.1	0.1
θ	°	30	30	30
T_p	mm	10	12.7	12.7
A	m ²	58.406	58.908	58.908
A_i	m ²	8.690	6.169	6.169
A_o	m ²	0.656	0.470	0.470
A_{fr}	m ²	0.857	0.495	0.495
D_h	mm	2.86	0.5	0.5

APPENDIX B
CFD RESULTS

List of Figures

Figure B1: Temperature contour for coarse and fine mesh for original flat tube	112
Figure B2: Pressure contour for coarse and fine mesh for original flat tube	112
Figure B3: Temperature cross-sections for coarse and fine mesh for original flat tube.....	113
Figure B4: Velocity contour cross sections for coarse and fine mesh for original flat tube.....	113
Figure B5: Temperature profile of outlet for coarse and fine mesh for original flat tube	113
Figure B6: Temperature profile for coarse and fine mesh of microchannel square tube	114
Figure B7: Pressure contours for coarse and fine mesh of microchannel square tube	114
Figure B8: Velocity profile at cross sections of coarse and fine mesh for microchannel square tube.....	114
Figure B9: Temperature profile at cross sections of coarse and fine mesh for microchannel square tube	115
Figure B10: Temperature profile of outlet for coarse and fine mesh for microchannel square tube	115
Figure B11: Temperature contour for coarse and fine mesh of microchannel round tube	115
Figure B12: Pressure contour of coarse and fine mesh for microchannel round tube	116
Figure B13: Velocity profile at cross sections of coarse and fine mesh for microchannel round tube.....	116
Figure B14: Temperature profile at cross sections of coarse and fine mesh for microchannel round tube	116
Figure B15: Temperature profile of outlet for coarse and fine mesh for microchannel round tube	117
Figure B16: Temperature profile of original fin as seen from above	117
Figure B17: Temperature profile of original fin as seen from side	118
Figure B18: Temperature profile at various cross sections of original fin	118
Figure B19: Pressure profile of original fin.....	119
Figure B20: Pressure profile of original fin.....	119
Figure B21: Velocity streamlines through original fin geometry	120

Figure B22: Temperature volume rendering of original fin	120
Figure B23: Temperature profile of original fin at pressure outlet and velocity inlet.....	121
Figure B24: Pressure profile at pressure outlet.....	121

Original Flat tube

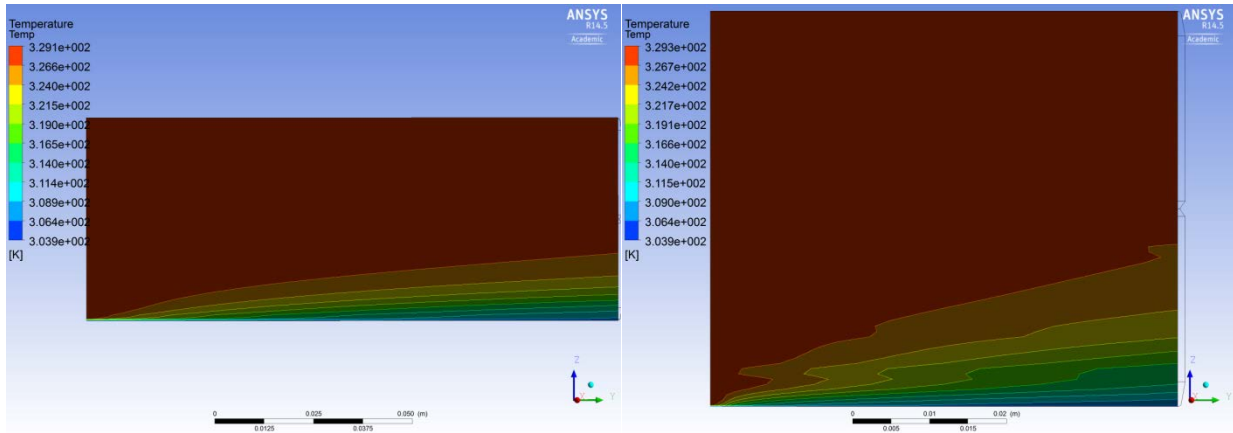


Figure B1: Temperature contour for coarse and fine mesh for original flat tube

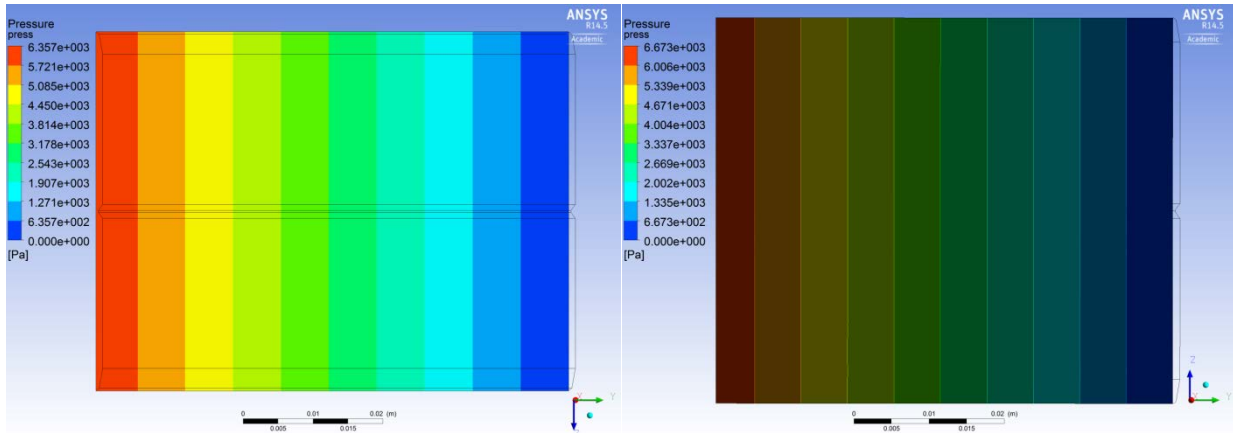


Figure B2: Pressure contour for coarse and fine mesh for original flat tube

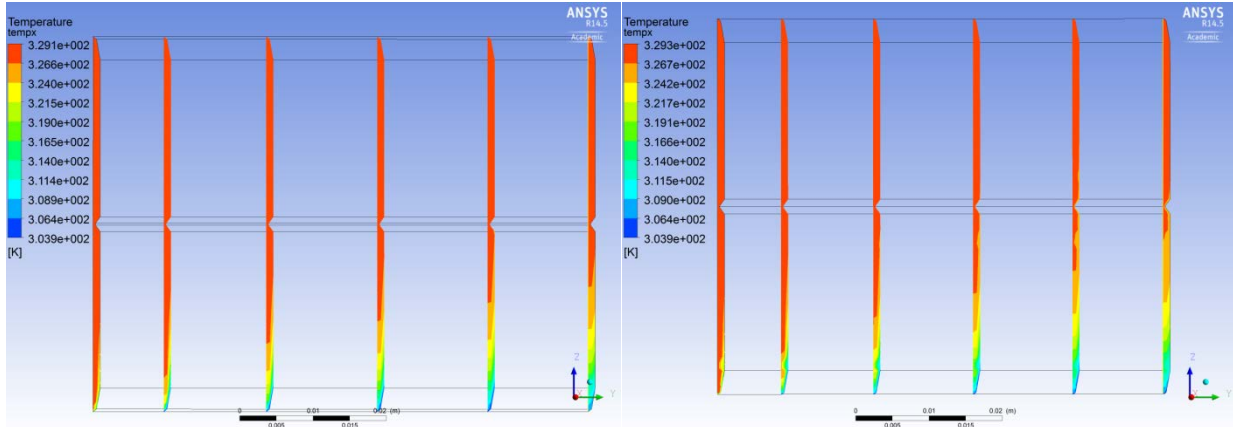


Figure B3: Temperature cross-sections for coarse and fine mesh for original flat tube

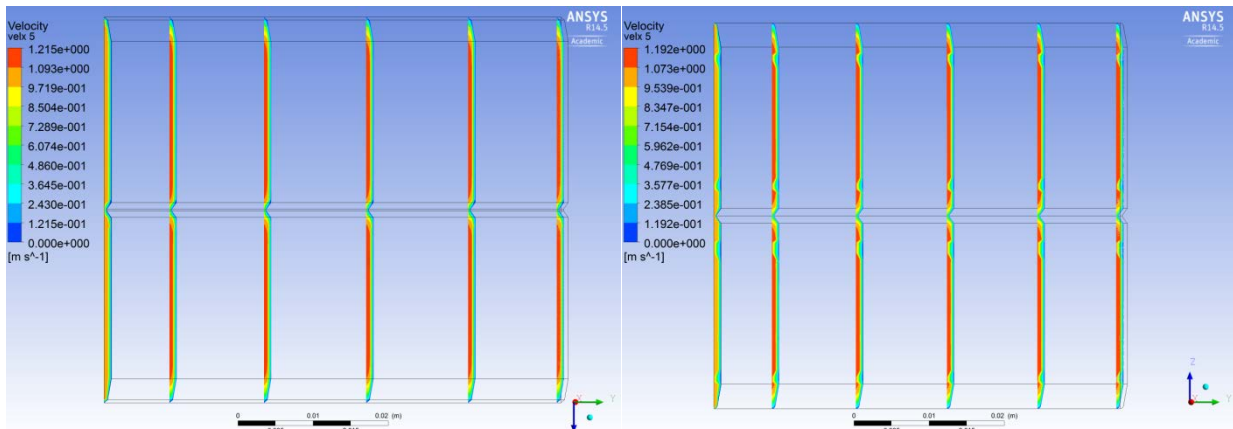


Figure B4: Velocity contour cross sections for coarse and fine mesh for original flat tube

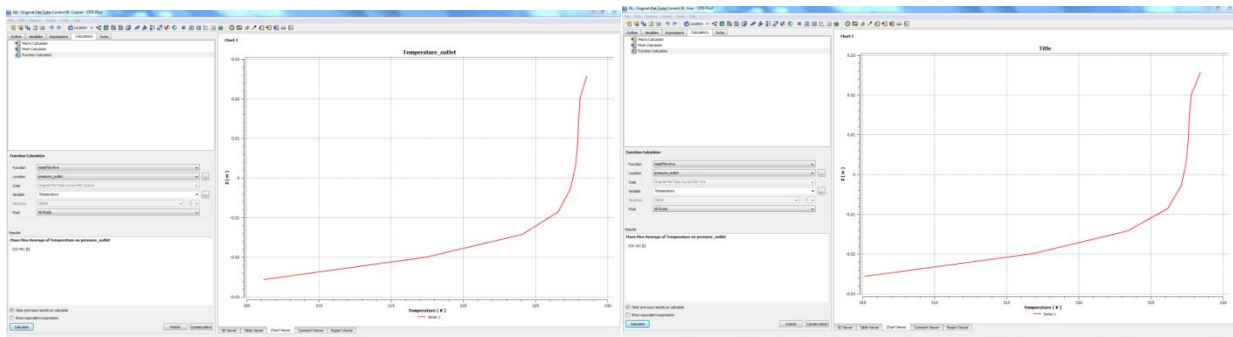


Figure B5: Temperature profile of outlet for coarse and fine mesh for original flat tube

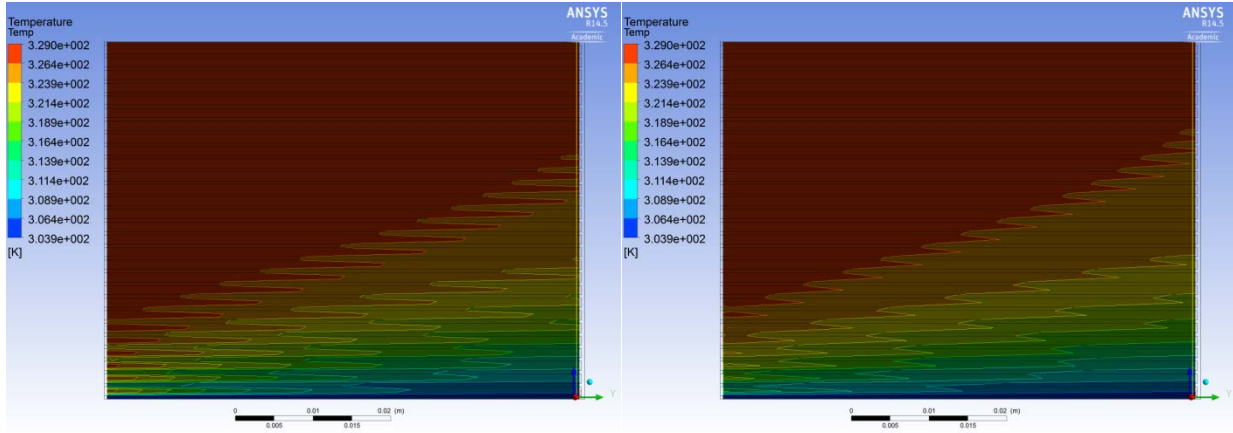


Figure B6: Temperature profile for coarse and fine mesh of microchannel square tube

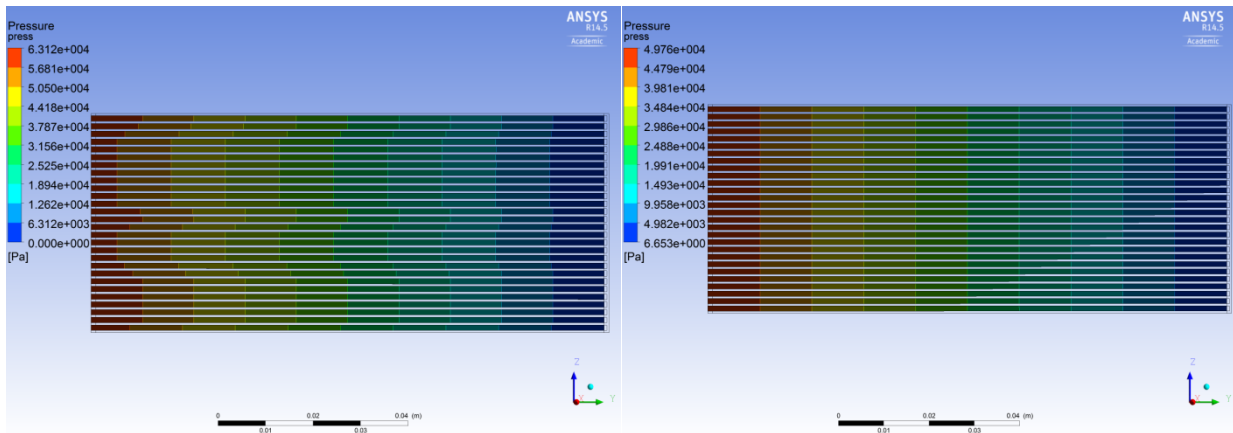


Figure B7: Pressure contours for coarse and fine mesh of microchannel square tube

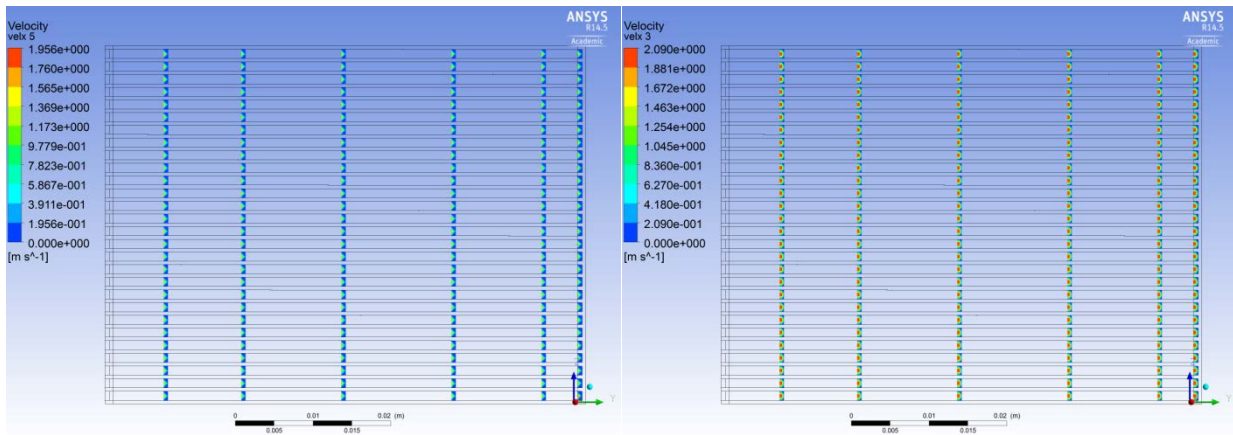


Figure B8: Velocity profile at cross sections of coarse and fine mesh for microchannel square tube

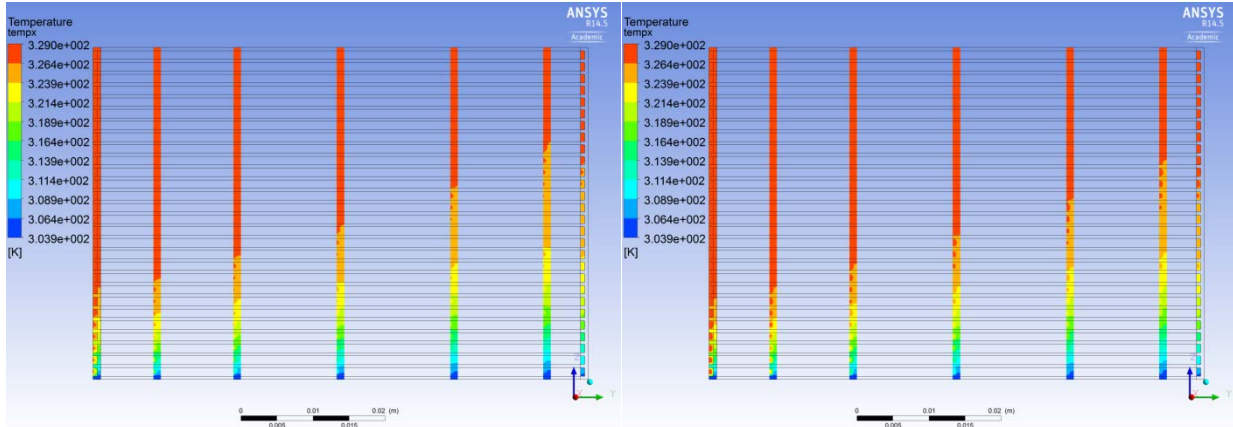


Figure B9: Temperature profile at cross sections of coarse and fine mesh for microchannel square tube

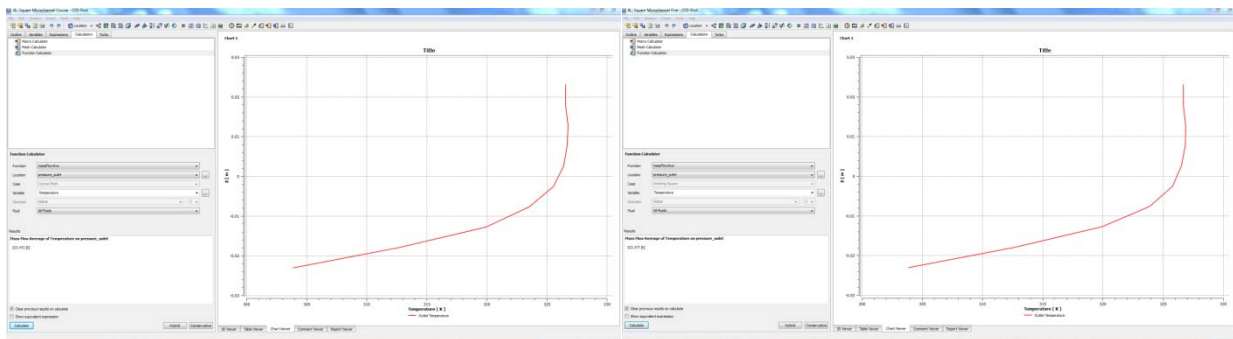


Figure B10: Temperature profile of outlet for coarse and fine mesh for microchannel square tube

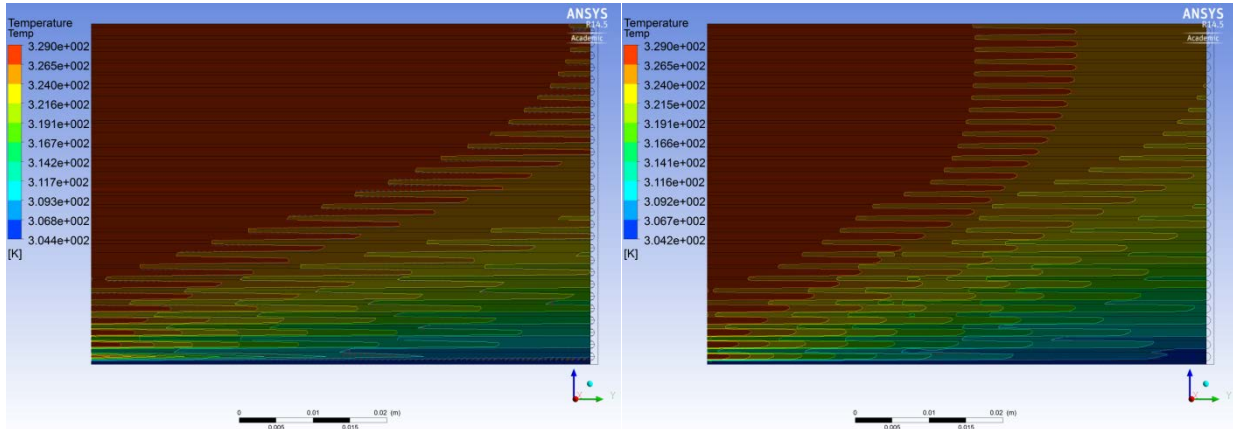


Figure B11: Temperature contour for coarse and fine mesh of microchannel round tube

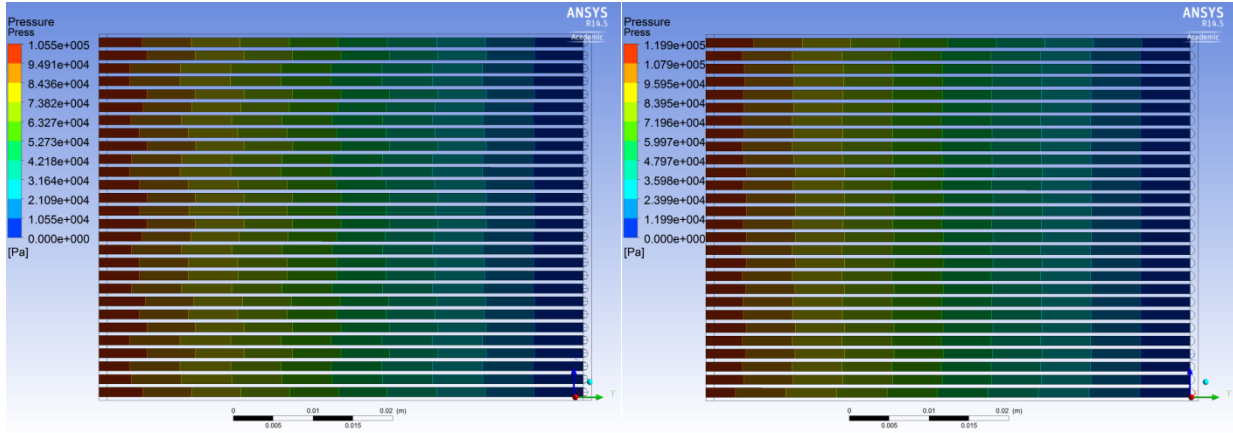


Figure B12: Pressure contour of coarse and fine mesh for microchannel round tube

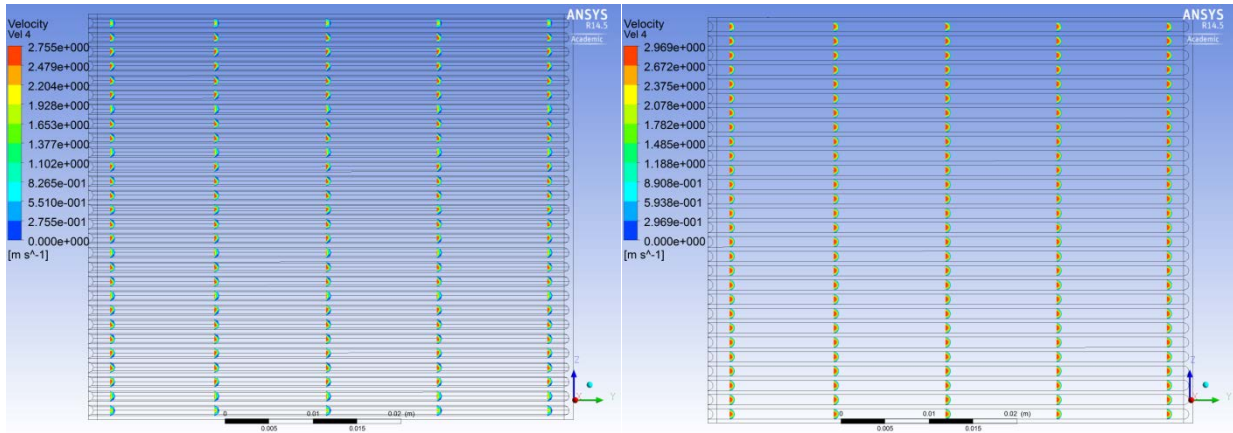


Figure B13: Velocity profile at cross sections of coarse and fine mesh for microchannel round tube

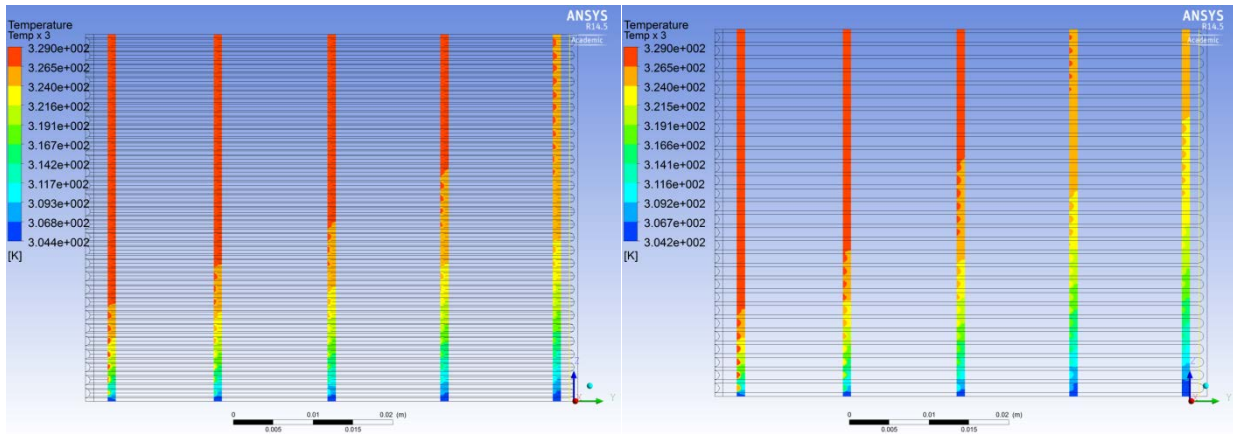


Figure B14: Temperature profile at cross sections of coarse and fine mesh for microchannel round tube

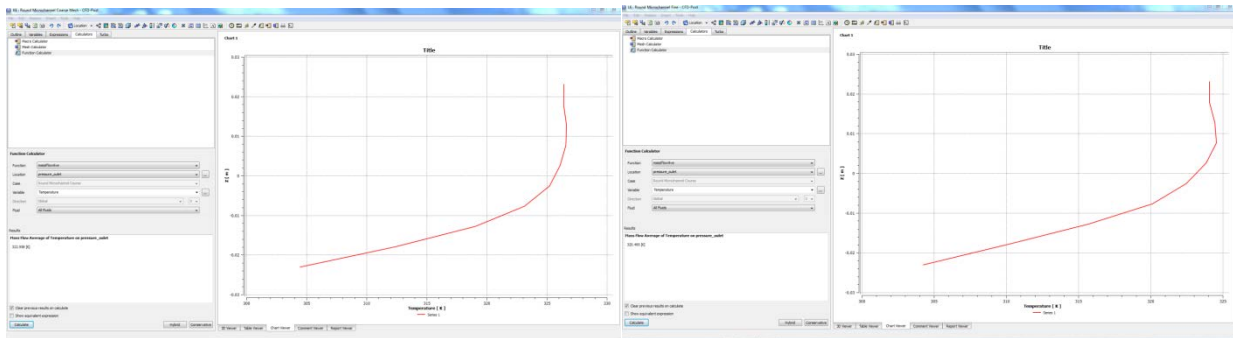


Figure B15: Temperature profile of outlet for coarse and fine mesh for microchannel round tube

Original Fin

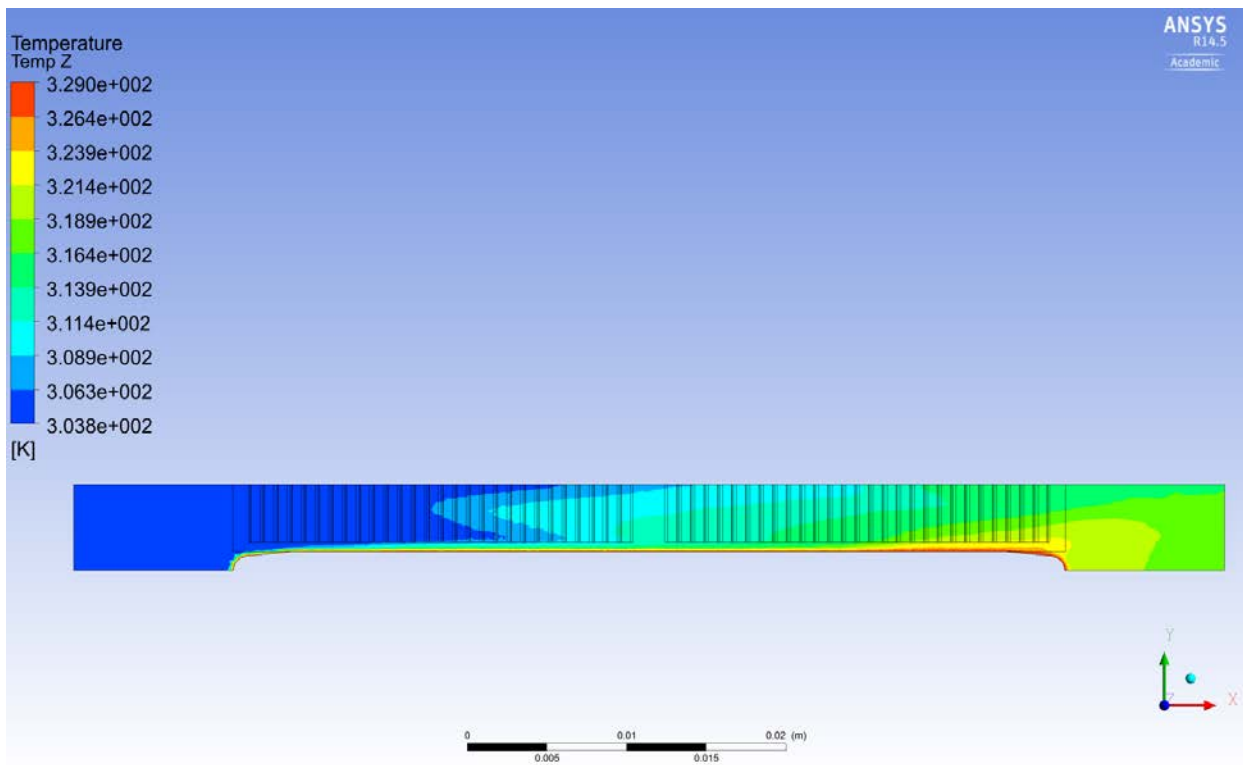


Figure B16: Temperature profile of original fin as seen from above

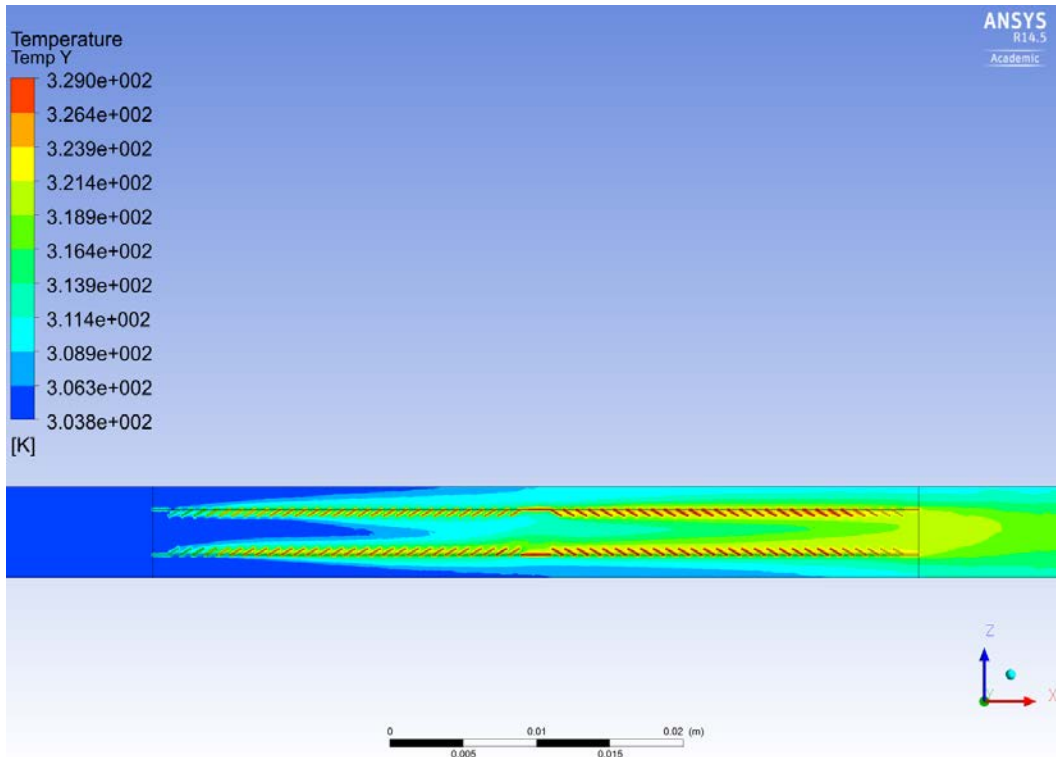


Figure B17: Temperature profile of original fin as seen from side

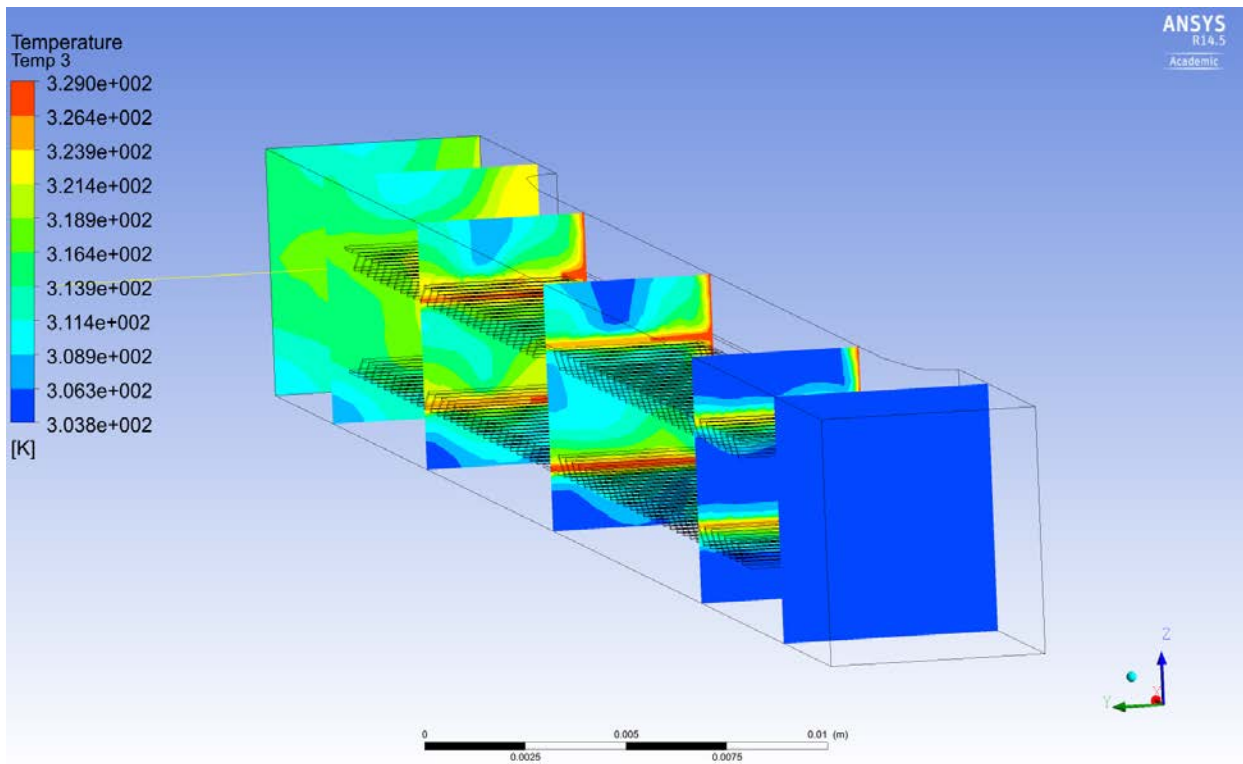


Figure B18: Temperature profile at various cross sections of original fin

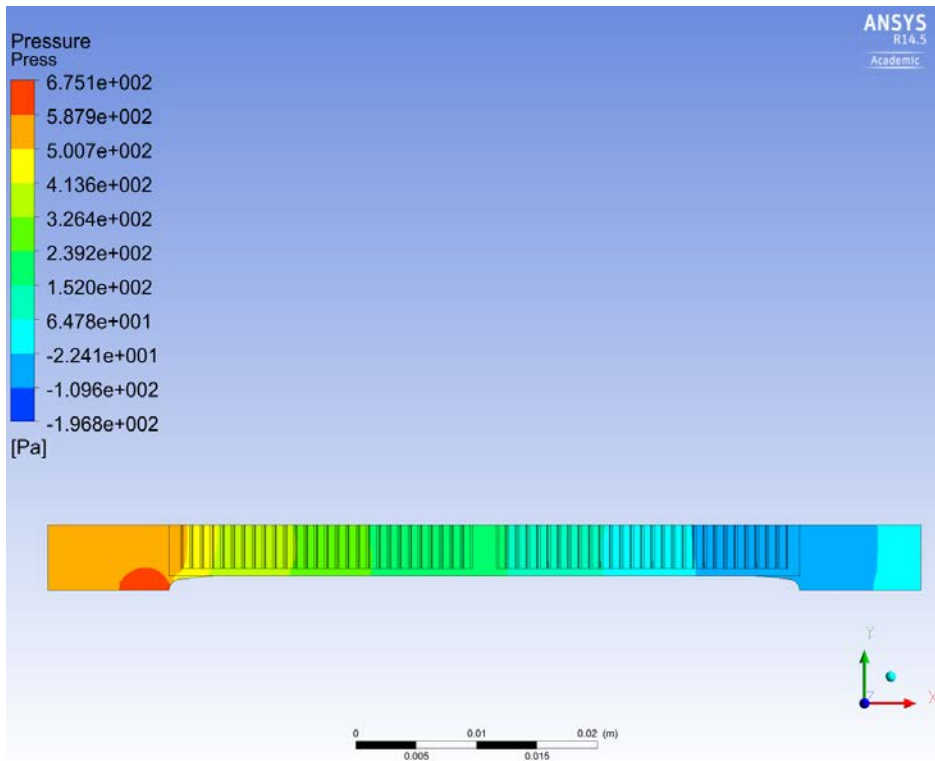


Figure B19: Pressure profile of original fin

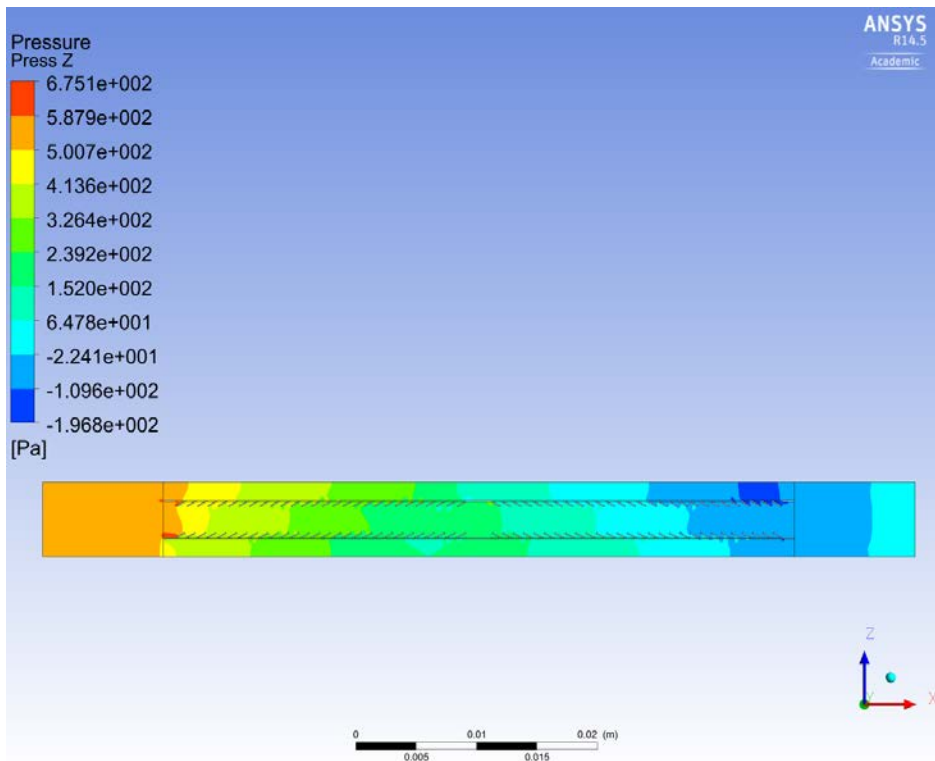


Figure B20: Pressure profile of original fin

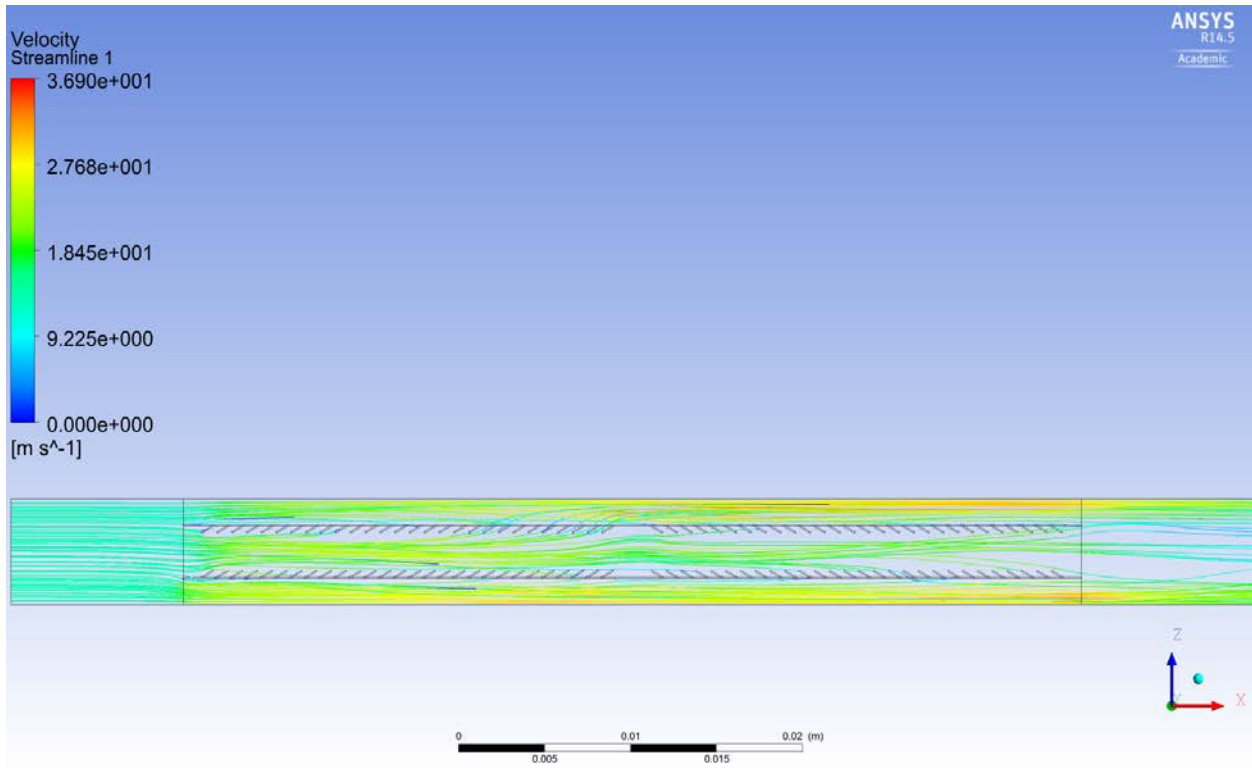


Figure B21: Velocity streamlines through original fin geometry

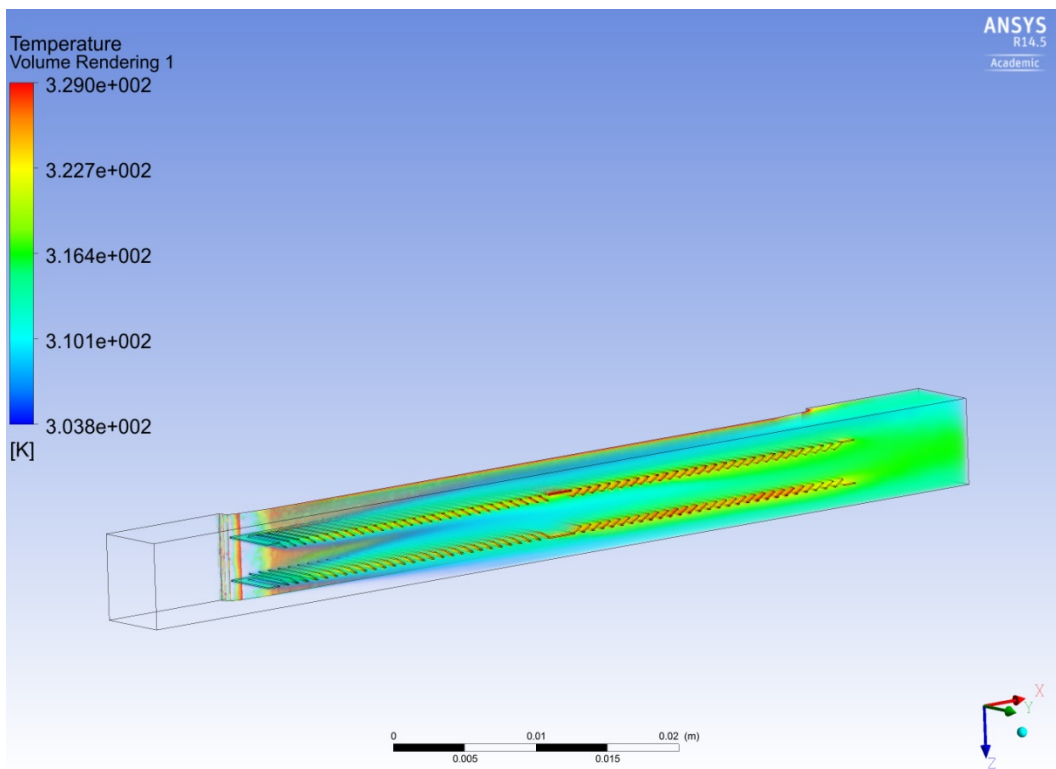


Figure B22: Temperature volume rendering of original fin

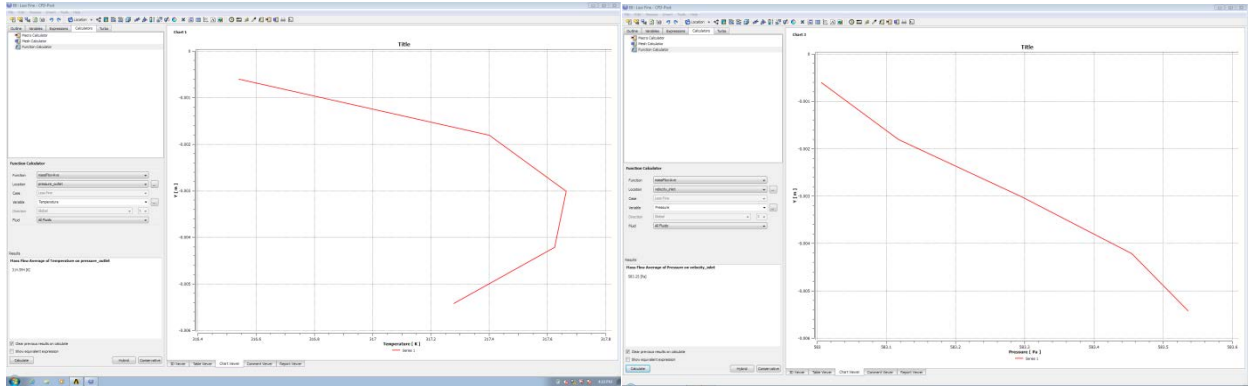


Figure B23: Temperature profile of original fin at pressure outlet and velocity inlet

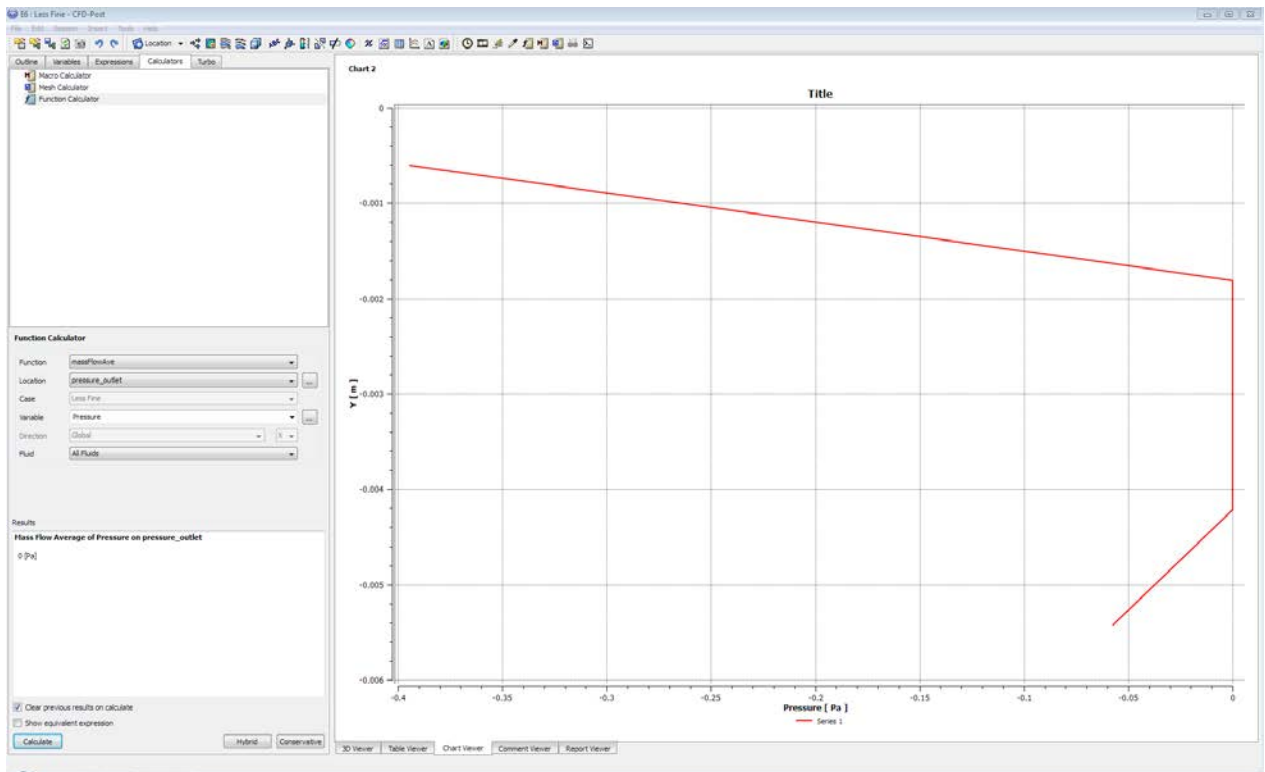


Figure B24: Pressure profile at pressure outlet

REFERENCES

- [1] EPA, "Sources of Greenhouse Gas Emissions," 2013. [Online]. Available: <http://www.epa.gov/climatechange/ghgemissions/sources/transportation.html>. [Accessed 7 March 2014].
- [2] NACFE, "Title of Presentation - North American Council for Freight Efficiency," 13 October 2011. [Online]. Available: <http://nacfe.org/wp-content/uploads/2011/10/NACFE-Baltimore-DI4-Presentations-101311.pdf>. [Accessed 7 March 2014].
- [3] R. Mihelic, *Peterbilt's new Super Truck*, Denton: Peterbilt, 2014.
- [4] US EPA, "Greenhouse Gas (GHG) Emission Requirements for Vocational Vehicles," August 2012. [Online]. Available: <http://www.epa.gov/otaq/climate/documents/vocational-only-presentation.pdf>.
- [5] American Trucking Association's Technology and Maintenance Council, "Relationships Between Truck Components And Fuel Economy," *Recommended Practice*, p. RP1111A, 2009.
- [6] "Peterbilt 579 on the road," 22 June 2012. [Online]. Available: <http://hankstruckforum.com/htforum/index.php?topic=61512.0>. [Accessed 17 March 2014].
- [7] P. Acoba, "Walmart reveals its WAVE concept hybrid powered semi-trailer truck," 17 February 2014. [Online]. Available: <http://www.examiner.com/article/walmart-reveals-its-wave-concept-hybrid-powered-semi-trailer-truck>.
- [8] EquipmentReady, "Cabover Trucks – Pros And Cons," 29 July 2012. [Online]. Available: <http://equipmentready.com/blog/tag/cabovers/>.
- [9] "Lonestar Peterbilt 367 hauling an oversized load through Lampasas, Tx.," 21 January 2012. [Online]. Available: <http://www.flickr.com/photos/51978442@N06/6779889043/>. [Accessed 12 March 2014].
- [10] Y. A. Cengel, *Heat Transfer: A Practical Approach*, New York: McGraw-Hill, 2003, p. 761.
- [11] D. Antonijevic, "An engineering procedure for air side performance evaluation of flat tube heat exchangers with louvered fins," *Heat and Mass Transfer*, vol. 2013, no. 49, p. 117–127, 2013.
- [12] S. R. P. Pawan S. Amrutkar, "Automotive Radiator Performance – Review," vol. 2, no. 3, 2013.
- [13] C. Oliet, C. D. P. Segarra and A. Oliva, "Numerical Simulation of Complex Thermal Systems Involving Multiple Fin-And-Tube Heat Exchangers," in *International Refrigeration and Air Conditioning Conference at Purdue*, Purdue University, 2004.

- [14] K. S. N. P. P. M.K. Rathod, "Performance evaluation of flat finned tube fin heat exchanger with different fin surfaces," vol. 2007, no. 27, 2007.
- [15] C. Oliet, A. Oliva, J. Castro and C. Perez-Segarra, "Parametric studies on automotive radiators," *Applied Thermal Engineering*, vol. 27, no. 11-12, p. 2033–2043, 2007.
- [16] Y.-J. Chang and C.-C. Wang, "A generalized heat transfer correlation for louver fin geometry," *International Journal of Heat and Mass Transfer*, vol. 40, no. 3, pp. 533-544, 1997.
- [17] D. Junqi, C. Jiangping, C. Zhijiu, Z. Yimin and Z. Wenfeng, "Heat transfer and pressure drop correlations for the wavy fin and flat tube heat exchanger," *Applied Thermal Engineering*, vol. 27, no. 11-12, pp. 2066-2073, 2007.
- [18] C. Oliet, C. D. Perez-Segarra and A. Olivia, "Thermal and Fluid Dynamic Simulation of Automotive Fin-and-Tube Heat Exchangers, Part 2: Experimental Comparison," *Heat Transfer Engineering*, vol. 29, no. 5, pp. 495-502, 2008.
- [19] C. D. Perez-Segarra, C. Oliet and A. Oliva, "Thermal and Fluid Dynamic Simulation of Automotive Fin-and-Tube Heat Exchangers, Part 1: Mathematical Model," *Heat Transfer Engineering*, vol. 29, no. 5, pp. 484-494, 2008.
- [20] C. Oliet, C. D. Perez-Segarra, S. Danov and A. Oliva, "Numerical Simulation Of Dehumidifying Fin-And-Tube Heat Exchangers, Model Strategies And Experimental Comparisons," in *International Refrigeration and Air Conditioning Conference*, Purdue University, 2002.
- [21] Y.-J. Chang, K.-C. Hsu, Y.-T. Lin and C.-C. Wang, "A generalized friction correlation for louver fin geometry," *International Journal of Heat and Mass Transfer*, vol. 43, no. 12, p. 2237–2243, 2000.
- [22] D. Junqi, C. Jiangping, C. Zhijiu, Z. Yimin and Z. Wenfeng, "Heat transfer and pressure drop correlations for the wavy fin and flat tube heat exchangers," *Applied Thermal Engineering*, vol. 27, no. 11-12, p. 2066–2073, 2007.
- [23] C. T'Joen, A. Jacobi and M. De Paepe, "Flow visualisation in inclined louvered fins," *Experimental Thermal and Fluid Science*, vol. 33, no. 4, p. 664–674, 2009.
- [24] I. H. Bell and E. A. Groll, "Air-side particulate fouling of microchannel heat exchangers: Experimental comparison of air-side pressure drop and heat transfer with plate-fin heat exchanger," *Applied Thermal Engineering*, vol. 31, no. 5, pp. 742-749, 2011.
- [25] K.-K. Chong and W.-C. Tan, "Study of automotive radiator system for dense-array concentration photovoltaic system," *Solar Energy*, vol. 86, no. 9, p. 2632–2643, 2012.
- [26] J. Yadav and B. R. Singh, "Study on Performance Evaluation of Automotive Radiator," *SAMRIDDHI-A Journal of Physical Sciences, Engineering and Technology*, vol. 2, no. 2, 2011.

- [27] K. Leong, R. Saidura, S. Kazi and A. Mamun, "Performance investigation of an automotive car radiator operated with nanofluid-based coolants (nanofluid as a coolant in a radiator)," *Applied Thermal Engineering*, vol. 30, no. 17-18, p. 2685–2692, 2010.
- [28] D. G. Charyulu, G. Singh and J. .. Sharma, "Performance evaluation of a radiator in a diesel engine-a case study," *Applied Thermal Engineering*, vol. 19, no. 6, p. 625–639, 1999.
- [29] J. Klett, C. Walls and T. Golubic, "Performance of Alternate Precursors for Graphite Foam," Oak Ridge National Lab, 2001. [Online]. Available: <http://web.ornl.gov/~webworks/cppr/y2001/pres/120073.pdf>. [Accessed 12 March 2014].
- [30] C. Harris, M. Despa and K. Kelly, "Design and Fabrication of a Cross Flow Micro Heat Exchanger," *Journal Of Microelectromechanical Systems*, vol. 9, no. 4, pp. 502-508, 2000.
- [31] D. Westphalen, K. W. Roth and J. Brodrick, "Microchannel Heat Exchangers," *ASHRAE Journal*, vol. 45, no. 12, pp. 107-109, 2003.
- [32] G. Khan, "Experimental Investigation Of Heat Transfer And Pressure Drop Characteristics Of Water And Glycol-Water Mixture In Multi-Port Serpentine Microchannel Slab Heat Exchangers," *University of Windsor*, no. 1, pp. 1-530, 2011.
- [33] Y. Fan and L. Luo, "Recent Applications of Advances in Microchannel Heat Exchangers and Multi-Scale Design Optimization," *Heat Transfer Engineering*, vol. 29, no. 5, p. 461–474, 2008.
- [34] M. G. Khan and A. Fartaj, "A review on microchannel heat exchangers and potential applications," *International Journal of Energy Research*, vol. 35, no. 7, p. 553–582, 2011.
- [35] C. W. B. M. H. Kim, "Air-Side Thermal Performance of Micro-Channel Heat Exchangers Under Dehumidifying Conditions," 2000.
- [36] K. D. Cole and B. Çetin, "The Effect of Axial Conduction on Heat Transfer in a Liquid Microchannel Flow," *International Journal of Heat and Mass Transfer*, vol. 54, no. 11-12, pp. 2542-2549, 2011.
- [37] S. C. Kim, M. S. Kim, I. C. Hwang and T. W. Lim, "Performance evaluation of a CO2 heat pump system for fuel cell vehicles considering the heat exchanger arrangements," *International Journal of Refrigeration*, vol. 30, no. 7, p. 1195–1206, 2007.
- [38] Y. J. Lee, P. S. Lee and S. K. Chou, "Enhanced Thermal Transport in Microchannel Using Oblique Fins," *Journal of Heat Transfer*, vol. 134, no. 10, pp. 101901-1-101901-10, 2012.
- [39] K. A. Moores, J. Kim and Y. K. Joshi, "Heat transfer and fluid flow in shrouded pin fin arrays with and without tip clearance," *International Journal of Heat and Mass Transfer*, vol. 52, no. 25-26, p. 5978–5989, 2009.

- [40] S. G. Kandlikar, S. Colin, Y. Peles, S. Garimella, R. F. Pease, J. J. Brandner and D. B. Tuckerman, "Heat Transfer in Microchannels—2012 Status and Research Needs," *Journal of Heat Transfer-Transactions of the ASME*, vol. 135, no. 9, pp. 1-18, 2013.
- [41] A. Kaneko, G. Takeuchi, Y. Abe and Y. Suzuki, "Condensation Behavior in a Microchannel Heat Exchanger," *Journal of Thermal Science and Technology*, vol. 4, no. 4, pp. 469-482, 2009.
- [42] "Experimental investigation of Cu-based, double-layered, microchannel heat exchangers," vol. 2013, no. 23, 2013.
- [43] Y. Tang, Z. He, M. Pan and J. Wang, "Ring-shaped microchannel heat exchanger based on turning process," *Experimental Thermal and Fluid Science*, vol. 34, no. 8, p. 1398-1402, 2010.
- [44] A. G. A. Nnanna, "Thermo-Hydraulic Behavior of Microchannel Heat Exchanger System," *Experimental Heat Transfer*, vol. 23, no. 2, pp. 157-173, 2010.
- [45] S.-W. Kang and S.-C. Tseng, "Analysis of effectiveness and pressure drop in micro cross-flow heat exchanger," *Applied Thermal Engineering*, vol. 27, no. 5-6, pp. 877-885, 2007.
- [46] B. Schneider, A. Kosar, C.-J. Kuo, C. Mishra, G. S. Cole, R. P. Scaringe and Y. Peles, "Cavitation Enhanced Heat Transfer in Microchannels," *Journal of Heat Transfer-Transactions of the ASME*, vol. 128, no. 12, pp. 1293-1301, 2006.
- [47] S. G. Kandlikar, "Fundamental issues related to flow boiling in minichannels and microchannels," *Experimental Thermal and Fluid Science*, vol. 26, no. 2-4, pp. 389-407, 2002.
- [48] Benjamin Newel, l Alexander Long and T. Newell, "A Microchannel Evaporator for Domestic Refrigerators," *ASHRAE Transactions*, vol. 117, no. 2, pp. 108-115, 2011.
- [49] X. Yang, J. Zhang, J. Yu, Y. Wu, Y. Luo and J. Guo, "Numerical Simulation on Flow and Heat Transfer at Shell-Side of Flat-Tube Heat Exchangers," *Wuhan University Journal of Natural Sciences*, vol. 15, no. 5, pp. 427-432, 2010.
- [50] N.-H. Kim, E.-J. Lee and H.-W. Byun, "Evaporation heat transfer and pressure drop of R-410A in flattened smooth tubes having different aspect ratios," *International Journal of Refrigeration*, vol. 36, no. 2, pp. 363-374, 2013.
- [51] R. Vajjha S., D. K. Das and P. K. Nambur, "Numerical study of fluid dynamic and heat transfer performance of Al₂O₃ and CuO nanofluids in the flat tubes of a radiator," *International Journal of Heat and Fluid Flow*, vol. 31, no. 4, pp. 613-621, 2010.
- [52] T. Perrotin and D. Clodic, "Thermal-hydraulic CFD study in louvered fin-and-flat-tube heat exchangers," vol. 2004, no. 27, 2004.
- [53] M. N. Bowman, Heat Transfer Log Mean Temperature Difference (Lmtd) Method, 2009.

- [54] T. Miller, Interviewee, *RE: Microchannel Heat Exchanger Manufacturing*. [Interview]. 4 February 2014.
- [55] "Micro-multiport extrusion tube," Yatal/Apalt, 2012. [Online]. Available: <http://www.yatal.com/en/products.asp?classid=29>. [Accessed 14 March 2014].
- [56] "Fluid Properties Calculator," Microelectronics Heat Transfer Laboratory, 1997. [Online]. Available: <http://www.mhtl.uwaterloo.ca/old/onlinetools/airprop/airprop.html>. [Accessed 15 March 2014].
- [57] "Thermophysical Properties of Brines Models," M. Conde Engineering, 2011. [Online]. Available: <http://www.mrc-eng.com/Downloads/Brine%20Properties.pdf>. [Accessed 2014 March 19].
- [58] "Ethylene Glycol Heat-Transfer Fluid," Engineering Toolbox, [Online]. Available: http://www.engineeringtoolbox.com/ethylene-glycol-d_146.html. [Accessed 15 March 2014].